

Machinability of Al-20Mg<sub>2</sub>Si-Cu Metal Matrix Composite  
Modified with Bismuth or Barium

By

Mohsen MARANI BARZANI

MANUSCRIPT-BASED THESIS PRESENTED TO  
ÉCOLE DE TECHNOLOGIE SUPÉRIEURE  
IN PARTIAL FULFILLMENT FOR THE DEGREE  
OF DOCTOR OF PHILOSOPHY  
Ph.D.

MONTREAL, APRIL 17, 2019

ÉCOLE DE TECHNOLOGIE SUPERIEURE  
UNIVERSITE DU QUEBEC

© Copyright

Reproduction, saving or sharing of the content of this document, in whole or in part, is prohibited. A reader who wishes to print this document or save it on any medium must first obtain the author's permission.

**BOARD OF EXAMINERS**

THIS THESIS HAS BEEN EVALUATED  
BY THE FOLLOWING BOARD OF EXAMINERS

Mr. Victor Songmene, Thesis Supervisor  
Department of Mechanical Engineering at École de Technologie Supérieure

Mr. Robert Hausler, President of the Board of Examiners  
Department of Construction Engineering at École de Technologie Supérieure

Mr. Mohammad Jahazi, Member of the jury  
Department of Mechanical Engineering at École de Technologie Supérieure

Mr. Marek Balazinski, External Evaluator  
Department of Mechanical Engineering at École Polytechnique Montréal

Mr. Fawzy-Hosny Samuel, Independent External Evaluator  
Department of Applied Sciences, Université du Québec à Chicoutimi (UQAC)

THIS THESIS WAS PRESENTED AND DEFENDED  
IN THE PRESENCE OF A BOARD OF EXAMINERS  
ON APRIL 10<sup>TH</sup>, 2019

AT ÉCOLE DE TECHNOLOGIE SUPÉRIEURE

## **ACKNOWLEDGMENT**

First of all I would like to express my sincere gratitude and deep appreciation to my supervisor professor Victor Songmene for his helpful guidance, indispensable advice, and continuous help through the course of this thesis.

I am also extremely grateful to Professor Fawzy Hosny Samuel in Université du Québec à Chicoutimi (UQAC) for the support of his laboratory in casting the workpieces used in this research work.

I also would like to thank the jury members, Professor Mohammad Jahazi and Professor Marek Balazinski for having accepted to evaluate my thesis and for their constructive comments.

I'm also grateful to Dr. Jules Kouam and Dr and Yasser Zedan for all technical help and support during the experimental tests.

I would like to thank Rio Tinto (Alcan) for the financial support (\$18000.00) for 1 year.

Finally, I would like to express my heartfelt gratitude for my parents, especially my mother, for their endless love and encouragement.

# Usinabilité du Composite Al-20Mg<sub>2</sub>Si-Cu à Matrice Métallique Modifié Avec du Bismuth ou du Baryum

Mohsen Marani Barzani

## RÉSUMÉ

Les composites à matrice métallique en aluminium (CMM) suscitent de plus en plus d'attention en raison de leurs excellentes propriétés, telles que leur excellente aptitude au moulage et leurs propriétés mécaniques. Ces propriétés les rendent utiles pour les applications à haute performance, spécialement pour les composants légers, en particulier pour la fabrication de pièces automobiles. Un composite à matrice métallique, Al-20Mg<sub>2</sub>Si-Cu, contenant une phase particulière de Mg<sub>2</sub>Si, s'est récemment révélé posséder certains avantages. Cependant, les propriétés mécaniques de ce composite coulé normalement ne sont pas satisfaisantes en raison de la morphologie grossière de la phase primaire Mg<sub>2</sub>Si. Par conséquent, la méthode de traitement à l'état fondu avec des éléments de raffinage a été choisie pour améliorer la morphologie des renforts Mg<sub>2</sub>Si et obtenir de meilleures propriétés mécaniques.

La plupart des pièces CMM nécessitent un certain usinage. Cependant, l'usinabilité du composite à matrice métallique Al-20Mg<sub>2</sub>Si-Cu n'est pas encore bien comprise. En ajoutant des éléments de raffinage au composite, les propriétés mécaniques et l'usinabilité, y compris les émissions de particules, seront affectées. Par conséquent, l'objectif principal de cette thèse est d'étudier l'usinabilité, les propriétés mécaniques et les émissions de particules du composite à matrice métallique Al-20Mg<sub>2</sub>Si-Cu contenant du bismuth ou du baryum comme éléments modificateurs.

Les résultats des différentes sections de cette thèse démontrent que des éléments modificateurs tels que le bismuth ou le baryum améliorent les propriétés mécaniques et l'usinabilité du composite. L'utilisation d'éléments modificateurs réduit les émissions de particules ultrafines au cours du processus d'usinage, ce qui est utile pour la santé de l'opérateur. De plus, des modèles mathématiques de prédiction du fini de surface et des efforts de coupe lors du l'usinage de ce composite ont été proposés.

**Mots-clés:** usinabilité, composite à matrice métallique, microstructure, propriétés mécaniques, bismuth, baryum.

# Machinability of Al-20Mg<sub>2</sub>Si-Cu Metal Matrix Composite Modified With Bismuth or Barium

Mohsen Marani Barzani

## ABSTRACT

Aluminum metal matrix composites (MMC) have been receiving growing attention largely owing to their excellent properties, such as excellent castability and mechanical properties. These properties make them useful for high performance applications, especially for lightweight components, particularly in the manufacture of automotive parts. Al-based composite reinforced with particulate Mg<sub>2</sub>Si phase has recently been shown to possess certain advantages. However, the mechanical properties of normal cast Al-20Mg<sub>2</sub>Si-Cu metal matrix composite are unsatisfactory due to the natural coarse morphology of the primary Mg<sub>2</sub>Si phase. Therefore, the melt treatment method with refiner elements was chosen due to improve the morphology of the Mg<sub>2</sub>Si reinforcement and achieve better mechanical properties.

Most of MMC parts require some machining. However, the machinability of Al-20Mg<sub>2</sub>Si-Cu metal matrix composite is not well understood yet. By adding refiner elements to the composite, the mechanical properties and machinability including particle emissions will be affected. Therefore, the main objective of this thesis is to study the machinability, and mechanical properties of Al-20Mg<sub>2</sub>Si-Cu metal matrix composite containing bismuth or barium as modifier elements.

Results from the different sections of this thesis demonstrate that modifier elements such as bismuth or barium improve the mechanical properties and machinability of the composite. Using modifier elements decreases ultrafine particle emissions during the machining process, which is beneficial for operator health. In addition, the proposed mathematical models for predicting surface roughness and cutting force for this composite are in good agreement with experiment data.

**Keywords:** machinability, metal matrix composite, microstructure, mechanical properties, bismuth, barium.

## TABLE OF CONTENTS

INTRODUCTION .....	1
CHAPTER 1      PROBLEM STATEMENTS, OBJECTIVES AND THESIS OUTLINE .....	5
1.1.    Problem statements .....	5
1.2.    Thesis objectives .....	6
1.3.    Thesis outline .....	6
CHAPTER 2      LITERATURE REVIEW .....	9
2.1.    Metal matrix composite .....	9
2.2.    Reinforcing material .....	10
2.3.    Effect of reinforcements on microstructure .....	12
2.4.    Machinability of aluminum metal matrix composite (MMC) .....	16
2.5.    Effect of reinforcements on machinability .....	19
2.6.    Machinability criteria .....	21
2.6.1.    Introduction .....	21
2.6.2.    Cutting tool material .....	22
2.6.3.    Cutting force .....	24
2.6.4.    Surface roughness .....	26
2.6.5.    Chip formation .....	28
2.6.6.    Dust formation .....	32
2.6.6.1.    Effect of machining process on particle emissions .....	35
2.7.    Adaptive network-based fuzzy inference system (ANFIS) .....	38
2.8.    Summary and conclusive remarks .....	41
CHAPTER 3      METHODOLOGY .....	43
3.1.    Experimental details .....	43
3.2.    Casting process .....	43
3.3.    Machining process .....	48
3.4.    Metallography .....	50
3.5.    Surface roughness and cutting force .....	54
3.6.    Dust emission .....	55
CHAPTER 4      MACHINABILITY CHARACTERISTICS AND MECHANICAL PROPERTIES OF Al-Mg <sub>2</sub> Si-Cu METAL MATRIX COMPOSITE WITH BISMUTH .....	59
4.1.    Abstract .....	59
4.2.    Introduction .....	60
4.3.    Experimental work .....	62
4.3.1.    Material .....	62
4.3.2.    Machining test .....	64

4.4.	Results and discussion .....	65
4.4.1.	Microstructure.....	65
4.4.2.	Mechanical properties.....	66
4.4.3.	Fracture surface.....	68
4.5.	Machinability of metal matrix composite.....	69
4.5.1.	Cutting force .....	69
4.5.2.	Surface roughness.....	75
4.5.3.	Chip morphology .....	79
4.6.	Conclusion .....	82
CHAPTER 5	EXPERIMENTAL INVESTIGATION ON MICROSTRUCTURE, MECHANICAL PROPERTIES AND DUST EMISSION WHEN MILLING Al-20Mg <sub>2</sub> Si-Cu METAL MATRIX COMPOSITE WITH MODIFIER ELEMENTS.....	83
5.1.	Abstract.....	83
5.2.	Introduction.....	84
5.3.	Experimental setup.....	88
5.3.1.	Work material and tooling .....	88
5.3.2.	Machining tests .....	88
5.4.	Results and discussion .....	91
5.4.1.	Microstructure and mechanical properties.....	91
5.4.2.	Fractography .....	95
5.5.	Dust emission.....	97
5.5.1.	Fine particle emission during milling.....	97
5.5.2.	Ultrafine particle emission during milling.....	104
5.6.	Conclusion .....	111
CHAPTER 6	NEURO-FUZZY PREDICTIVE MODLE FOR SURFACE ROUGHNESS AND CUTTING FORCE OF MACHINED Al- 20Mg <sub>2</sub> Si-Cu METAL MATRIX COMPOSITE USING ADITIVES .....	113
6.1.	Abstract.....	113
6.2.	Introduction.....	114
6.3.	Experimental procedure .....	117
6.3.1.	Workpiece fabrication.....	117
6.3.2.	Machining tests .....	117
6.3.3.	Adaptive network-based fuzzy inference system (ANFIS) .....	118
6.4.	Result and discussion.....	120
6.4.1.	ANFIS structure and membership function selection.....	120
6.5.	ANFIS prediction result.....	125
6.5.1.	Surface roughness prediction.....	125
6.5.2.	Cutting force prediction .....	131
6.6.	Conclusion .....	138
CONCLUSION	141	
CONTRIBUTIONS .....		144

RECOMMENDATIONS.....145  
LIST OF BIBLIOGRAPHICAL REFERENCES.....147

## LIST OF TABLES

	Page
Table 3. 1	Machining parameters .....44
Table 3. 2	Chemical composition of base aluminum alloy used .....44
Table 4. 1	Chemical composition of Al-20Mg2Si metal matrix composite.....64
Table 4. 2	Cutting tool and tool holder.....64
Table 5. 1	Composition of Al20%Mg2Si composite .....89
Table 5. 2	Cutting tool and tool holder.....89
Table 5. 3	Cutting conditions and parameters .....90
Table 6. 1	Experimental results used as training data for ANFIS structure .....119
Table 6. 2	Applied equation of each layer.....121
Table 6. 3	Specifications of MFs employed in ANFIS model .....122
Table 6. 4	RMSE values of different structures of the ANFIS model .....123
Table 6. 5	MF arrangements for each input .....124
Table 6. 6	Utilized MF types.....124
Table 6. 7	ANFIS model for surface roughness prediction.....125
Table 6. 8	Values of premise and consequent parameters in proposed ANFIS structure for surface roughness prediction.....131
Table 6. 9	ANFIS model for cutting force prediction .....132
Table 6. 10	Values of premise and consequent parameters in proposed ANFIS structure for cutting force prediction .....137
Table 6. 11	Comparison of estimated outputs and RMSE .....138

## LIST OF FIGURES

Figure 0. 1	Optical microstructures of machined surface for (a) base alloy, (b) Bi-containing, and (c) Sb-containing (Barzani <i>et al.</i> , 2013).	2
Figure 2.1	Application of metal matrix composite (Fadavi <i>et al.</i> , 2015).	10
Figure 2.2	Optical microstructures for (a) base alloy, (b) bi-containing composite, (c) sb-containing composite, and (d) Sr-containing composite (Barzani <i>et al.</i> , 2015).	12
Figure 2.3	Optical micrographs showing the microstructure of primary Mg <sub>2</sub> Si (a) without and (b) with addition of Sr (Farahany <i>et al.</i> , 2016)	14
Figure 2.4	Built-up edge formation in (a) base alloy and (b) Sr-containing workpieces (Barzani <i>et al.</i> , 2013).	17
Figure 2.5	Micrograph of machined subsurface of (a) untreated Al-11%Si and (b) Sb-treated workpiece at cutting speeds 70 m/min (Barzani <i>et al.</i> , 2013).	20
Figure 2.6	The face milling cutter machine (Shaw <i>et al.</i> , 2005)	21
Figure 2.7	Common properties of cutting tool materials (Galoppi <i>et al.</i> , 2006).	23
Figure 2.8	Measured cutting force component (Galoppi <i>et al.</i> , 2006)	25
Figure 2. 9	Composite cutting force circle (Shaw, 2005).	25
Figure 2.10	Surface roughness graph (Barzani <i>et al.</i> , 2015)	28
Figure 2.11	Chip formations (a) discontinuous, (b) continuous, and (c) continuous with BUE (Peach, 2009)	29
Figure 2.12	Chip formations and BUE formation at cutting speed of 250 m/min (a, b) base alloy,(c, d) Bi-containing, and (e, f) Sb-containing alloys (Barzani <i>et al.</i> 2015)	31
Figure 2.13	Dust production zones in the case of milling (Kouam, 2012).	34
Figure 2.14	ANFIS structure (Mohammad <i>et al.</i> , 2015)	39
Figure 3. 1	(a) Melting furnaces and (b) furnace for preheating the permanent mold (Université du Québec à Chicoutimi)	45
Figure 3. 2	Image of the workpiece specimens	46

Figure 3. 3	Optical micrographs showing changes of morphologies for Mg <sub>2</sub> Si with (a) 0.0wt% Bi, (b) 0.2 Bi, (c) 0.4wt% and (d) 0.8wt%Bi	47
Figure 3. 4	Optical micrographs showing changes of morphologies for Mg <sub>2</sub> Si with (a) 0.0wt% Ba, (b) 0.2 Ba, (c) 0.4wt% Ba and (d) 0.8wt%Ba	48
Figure 3.5	CNC machine tool used	49
Figure 3.6	(a) Cutting inserts and (b) tool holder	49
Figure 3.7	Mounted specimens	50
Figure 3.8	Scanning electron microscopy (SEM)	51
Figure 3.9	Optical microscope	51
Figure 3.10	Universal mechanical tensile testing machine	52
Figure 3.11	Hardness machine testing	52
Figure 3.12	Zwick impact testing machine (Courtesy of Ecole Polytechnique de Montréal)	53
Figure 3.13	Tensile samples	53
Figure 3.14	Impact test samples	54
Figure 3.15	Surface roughness tester	55
Figure 3.16	Aerodynamic particle sizer (APS) and scanning mobility particle size (SMPS)	56
Figure 3.17	Summary of the overall methodology	57
Figure 4.1	Tensile sample dimension (mm)	63
Figure 4.2	Optical micrographs of Al-20Mg <sub>2</sub> metal matrix composite (a,b) without Bi and (c,d) with 0.4 wt.% Bi additions	65
Figure 4.3	(a) Stress-strain curve and (b) variation of impact toughness with hardness value for Al-20Mg <sub>2</sub> Si (MMC), and Bi-containing composite	67
Figure 4.4	SEM micrographs of tensile samples for (a,b) Base composite (c,d) Bi-containing composite	69
Figure 4.5	Variation of forces at cutting speed of (a) 90 mm/min (b) 180 m/min and (c) 270 m/min	71

Figure 4.6	Images of inserts (BUE formation) at cutting speed of 270 m/min for (a,b) base composite, and (c,d) Bi-containing composite	72
Figure 4.7	BSE image of Al-20Mg2Si and elemental mapping	73
Figure 4.8	BSE image of Al-20Mg2Si and elemental mapping indicating Bi white compound	74
Figure 4.9	Surface roughness value with feed rate at cutting speed of (a) 90 mm/min (b) 180 m/min and (c) 270 m/min.	76
Figure 4.10	Optical 3D micro coordinate system (a) base composite (b) Bi-containing composite.	77
Figure 4.11	Scanning electron image of machined surface (a) and (b) for Base composite, (c) and (d) for Bi-containing composite	79
Figure 4.12	Optical images of the chip formed (a, b, c) for base composite and (d, e, f) Bi-containing composite	81
Figure 4.13	SEM micrograph of chip formation for Bi-containing composite	81
Figure 5. 1	Schematic representation of machining and dust sampling system	90
Figure 5. 2	Optical micrographs and EDS showing primary and secondary <i>Mg</i> 2Si for (a, b, c) Base composite, (d, e, f) Bi-containing, and (g, h, i) Ba-containing	93
Figure 5.3	Comparison of size and aspect ratio of primary <i>Mg</i> 2Si for the base composite, Bi and Ba-containing	94
Figure 5.4	Vickers hardness values of base composite as a function of Bi and Ba-containing.	95
Figure 5.5	Variations of UTS and El values as a function of Bi and Ba-containing.	96
Figure 5.6	Fracture surface for (a) base composite (b) Bi-containing and (c) Ba-containing.	97
Figure 5.7	Comparison of (a) fine particle number concentration (b) specific area concentration and (c) mass concentration as function of diameter of particles at cutting speed of 700 m/min and feed rate of 0.2 mm/tooth	99
Figure 5.8	Total fine particle number concentration (b) surface concentration and (c) mass concentration as function of cutting speed for all workpieces at feed rate of 0.2 mm/tooth	102

Figure 5.9	Comparison of (a) ultrafine particle number concentration (b) specific area concentration and (c) mass concentration as function of diameter of particles at cutting speed of 700 m/min and feed rate of 0.2 mm/tooth	105
Figure 5.10	Variation of forces with feed rate at cutting speed of (a) 300 (b) 700 and (c) 1100 m/min	107
Figure 5.11	Total ultrafine particle number concentration (b) surface concentration and (c) mass concentration as function of cutting speed for all workpieces at feed rate of 0.2 mm/tooth.	110
Figure 6.1	The structure of proposed ANFIS model	120
Figure 6.2	Plots of MFs for (a) feed rate, (b) cutting speed and (c) particle size inputs in prediction model of surface roughness	126
Figure 6.3	The surface roughness predicted by ANFIS as function of cutting speed, feed rate and workpiece material: (a) Ba-containing composite (b) Bi-containing composite, (c) Base composite	127
Figure 6.4	Optical microstructure of (a) Base composite, (b) Ba-containing composite, (c) Bi-containing composite.	129
Figure 6.5	Plots of MFs for (a) feed rate, (b) cutting speed and (c) particle size inputs in cutting force prediction model.	133
Figure 6.6	Cutting force predicted by ANFIS in relation to cutting speed, feed rate and workpiece material: (a) Ba-containing composite, (b) Bi-containing composite, (c) Base composite.	134
Figure 6.7	Optical images of chips during machining of the (a) base composite, (b) Ba-containing composite, and (c) Bi-containing composite	136

## LIST OF ABBREVIATION

APS	Aerodynamic particle sizer
ANFIS	Adaptive network-based fuzzy inference system
BUE	Built-up edge
Bi	Bismuth
Ba	Barium
CNC	Computer numerical control
EL	Elongation
EDS	Electronic diffusion spectroscopy
MMC	Metal matrix composite
MF	Membership function
Pb	Lead
RMSE	Root mean square error
SEM	Scanning electron microscopy
SMPS	Scanning mobility particle sizer
Sr	Strontium
Sn	Tin
UTS	Ultimate tensile test

## LIST OF SYMBOLS AND UNITS OF MEASUREMENTS

$V$	Cutting speed (m/min)
$F$	Feed rate (mm/tooth)
$D$	Depth of cut (mm)
$F_c$	Cutting force (N)
$P_s$	Particle size ( $\mu\text{m}$ )
$R_a$	Arithmetic Surface roughness ( $\mu\text{m}$ )
$a, a_i, b, c, c_i, a_1, a_2, c_1, c_2$	Premise parameters
$P, q, r, s$	Consequent parameters value

## INTRODUCTION

Particulate-reinforced aluminum and magnesium metal matrix composites (MMCs) are extensively used in various commercial applications owing to their high wear resistance, low thermal expansion coefficient and low melting point. These advantages increase their potential for use in the automobile industry in parts such as cylinder blocks, cylinder heads, and discs (Nur *et al.*, 2013). A hypereutectic Al-Si alloy with high Mg content is an in-situ aluminum matrix composite containing a large number of hard particles of Mg<sub>2</sub>Si. Al-based alloy reinforced with a particulate Mg<sub>2</sub>Si phase presents attractive advantages such as weight reduction due to the low density of particulate Mg<sub>2</sub>Si and a low-cost process (Hadian *et al.*, 2009). These improved properties also make the material suitable as a replacement for Al-Si cast alloy in the automobile industry.

Although Mg<sub>2</sub>Si intermetallic particles exhibit certain advantages, their coarse morphology, in the Al matrix, is believed to be at the root of the low ductility observed in these materials (Hengcheng *et al.*, 2003). Melt treatment with the addition of inoculation agents is used to produce a very fine matrix structure as well as the morphology of the Mg<sub>2</sub>Si structure. It is also suitable for general engineering applications due to low production cost (Guo *et al.*, 2008). Lithium (Li) (Hadian *et al.*, 2008), strontium (Sr) (Yang *et al.*, 2009) and bismuth (Bi) (Guo *et al.*, 2008) have been used as reinforcement materials. The melt treatment of composite leads to a change in the morphology of coarse primary Mg<sub>2</sub>Si and improves its mechanical properties.

For instance, Figure 0.1 shows the optical microstructures for machining Al-Si alloys. Figure 0.1a presents, the eutectic Si in the base alloy with large flake-like morphology embedded in

the Al matrix. Figure 0.1b illustrates the eutectic Si morphology after the addition of Bi where the large plate-like Si changes into lamellar or refined shapes. Moreover, the addition of Sb also exhibits a similar effect to Bi addition, as seen in Figure 0.1c. It was observed that the addition of Bi or Sb has a profound influence on the microstructures of the cast alloys. Therefore, it can be deduced that the changes in topography and surface roughness are associated with the morphology changes of the silicon hard phase in the aluminum soft matrix.

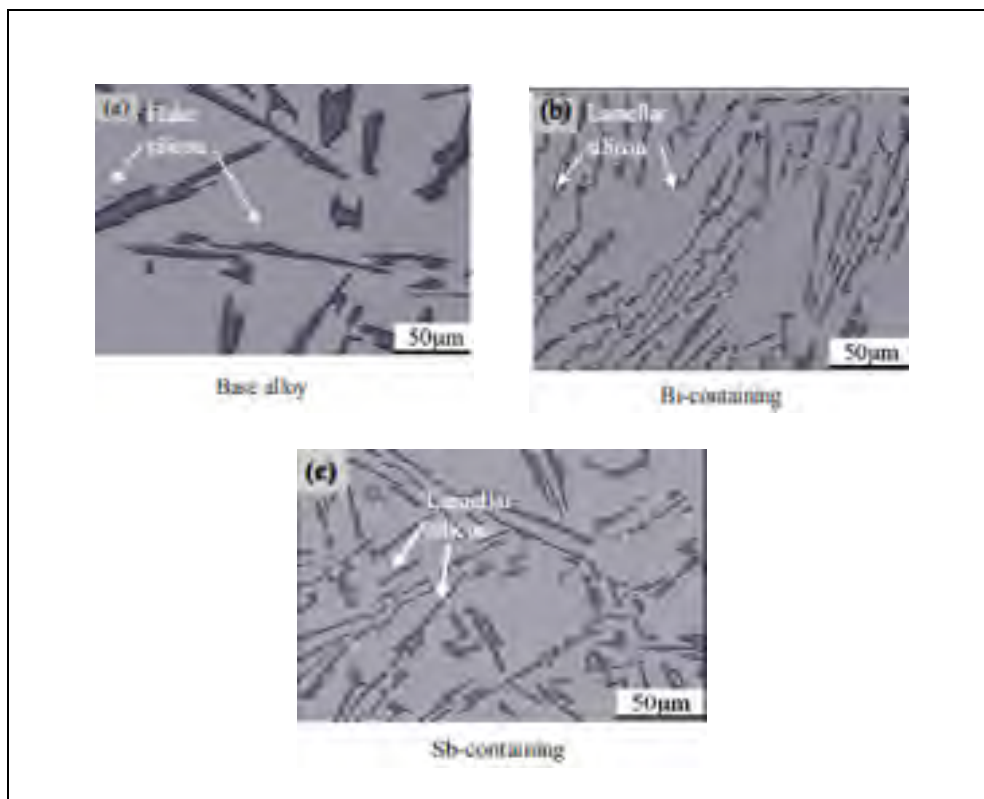


Figure 0. 1      Optical microstructures of machined surface for (a) base alloy, (b) Bi-containing, and (c) Sb-containing (Barzani *et al.*, 2013).

Some studies have indicated that the machining of metal matrix composites leads to excessive tool wear and possible sub-surface damage, thereby resulting in increased machining cost and production time. Modifying the melt treatment also has a direct effect on machinability indicators such as cutting forces, surface roughness and chip morphology. It has been reported that the addition of refiner elements can be used to improve the machinability of alloys and composites (Nur *et al.*, 2013). Barzani *et al.* (2015) reported that machinability of metal matrix composite depends on the type of material, microstructure, and machining conditions. Yang *et al.* (2006) found an improvement of wear resistance after the addition of Sb and Sr to A357 cast alloy. Barzani, *et al.* (2015) also reported that Bismuth is considered to be a free-machining element for aluminum alloys. In this study, Bi and barium (Ba) were used as refine elements.

In spite of the multiple advantages of machining, it is considered hazardous for operators and for the environment. In fact, most machining processes generate aerosols in liquid or solid form. It has been concluded that a major concern in the metal cutting industry is the health hazard associated with using cutting fluids in wet machining (Arumugam *et al.*, 2003). Long-term exposure to cutting fluids can lead to increased cancer risk. Dry machining, where no mist is generated and metal chips are not contaminated by cutting fluids, is known as an alternative for wet machining (Arumugam *et al.*, 2003).

Recently, a lot of research work has been carried out to reduce the experimental work. Soft computing tools are widely used to model and control machining processes. An adaptive network-based fuzzy inference system (ANFIS) is an artificial intelligence method in which the neural networks are utilized to elaborate the fuzzy rules for the fuzzy inference approach (Zeinali et Mazlan, 2013). The membership function (MF) is an important portion of the

ANFIS method that must be correctly defined in order to achieve an accurate relationship between inputs and outputs ( Pourtousi *et al.*, 2015).

Dong et Wang (2011) proposed a method for modeling surface roughness with ANFIS in the milling process. Ho *et al.* (2009) reported a surface reconstruction model based on a methodology developed for predicting machinability in a milling process. Ekici *et al.* (2009) investigated an ANFIS model for Wire-EDM. They found that the ANFIS model developed the prediction of the white layer thickness and surface roughness achieved as a function of the process parameters and improved machining performances. They reported that ANFIS introduced technological knowledge base on the selection of machining parameters in order to have high productivity and satisfactory surface quality. In fact, this technique is used to reduce the cost and repetition of the experiment.

Although, some studies have been carried out on the microstructure and machinability of alloys and composites, there is still a lack of knowledge about the effect of modifiers on the mechanical properties and machinability of Al-20Mg<sub>2</sub>Si-Cu metal matrix composite. In addition, systematic studies on the effect of machining parameters and reinforcements on particle emissions for this type of composite are not available. Therefore, the aim of this study is to evaluate and predict the influence of reinforcements on the mechanical properties and machinability of Al-20Mg<sub>2</sub>Si-Cu metal matrix composite containing Bi and Br.

## CHAPTER 1

### PROBLEM STATEMENTS, OBJECTIVES AND THESIS OUTLINE

#### 1.1. Problem statements

The high performance of Al-Mg-Si composite containing an  $Mg_2Si$  reinforcing phase has led to the material becoming an attractive candidate to manufacture most industrial products, especially automotive and aerospace components. However, the Al- $Mg_2Si$ -Cu metal matrix composite contains coarse dendritic primary  $Mg_2Si$  particles that can have adverse effects on its mechanical properties. These particles need to be modified to ensure that the desired mechanical properties are obtained.

In terms of machinability, composites are difficult to machine due to the high abrasiveness of reinforcement constituents. This results in damage being introduced into the workpieces and rapid wear of the cutting tool. Therefore, there is a need to optimize the machining process based on certain output variables, such as cutting forces, surface finish and chip morphology. In addition, machining processes produce liquid and solid aerosols that can be harmful to the operator and the environment. The protection of operators and the environment has become another machining performance variable to consider. Thus, there is a need to control dust emission during the machining process in order to protect the operator's health and the industrial environment.

There is also insufficient knowledge about the prediction of machining Al- $Mg_2Si$ -Cu metal matrix composite, which is a vital factor to improve machinability of the composite. Hence, an ANFIS model was used to accurately predict the machinability of this type of composite.

Al-20Mg<sub>2</sub>Si-Cu metal matrix composite has recently caught the attention of materials engineering researchers, but no past studies were found in the literature that extensively addresses the evaluation of reinforcement and cutting conditions on the machinability characteristics and particle emissions of Al-20Mg<sub>2</sub>Si-Cu metal matrix composite. Therefore, the aim of this study is to evaluate the influence of reinforcements on microstructure and machinability (including particle emissions) of Al-20Mg<sub>2</sub>Si-Cu metal matrix composite.

## **1.2. Thesis objectives**

- To investigate the effect of reinforcements on the microstructure and mechanical properties of Al-20Mg<sub>2</sub>Si-Cu metal matrix composite.
- To determine the influence of reinforcements on the machinability of Al-20Mg<sub>2</sub>Si-Cu metal matrix composite containing modifier element.
- To evaluate feasibility of predicting surface roughness and cutting force when machining Al-20Mg<sub>2</sub>Si-Cu metal matrix composite containing additives.

## **1.3. Thesis outline**

The thesis content is presented in six chapters as a thesis by publication. The first chapter provides problem statements and objectives that defend the scope of this research. Chapter 2 reviews related previously published research and ends with a summary. Experimental procedure details are presented in Chapter 3. That chapter explains the methodology of the experiments, including the name of the equipment and different steps of the experiment.

Chapter 4 presents the first article, published in *Measurement* (Marani *et al.*, 2017). In that article, the machinability characteristics and mechanical properties of Al-20Mg<sub>2</sub>Si-Cu metal matrix composite with Bi were investigated. From the investigation, it was concluded that the structure of the primary Mg<sub>2</sub>Si reinforcement particle changed from coarse to fine polygonal type. In addition, the addition of Bi improved ultimate tensile strength (UTS) and elongation (El%). Machining tests were carried out with various cutting conditions and feed rates. The results showed that the surface roughness and cutting force improved with the addition of Bi due to a change in Mg<sub>2</sub>Si particle size with a less built-up edge.

Chapter 5 presents the second article, published in *Advanced Manufacturing Technology* (Marani *et al.*, 2018). In this chapter, a specific focus is put on microstructure, mechanical properties and dust emission when milling Al-20Mg<sub>2</sub>Si-Cu metal matrix composite. In addition, the effect of modifier elements such as Bi and Ba on mechanical properties and dust emission was investigated. Experiments were carried out using dry CNC milling by uncoated carbide tools. An aerodynamic particle sizer (APS) and a scanning mobility particle sizer (SMPS) were used to measure microparticle and ultrafine particle emissions, respectively. The results show that ultrafine particle number concentration, specific area concentration, and mass concentration decreased with the addition of modifiers. It was also confirmed that cutting conditions and the microstructure of workpieces have a direct effect on dust emission during the milling process.

Finally, Chapter 6 presents the third article, submitted to *Neural Computing and Applications*. In this research work, an adaptive network-based fuzzy inference system (ANFIS) predictive model for surface roughness and cutting force was investigated while machining Al-20 Mg<sub>2</sub>Si-Cu metal matrix composite. In fact, various ANFIS structures were

constructed to evaluate the effects of feed rate, cutting speed and particle size on the machinability of the composite. Two ANFIS models were selected as the most precise models to predict surface roughness and cutting force when machining the composite. The thesis conclusion drawn from the current research work and recommendations for future work are provided at the end of this thesis.

## **CHAPTER 2**

### **LITERATURE REVIEW**

#### **2.1. Metal matrix composite**

Recently, aluminum metal matrix composites have found widespread engineering applications. They are being considered as a replacement material for the conventional alloys used in many engineering industries. Their properties such as excellent castability, good wear resistance, excellent mechanical properties and low production cost are more attractive to meet future application demands especially for lightweight components (Razaghian *et al.*, 2012). With the expansion of modern industry, lightweight materials are receiving consideration due to their technological applications. Figure 2.1 shows the most important application of metal matrix composites such as cylinder head, engine block and transmission housing in the automobile industry.

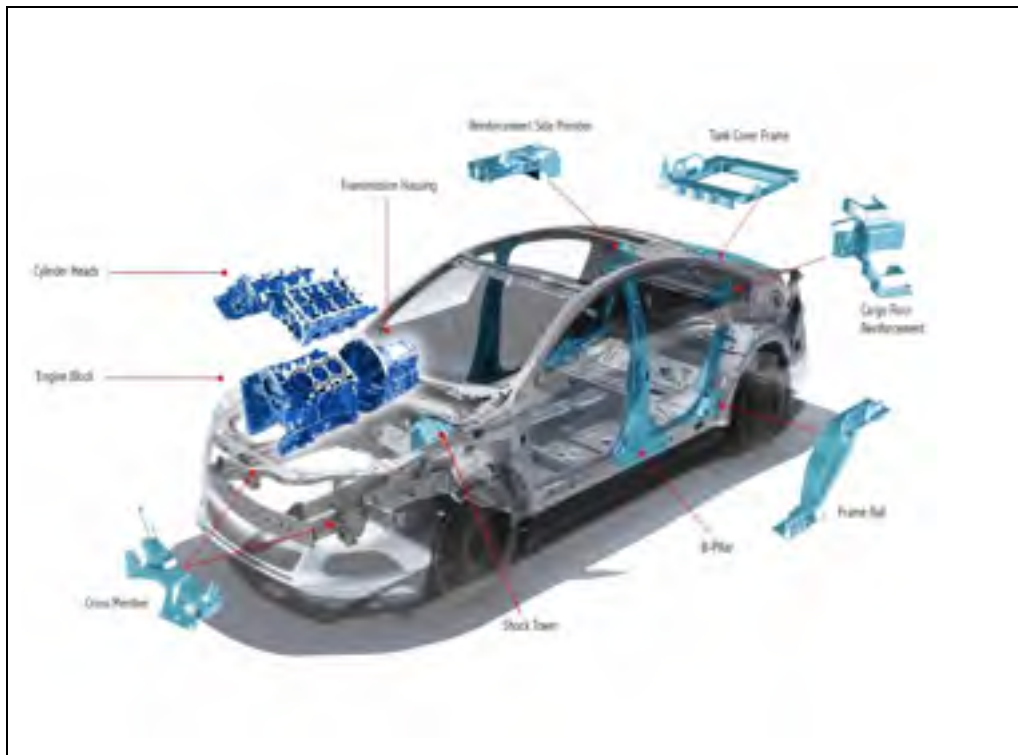


Figure 2.1 Application of metal matrix composite (Fadavi *et al.*, 2015).

Al-based alloy reinforced with particulate  $Mg_2Si$  particles has been introduced as a new group of particulate metal matrix composites (PMMCs) that offer attractive advantages such as weight reduction due to the low density of particulate  $Mg_2Si$  and better mechanical properties (Hadian *et al.*, 2009). These advantages make them suitable to replace Al-Si cast alloy (Hadian *et al.*, 2008).

## 2.2. Reinforcing material

Most composite materials are formed from two or more materials. In fact, one of the constituent materials acts as the matrix, and the other constituent materials act as the

reinforcement in the composite. The role of the matrix material is to protect the reinforcement materials and distribute stress to the other reinforcements, while the main role of reinforcement materials is to increase the mechanical properties of the composite (Farahany *et al.*, 2014). Some materials such as alumina and silicon are added to composite materials as reinforcements. Most reinforcements are brittle, and material separation is accomplished by brittle fracture rather than plastic deformation ahead of the tool (Koch *et al.*, 2008).

It has been found that composite materials are difficult to machine. In fact, cutting tool wear rates are experienced during the machining process (Andrewes *et al.*, 2000). Bismuth (Bi), antimony (Sb), and strontium (Sr) have been found to be free cutting elements (Barzani *et al.*, 2008). Figure 2.2 shows the microstructure of Al-Si alloy. As can be seen in Figure 2.2a, coarse plate-like Si formations are observed in a matrix of aluminum for the base alloy.

It is considered harmful for elongation due to the shape of the silicon in the matrix. Therefore, it is modified by the addition of a certain amount of Bi (Figure 2.2b). In fact, silicon morphology changed from a plate-like formation to a lamellar structure with Bi. It is also observed that the addition of Sb had a similar effect as Bi (Figure 2.2c). The addition of Sr changed the silicon morphology from plate-like to fine fibrous form (Figure 2.2d). Therefore, it can be concluded that changes in topography are related to a change in morphology of the silicon in the aluminum soft matrix (Barzani *et al.*, 2015).



Figure 2.2 Optical microstructures for (a) base alloy, (b) bi-containing composite, (c) sb-containing composite, and (d) Sr-containing composite (Barzani *et al.*, 2015).

### 2.3. Effect of reinforcements on microstructure

Numerous efforts have been carried out to discover the relationship between the microstructure and deformation behavior in the new group of particulate metal matrix composites (PMMCs). It has been reported that the mechanical properties of PMMCs significantly affected by their microstructure, such as particle aspect ratio, particle size, volume fraction and Young's modulus of the particle (Emamy *et al.*, 2013).

Refinement and modification of Mg<sub>2</sub>Si can be achieved by different techniques such as adding modifiers, rapid solidification, and spray forming. However, chemical modification by adding modifiers has been used in the casting process due to its effectiveness and simplicity in comparison with other methods. Emamy *et al.*, (2013) paid attention to the

effect of Cu addition on the microstructure and hardness of Al-15Mg<sub>2</sub>Si-15Li. They reported that the addition of more than 1% Cu has a marginal effect on the primary and secondary Mg<sub>2</sub>Si particles. It was also found that the addition of more than 3% Cu content leads to the fracture behaviour changing from ductile to brittle.

Farahany *et al.* (2016) studied the effect of strontium addition on the microstructure and impact toughness of Al-Mg<sub>2</sub>Si metal matrix composite. The results show that the impact toughness of the composite increased from 0.8 J to 1.4 J when 0.01 wt.% Sr was introduced into the melt. Figure 2.3 shows the microstructure of primary Mg<sub>2</sub>Si (a) without and (b) with the addition of Sr. As it can be seen, the addition of 0.01 wt.% Sr causes the average size and aspect ratio to decrease by decreasing the size of the Mg<sub>2</sub>Si particles in the microstructure.

It has been reported that the addition of 0.155Li to Al-15 Mg<sub>2</sub>Si (MMC) decreases the size of the primary Mg<sub>2</sub>Si particles from 32 μm to 4 μm. It was also concluded that Li changes the morphology of primary Mg<sub>2</sub>Si from plate-like to coral-like which can create a good distribution of primary Mg<sub>2</sub>Si in the microstructure (Emamy *et al.*, 2013)

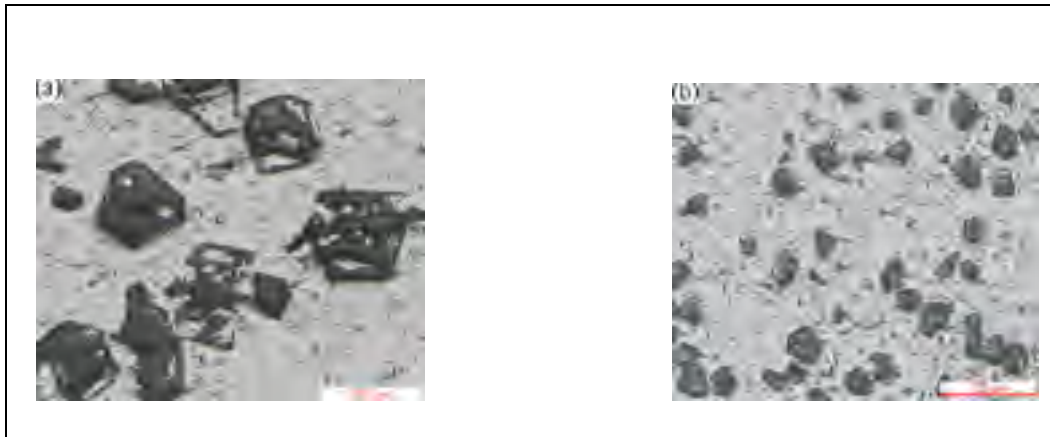


Figure 2.3 Optical micrographs showing the microstructure of primary  $Mg_2Si$  (a) without and (b) with addition of Sr (Farahany *et al.*, 2016)

Azarbarmas *et al.* (2011) studied the effect of boron additions on the microstructure and mechanical properties of Al-15%  $Mg_2Si$  composite. They found that ultimate tensile strength (UTS) and elongation values increased with the addition of 0.3% boron. The addition of boron decreased the hardness values of the composite.

Bahrami *et al.* (2012) studied the effect of Zr on the microstructure of hot-extruded Al- $Mg_2Si$  composite. They reported that adding Zr has no significant effect on the morphology of the primary  $Mg_2Si$  particle. However, the morphology of the  $Mg_2Si$  phase changed from an irregular to a more spherical shape by the hot-extrusion process. The results showed that the average size of  $Mg_2Si$  particles decreased with the addition of 0.1% Zr in hot-extrusion conditions. In addition, UTS and elongation values increased with the addition of more than 1wt% Zr. The fracture surface also showed a transition from brittle fracture to ductile fracture due to changes in the size and morphology of the intermetallic  $Mg_2Si$  content.

Emamy *et al.* (2013) investigated the effect of Fe-rich intermetallic on the microstructure and mechanical properties of Al-15Mg<sub>2</sub>Si die-cast composite. It was concluded that the morphology of primary Mg<sub>2</sub>Si particles changed from an irregular to a polyhedral shape with the addition of 2 wt.% Fe. The small amount of certain Fe also improved hardness, UTS and elongation with a slight reduction in ductility. Emamy *et al.* (2011) studied the microstructure, hardness and tensile properties of Al-15Mg<sub>2</sub>Si composite with yttrium (Y) addition. They found that the addition of Y did not change the size or morphology of primary Mg<sub>2</sub>Si particles, but the eutectic Mg<sub>2</sub>Si was changed from a flake-like to a fine fibrous shape. It was found that the addition of Y increased UTS, hardness and elongation values.

Nami *et al.* (2011) studied the microstructure and mechanical properties of friction stir welded Al-15Mg<sub>2</sub>Si cast composite. They found that the hardness value increased in the stir zone due to the homogeneous distribution of Mg<sub>2</sub>Si needle particles. The addition of extra Si up to 2 wt.% reduced the average Mg<sub>2</sub>Si particle size and increased the volume fraction of the Al phase. In addition, extra Si improved the UTS and elongation values of the composite. Using more than 7% silicon decreased the size of dimples and increased elongation values while changing the mode of fracture from brittle to ductile.

Nasiri *et al.*, (2012) investigated the effects of phosphorous addition and heat treatment when casting Al-15Mg<sub>2</sub>Si composite. It was concluded that adding phosphorous changed the primary of Mg<sub>2</sub>Si particle from dendritic to a regular shape and reduced Mg<sub>2</sub>Si particle size. The result also showed that both solution heat and phosphorous addition improved UTS and elongation values.

Li *et al.* (2013) studied the effect of rare earth addition on the microstructure and mechanical properties of Al-20%Si alloy. They reported that primary silicon refined from a coarse star-

like shape to a fine blocky shape with the addition of 0.5% Er. The UTS and elongation values were significantly improved with the addition of 0.5% Er due to the refinement and modification of primary and eutectic Si crystals.

Li *et al.* (2013) investigated the effect of in situ  $\gamma\text{-Al}_2\text{O}_3$  particle on the microstructure of Al-20%Si alloy. They reported that primary Si refined from a plate-like to a fine blocky shape. The eutectic silicon structure changed from a coarse acicular structure to a fine flake-like one. In addition, increasing  $\gamma\text{-Al}_2\text{O}_3$  particle to 0.8% reduced the size of primary silicon and improved the mechanical properties of the composite.

#### **2.4. Machinability of aluminum metal matrix composite (MMC)**

Some research work based on the machinability of aluminum alloys and aluminum metal matrix composite have been reported. Gallab *et al.* (2004) studied the machinability of Al-20%Si using polycrystalline diamond tools. They reported that surface roughness improves with decrease feed rate but slightly deteriorates with an increase in depth of cut. It was found that machining this type of composite is most economical and safe at a speed of 894 m/min and feed rates as high as 0.45 mm/ rev.

Manna et Bhattachary (2002) investigated the machinability of Al-Si alloy. The results showed that the value of surface roughness (Ra) increased by 40% when cutting speed was tripled from 60 to 180 m/min. They also found that cutting speed and feed rate had equal influence on the surface finish when both are increased simultaneously.

Figure 2.4 shows two different behaviours of built-up edge (BUE) formation after turning of Al-Si alloy (base alloy) and strontium-containing workpieces. It can be observed that BUE

widely covered the flank face of the tool when machining strontium-containing alloy and changed the tool geometry. The highest and the lowest cutting force values were obtained for strontium and bismuth-containing alloys, respectively (Barzani *et al.*, 2013).

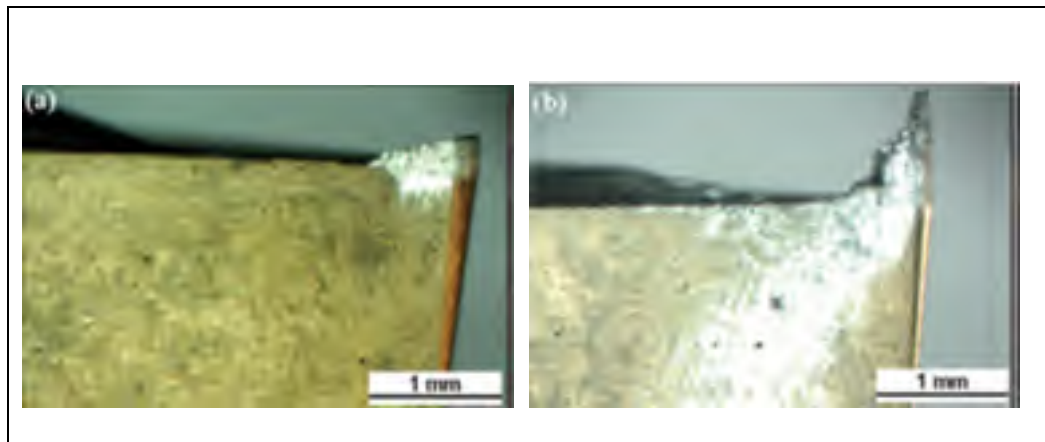


Figure 2.4 Built-up edge formation in (a) base alloy and (b) Sr-containing workpieces (Barzani *et al.*, 2013).

Basavakumar *et al.* (2007) investigated the influence of melt treatments (grain refinement and modification) and different inserts (un-coated, PVD, and polished CVD diamond coated) on cutting force and surface integrity when turning Al-12Si and Al-12Si-3Cu cast alloys in dry conditions. They found that the combined addition of a grain refiner and a modifier (Al-1Ti-3B-Sr) to the Al-12Si-3Cu cast alloy lowered the cutting forces and improved the surface finish in contrast to untreated alloys. It was also found that the performance of the polished CVD diamond-coated insert resulted in lower cutting forces and less surface roughness.

Arumugam *et al.*, (2006) studied CVD diamond-coated and -uncoated carbide tool performance in machining. Results have shown that the main advantages were the possibilities of using multiple edges per tool insert and advanced chip breaker technology. Compared to an uncoated carbide tool, the CVD diamond-coated insert exhibited much more

abrasive wear resistance, less built-up edge and a lower cutting force, resulting in a much-improved surface finish.

Ozben *et al.* (2008) analyzed tool wear and surface roughness in the machining of homogenized SiC reinforced aluminum metal matrix composite. Two types of K10 cutting tools (uncoated and TiN-coated) were used at different cutting speeds (50, 100 and 150 m/min), feed rates (0.1, 0.2 and 0.3 mm/rev) and depths of cut (0.5, 1 and 1.5 mm). The cutting speed and feed rate influenced the surface roughness values. In fact, higher cutting speeds and lower feed rates produced better surface quality.

Noordin *et al.* (2001) investigated cutting forces when turning automotive AISI 1010 steel. A coated tungsten-based cemented carbide insert and an uncoated titanium-based cemented carbide insert were tested. The results showed that tangential force increased when the cutting speed was increased from low to medium. For the uncoated insert, the tangential force remained constant when the cutting speed was increased from low to medium and decreased when the cutting speed was at maximum.

Gallab *et al.* (2004) studied the machining of Al-SiC particulate metal-matrix composites using a series of dry high-speed turning tests to select the optimum tool material, tool geometry and cutting parameters for turning Al-20%Si metal-matrix composites. The results indicated that polycrystalline diamond tools (PCD) provide satisfactory tool life compared to alumina and coated-carbide tools. Furthermore, the cost of PCD tools could be justified by using dry cutting at feed rates as high as 0.45 mm/rev, cutting speeds of 894 m/min and a depth of cut of 1.5 mm. PCD tools sustained the least tool wear compared to TiN-coated

carbide tools due to PCD's superior hardness and wear resistance, as well as a low coefficient of friction, together with high thermal conductivity.

## **2.5. Effect of reinforcements on machinability**

It has been found that some low melting point elements such as lead (Pb), Bi and indium (In) minimize the chip size when machining aluminum alloys. In fact, these elements have limited solubility in the aluminum solid solution. They are able to support chip breakage and lubricate the tool. From the chip breaking alloying elements, it is concluded that the elements are insoluble in solid aluminum and have a lower melting point compared to aluminum alloys (Koch *et al.*, 2008).

Koch et Antrekowitsch (2008) studied free cutting aluminum alloys with tin as a substitution for lead. They reported that the inclusion of tin distributed mainly at the grain boundaries together with other phases improved the machinability of aluminum alloys. It was found that the strength of alloy can especially be increased by the addition of Cu and Mg. In addition,  $\text{Cu} \geq 2.7\%$  and  $\text{Mg} < 0.5\%$  are suggested for good machinability.

Barzani *et al.* (2013) investigated the machinability of Al-Si cast alloy containing bismuth and antimony. They found that the addition of bismuth improved alloy machinability due to the fact that Bi particles act as a lubricant during the machining process. Chips were longer when machining the base alloy compared to the Bi-containing alloy and increased the value of cutting force by a massive amount of build-up edge (BUE).

Figure 2.5 shows an image of a machined sub-surface for Al-11%Si alloy and Sb-containing alloy, respectively. As can be seen in Figure 2.5a, there is a smooth machined surface for the

base alloy while a torn surface is shown for the Sb-containing alloy, which increased surface roughness values during the machining process. Surface roughness also decreased by increasing cutting speeds from 70 to 250 m/min (Barzani *et al.*, 2013).

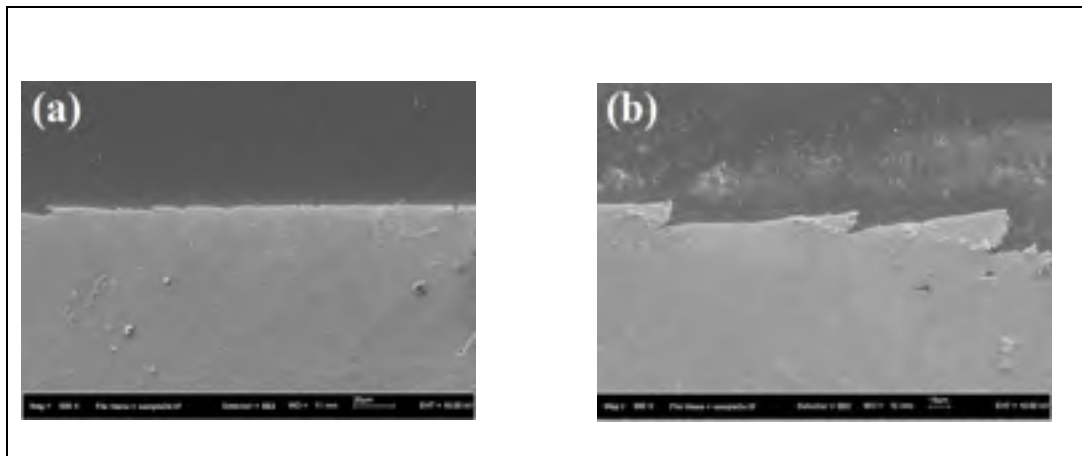


Figure 2.5 Micrograph of machined subsurface of (a) untreated Al-11%Si and (b) Sb-treated workpiece at cutting speeds 70 m/min (Barzani *et al.*, 2013).

Elgallad *et al.* (2010) studied machinability aspects of new Al-Cu alloys intended for automotive applications. It was observed that the addition of Sn and Bi decreased total drilling force compared to the base alloy. Chip fragility also increased with the addition of Bi. Zedan (2010) investigated the effect of Fe intermetallic on the machinability of heat treated Al-Si alloy. It was found that the tool life for 396 alloy decreased by 50% compared with 396-M containing Fe intermetallic. Increasing the Fe content from 0.5% to 1% produced a distinct improvement in terms of tool life and cutting force.

## 2.6. Machinability criteria

### 2.6.1. Introduction

The machining process is known as one of the most used techniques for producing different components. Milling is a process of producing flat and complex shapes with the use of a multi-tooth cutting tool. Planar surfaces, two-dimensional surfaces and three-dimensional surfaces are known as three major groups of geometric forms that are created by the milling process. As it can be seen in Figure 2.6, in face milling, machining is performed by a tooth on both the end and the periphery of the face milling cutter. A high production rate is known as an important advantage of face milling due to the large cutter diameter in this process.

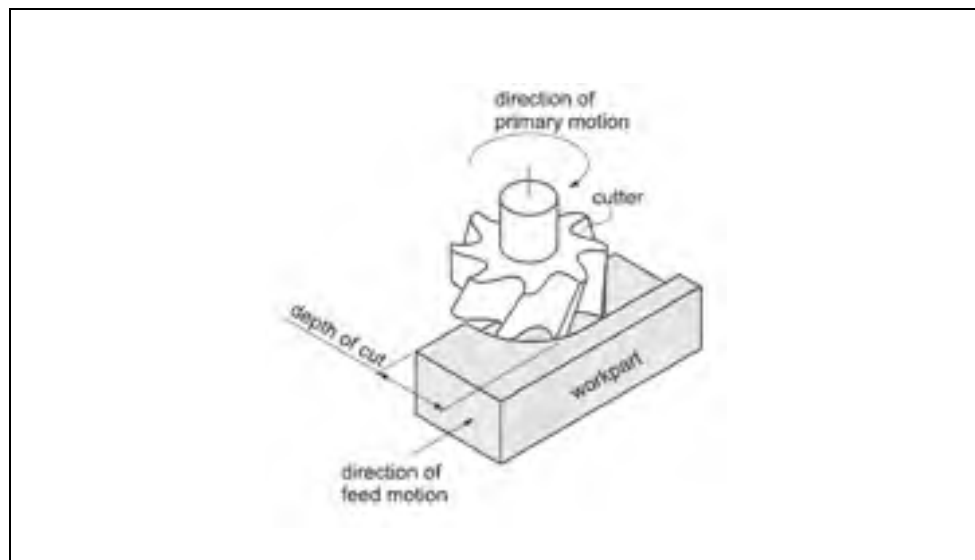


Figure 2.6 The face milling cutter machine (Shaw et al., 2005)

### **2.6.2. Cutting tool material**

A large variety of cutting tool materials have been developed to cater to various programmers such as those found in the aerospace industry (Shaw, 2005). Some important characteristics expected in cutting tool materials are:

- Hardness greater than that of the workpiece material.
- Hot hardness where the tool should be able to retain hardness at an elevated temperature.
- Wear resistance with high abrasion resistance to improve the effective life of the tool.
- Toughness to withstand the impact loads at the beginning of the cut and force fluctuation due to imperfections in the workpiece material.
- Thermal characteristics where the tool material should have higher thermal conductivity to dissipate heat quickly.

These characteristics will ensure better cutting performance. The continuous development of the cutting tool will help to achieve these characteristics (Figure 2.7).

The various cutting tool materials commercially available today have the ability to satisfy the requirements for cutting tool properties such as high hot hardness, toughness, and chemical stability. Several cutting tool materials have been developed for different applications and have different properties for these applications (Shaw, 2005)

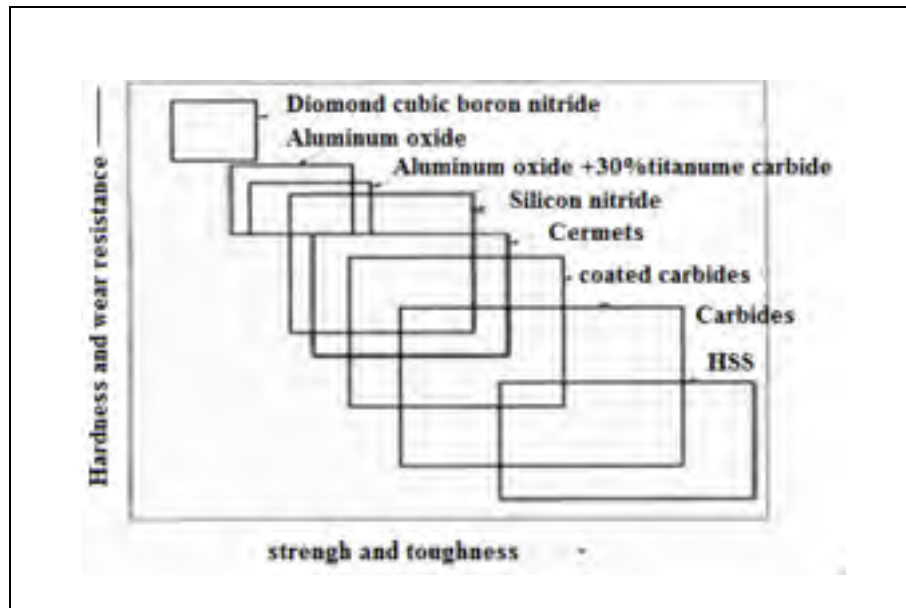


Figure 2.7 Common properties of cutting tool materials (Galoppi *et al.*, 2006).

Machinability may be seen as an interactive phenomenon between the work piece (material type and form), the cutting tool (material type and geometry), and the cutting medium such as air and liquid, in a number of different removal sequences, which include turning, milling, sawing, and cutting conditions. In a collective sense, the indicators of machinability are: (i) specific power consumed, cutting forces, and temperature increase; (ii) tool life, wear, and fracture probability; (iii) chip control including chip breakability, chip shape, and built-up edge; (iv) dimensional tolerances in terms of surface roughness and microstructure; and (v) machining rate. All effort-related parameters are relatively more difficult to evaluate, but can often provide an explanation for good or bad machinability results ( Davim, 2010).

It has been noticed that the machining parameters are strongly linked to the material parameters when optimizing the material with regards to machinability. Material parameters have an individual contribution to machinability and are cross-correlated with each other. For

instance, one type of cutting tool can exhibit a correlation with one type of silicon morphology, while another type of cutting tool could behave in a different way. Therefore, it is necessary to identify the optimal process parameters for certain materials.

### **2.6.3. Cutting force**

Cutting force is one of the few quantitative responses that can be measured during the machining operation, and it can be used as a basis for further analysis. Cutting forces in milling can be measured in several ways. The most common method is by a fixed force plate dynamometer on which the workpiece is placed. This enables the measurement of the three cutting force components in a fixed coordinate system relative to the table. However, this method has its limitations, with respect to the size of the part that can be clamped. Also, the recorded cutting forces could vary during the machining experiments, since the dynamometer will be affected by the changing of the workpieces. Figure 2.8 shows the measured cutting force component.

The geometrical resolution of the total cutting force is usually done by assuming that the chip is a solid body in a stable mechanical equilibrium under the action of the forces exerted on it at the rake face and at the shear plane as suggested by Merchant on the basis of the following assumptions (Shaw, 2005) : (i) the chip is continuous with no built-up edge; (ii) the tool tip is perfectly sharp, which leads to absolutely no contact between the machined surface and the flank of the tool; (iii) the shear plane is perfectly planar, and shearing occurs along it as the tool tip pushes into the material, extending from the tool tip to the chip root; (iv) the depth of cut is assumed to be very large with respect to the feed of cut, thus reducing the problem to

one of plane strain; and (v) shear stress, strain and strain rates are all assumed to be uniform. The relationship between the various forces determined using these force diagrams (Figure 2.9) is as follows (Shaw, 2005):

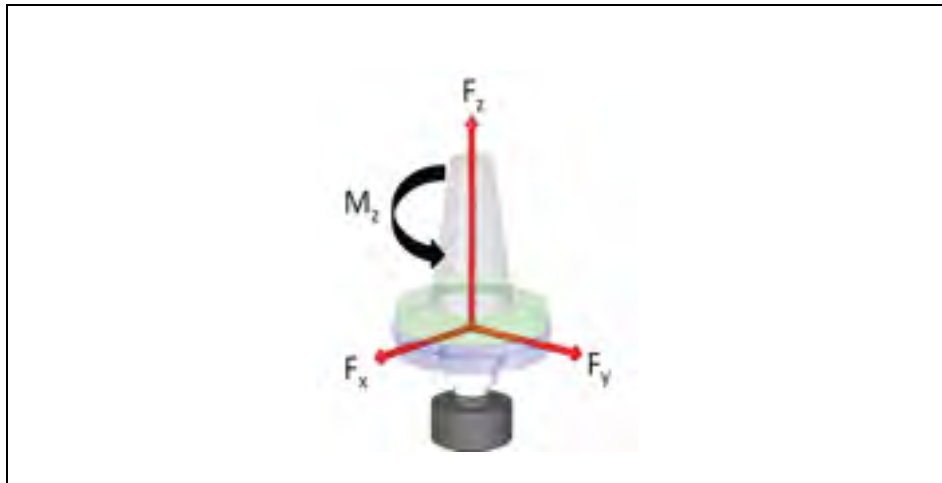


Figure 2.8 Measured cutting force component (Galoppi *et al.*, 2006)

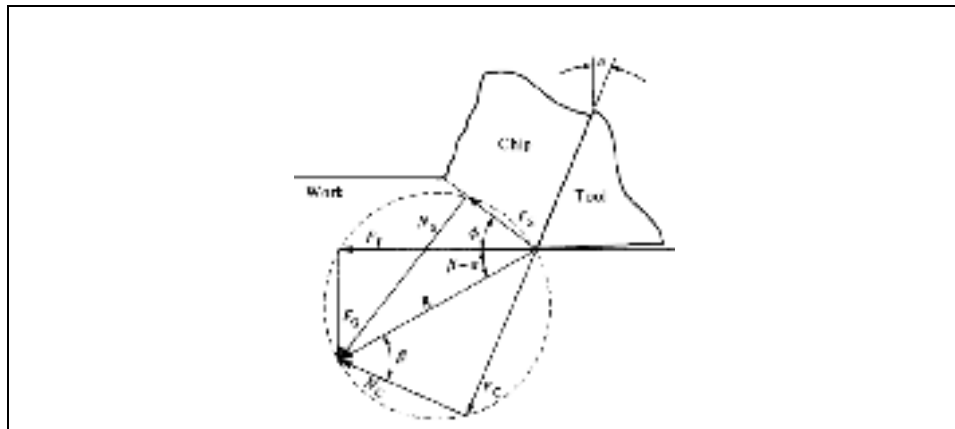


Figure 2.9 Composite cutting force circle (Shaw, 2005).

$$F_S = F_p \cos \phi - F_Q \sin \phi \quad (2.1)$$

$$N_S = F_Q \cos \phi + F_p \sin \phi = F_S \tan (\phi + \beta - \alpha) \quad (2.2)$$

$$F_C = F_p \sin \alpha + F_Q \cos \alpha \quad (2.3)$$

$$N_C = F_p \cos \alpha - F_Q \sin \alpha \quad (2.4)$$

Where  $F_S$  is the shear force on the shear plane,  $F_p$  is the cutting force,  $F_Q$  is the thrust force,  $N_S$  is the normal force on the shear plane,  $F_C$  is the shear force on the rake face,  $N_C$  is the normal force on the rake face,  $\phi$  is the shear angle,  $\alpha$  is the true rake angle of the cutting tool and  $\beta$  is the friction angle.

The coefficient of friction ( $\mu$ ) at the tool face can be computed as (Shaw, 2005):

$$\mu = \frac{F_C}{N_C} = \frac{F_p \sin \alpha + F_Q \cos \alpha}{F_p \cos \alpha - F_Q \sin \alpha} = \frac{F_Q + F_p \tan \alpha}{F_p - F_Q \tan \alpha} \quad (2.5)$$

#### 2.6.4. Surface roughness

Surface integrity in the engineering sense can be defined as a set of properties of an engineering surface that affect the performance of the surface in service. These properties primarily include surface finish, texture and profile, fatigue corrosion and wear resistance, and adhesion and diffusion properties. In addition, numerous investigations confirm that the quality and especially the lifetime of dynamically loaded parts are very much dependent on the properties of the surface material (Basavakumar *et al.*, 2007). Severe failures produced by fatigue, creep and stress corrosion cracking invariably start at the surface of components, and their origins depend to a great extent on the quality of the surface. Therefore, when machining any component, it is first necessary to satisfy the surface integrity requirements.

Surface integrity refers to residual stress analysis, microhardness measurements, surface roughness and the degree of work hardening in the machined sub-surfaces, which are used as criteria to obtain optimum machining conditions that ensure machined surfaces with high integrity (Grum et Kisin, 2006). Surface integrity is built up by the geometrical values of the surface, such as surface roughness, and the physical properties, such as residual stresses, hardness and structure of the surface layers (Davim, 2010).

In fact, the surface quality of a machined surface is one of the most important concerns in a machining operation. Surface roughness measurements and optically observed features on the finished surface give important information about the quality of the surface produced and therefore the machinability of the given alloy under the conditions used for the process. The surface roughness value in machining depends on cutting conditions, tool geometry and chip formation.

It has been found that average arithmetic surface roughness (Ra) and the average distance between highest and lowest points per sampling length (Rz) are commonly used. It is also concluded that Ra can be calculated with the feed rate (F) and nose radius (R) of the cutting insert.

$$Ra = \frac{F^2}{32.R} \quad (2.6)$$

Equation 2.7 is used to calculate the actual Ra values of a casting metal. The data are collected using an optical profilometer with a fixture.

$$Ra = \frac{1}{n} \sum_{i=1}^n y_i \quad (2.7)$$

Where  $n$  is the number of data points collected,  $y_i$  is the height of the  $i$ th measure data point (Peach, 2009). Figure 2.10 shows the surface roughness graph (Ra) at (a) the lowest cutting speed (70 m/min) and (b) the highest cutting speed (130 m/min) when machining Al-Si alloy (Barzani *et al.* 2015).

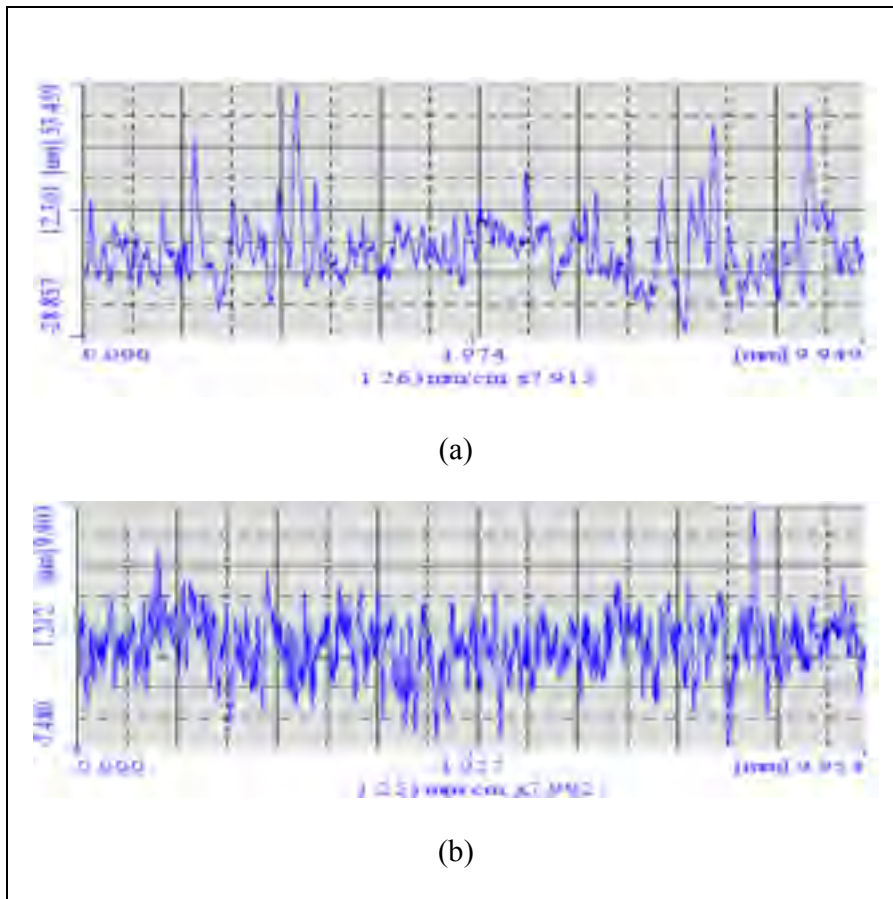


Figure 2.10 Surface roughness graph (Barzani *et al.*, 2015)

### 2.6.5. Chip formation

It has been found that three major chip formation phenomena are produced during the machining process, and the ductility of the material plays an important role to produce the different shaped

chips. They are called discontinuous, continuous and continuous with a built-up edge (BUE). Figure 2.11 illustrates the chip formation mechanisms studied by Peach (2009). The brittle and ductile microstructure caused the chip formation characteristics to show different mechanisms. It should also be considered that machining parameters have an important effect on chip formation during the machining process.

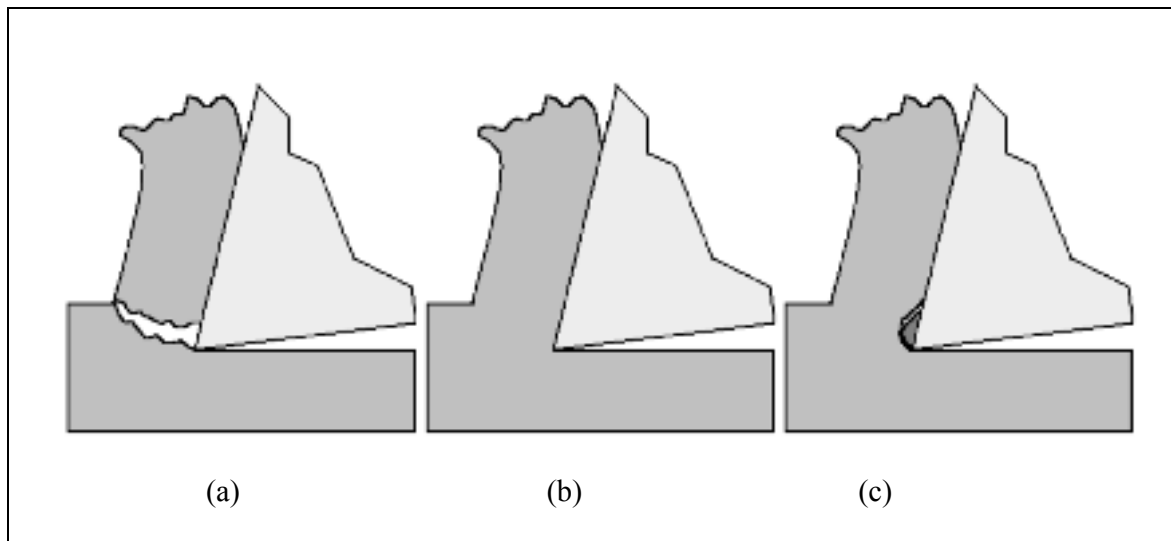


Figure 2.11 Chip formations (a) discontinuous, (b) continuous, and (c) continuous with BUE (Peach, 2009)

The transition from continuous to discontinuous chip formation depends on the thermo-physical properties and the metallurgical state of the workpiece material, as well as the cutting process (Dabade et Joshi, 2009). Chips become more segmented (discontinuous) with decreasing cutting speeds and increasing feed rates (Palanikumar et Karthikeyan, 2007). Low rake angles, the rigidity of the tool, high feed rates and the presence of inhomogeneities in the workpiece material lead to the formation of discontinuous chips in metals. For a completely homogeneous material, the transition from continuous to discontinuous chips would be abrupt. However, it would be

rather gradual for a non-homogeneous material. At lower speeds, fractures produced in the chips are almost complete and deep, leading to the formation of segmented chips.

Barzani *et al.* (2015) investigated the machinability of Al–Si–Cu cast alloy containing bismuth and antimony using a coated carbide insert. They found that Si shape (flake or lamellar) has a major effect on chip formation. Figure 2.12 shows chip adhesion on the cutting tools during the machining process. It is obvious that the base alloy produced large chips while the Bi-containing alloy exhibits short chips under the same cutting conditions. In addition, the Sb-containing alloy and the base alloy produced massive BUE during machining, which deteriorated the machined surface and finally decreased the machinability of the alloys.

BUE was found on the tools and cracks were seen on the machined surface despite increasing the cutting speed. However, at a high cutting speed, the depth of the cracks was shallow the cracks were far from each other. Formation of a small amount of BUE at a high cutting speed reduced the number of defects on the machined surface. The addition of Bi improved the surface roughness value by decreasing adhesion to the cutting tools. It was also found that Sb increased the surface roughness value by increasing BUE formation during the machining process (Figure 2.13f).

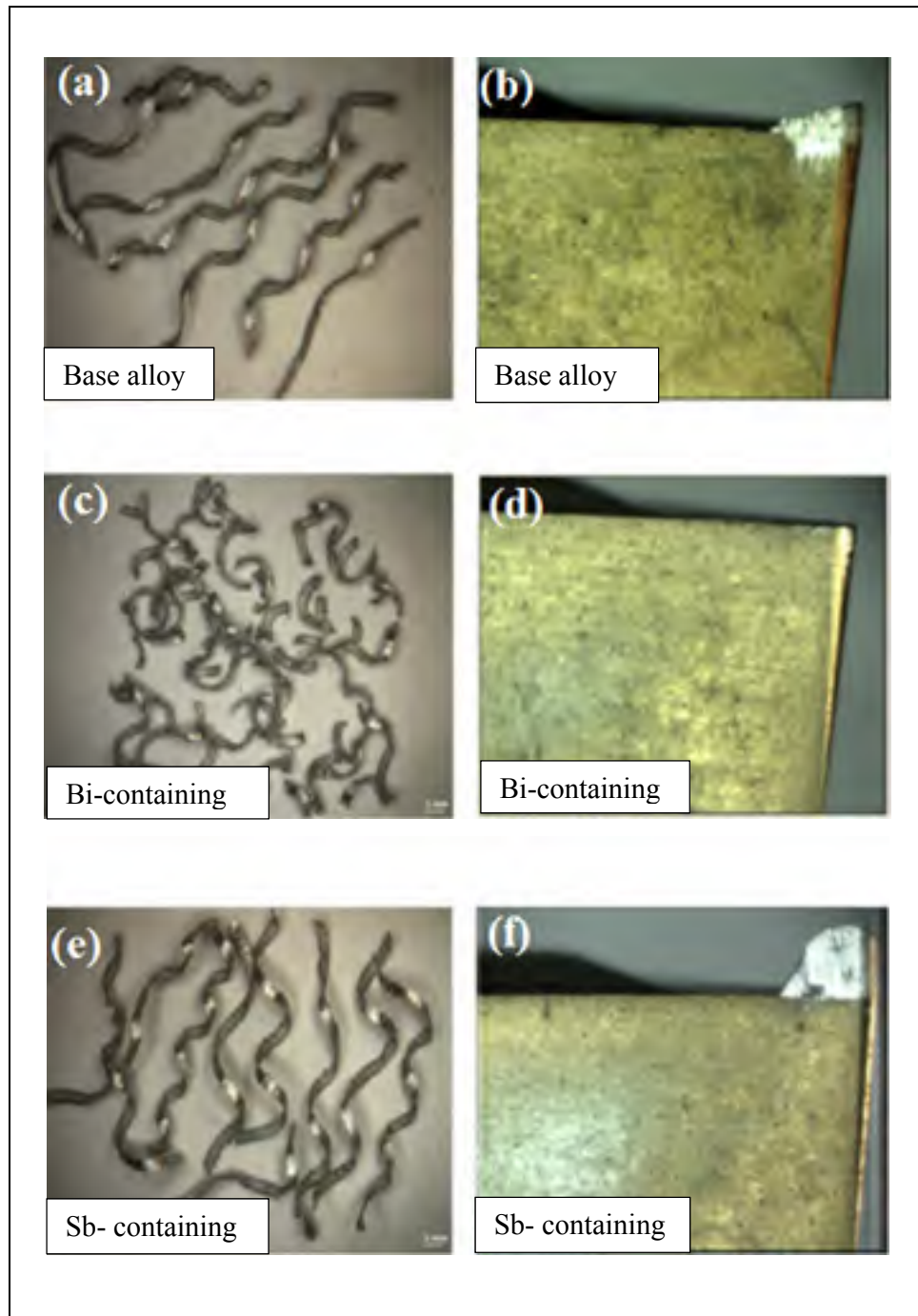


Figure 2.12 Chip formations and BUE formation at cutting speed of 250 m/min (a, b) base alloy, (c, d) Bi-containing, and (e, f) Sb-containing alloys (Barzani et al. 2015)

Kannan *et al.* (2009) explained the steps in the formation of discontinuous chips based on the single shear plane concept. The chip formation process starts at a high shear angle, which is followed by the sliding of the chip on the rake face and leads to an increase in the frictional force deterring the motion of the newly formed chip, which causes it to bulge, and there is a simultaneous decrease in the shear angle. The strain along the shear plane increases constantly while the bulging occurs until it reaches the point of ductile shear fracture. This fracture leads to the formation of segments similar to saw-teeth. This process continues cyclically leading to discontinuous or serrated chip formation.

#### **2.6.6. Dust formation**

Clean manufacturing is becoming one of the important issues at stake in future manufacturing. This technology has become attractive because of the serious problems associated with traditional machining such as health and environmental issues. Most of these issues are caused by metallic particles generated during the cutting process (turning, milling, and drilling) (Bell *et al.*, 1999). In fact, the process performance of modern metalworking is not limited to criteria such as productivity, precision, surface quality and cycle time. The protection of operators and the environment has become an additional machining process performance indicator that must be taken into consideration (Riad *et al.*, 2010).

In the U.S., regulations of the Occupational Safety and Health Administration (OSHA) stipulate that worker exposure to fine dust and PM<sub>2.5</sub> during an 8-hour work shift must not exceed 15 mg/m<sup>3</sup> (Sutherland *et al.*, 2000). It has been concluded that most machine operators are not aware of the presence of metallic dust and its associated risks, except for

those machining materials such as graphite or gray cast iron, which generated a large amount of visible dust (Geneva, 1999). It has been found that particulates of potentially hazardous sizes are present if dust clouds are seen in the air (Geneva, 1999). However, there may still exist dangerous concentrations of small particulates even if no dust is visible.

McLellan et Miller (1997) found that dust particles less than 2.5 microns (PM<sub>2.5</sub>) in size represent a fraction of the breathable particles that penetrate deep into human lungs. They noticed that current regulations of the U.S. OSHA require maximum exposure levels (PELs) of 5 mg/m<sup>3</sup> for a particulate substance such as machining dust. It has been found that microparticles (generally PM<sub>2.5</sub>) or ultrafine particles can be considered a serious problem. The fine particles are inhalable and can affect the respiratory system.

Khettabi *et al.* (2007) studied the effect of the tool, lead angle and chip formation mode on dust emission. They found that tool geometry has a significant influence on dust emission in machining. It was also concluded that a tool having a lead angle of 90° generates less dust than one having an angle of 70° and 110°. Brittle chips emit less dust in comparison with ductile chips. The chip microstructure showed that dust production during machining is due to the formation of micron-bands within the chip, and chip micron-band width was largely influenced by cutting speed.

A schematic of the process illustrates different models of dust emission during the machining process (Figure 2.13). Q1 shows the shearing action taking place at the shear plane generates a certain amount of dust. Q2 shows the deformation of the chip and friction during its formation and leads to an additional quantity of dust. Q3 illustrates the chip sliding on the rake face of the insert, undergoing a second deformation and more friction, which leads to the generating of a certain amount of metallic dust. Q4 shows the tool rubbing on the

machined surface and generating dust. It may release large solid metal particles when there is BUE during machining and will create additional dust.

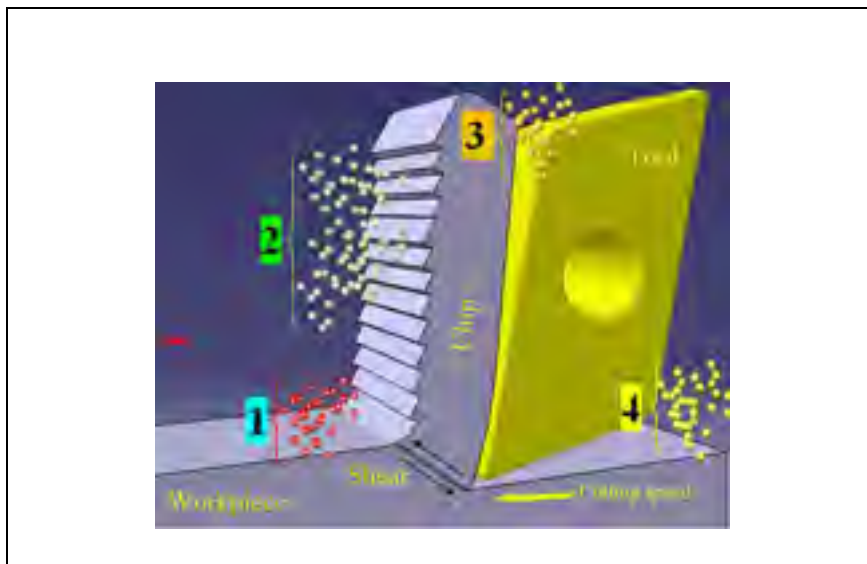


Figure 2.13 Dust production zones in the case of milling (Kouam, 2012).

The machining process is a widely used technique for shaping metallic and non-metallic materials. Despite the multiple advantages of machining, it is considered hazardous for operators and for the environment. In fact, most machining processes generate aerosols in liquid or solid form that are harmful both to operator health and to the environment. Solid aerosols are generated from part materials during dry and wet machining, while liquid aerosols are produced when cutting fluids are used (Yue *et al.*, 2000).

It has been found that long-term exposure to fluids can lead to an increase in cancers. The International Agency for Research on Cancer has concluded that there is sufficient evidence that the mineral oils used in the workplace are carcinogenic (Raynor *et al.*, 1996). On the other hand, cutting fluids generate fine liquid droplets that are under 5 microns in diameters.

Mist poses a major health threat to machinists because drops in this range remain airborne for extended periods of time. Therefore, it is necessary to decrease dust emissions during the machining process to improve operators' safety and health.

A general feeling in machining is that dry machining is a viable option over the wet process in terms of the environmental hazards (Arumugam *et al.*, 2003). Solid aerosols are generated from part materials during dry and wet machining, while liquid aerosols are produced when cutting fluids are used (Sun *et al.*, 2004). In fact, the primary mechanisms responsible for wet aerosol production include the fluid impact on the workpiece and evaporation. Cutting fluids are toxic as well as costly, given the price of initial purchase and the cost of treating used fluids (Raynor *et al.*, 1996).

Despite, dry machining presenting the problem of solid aerosol production, it is an alternative to wet machining. Eliminating cutting fluids reduces manufacturing costs and some of the aerosols that are generated. Wet machining has also been found to generate more fine and ultrafine particles than dry machining (Sutherland *et al.*, 2000).

#### **2.6.6.1. Effect of machining process on particle emissions**

Different measuring instruments are used to measure particle emissions in the machining process. It has been found that the size of particles plays an important role in the process.

According to the literature review, a laser photometer, an aerosol particle sizer (APS) and a scanning mobility particle sizer (SMPS) from TSI instruments have been used to quantify the particles produced. A laser photometer has also used to measure particle concentration, especially for those with an aerodynamic diameter below 2.5 micron.

A particle's aerodynamic size determines its rate of acceleration, with smaller particles accelerating more quickly due to decreased inertia. The SMPS spectrometer measures the aerosol's particle size distribution ranging from 2.5 to 1000 nm using an electrical mobility detection technique. The particles are then classified based on their ability to pass through an electrical field and are counted with a condensation particle counter (CPC) (Khettabi *et al.*, 2007).

Khettabi *et al.* (2010) reported that the quantity and particle size of machining dust was found to be dependent on cutting parameters, tool material, workpiece material, and tool geometry. They also concluded that lubrication has a direct impact on the quantity and size of the particles produced. They also found that cutting speed and feed rate have no significant influence on nanoparticle mass concentrations using wet milling. In fact, the shearing zone is the main source of dust emission during machining.

Sutherland *et al.* (2004) noticed that the quantity of mist and dust produced increased with the speed, feed rate and cutting depth. Ramulu *et al.* (1999) reported that dust generated during the machining process can affect the torque during a drilling process of graphite composite material. They found that tool geometry must be designed and chosen to minimize the amount of holes damaged in the form of delamination. They reported a PCD four-face drill produced the highest-quality holes and suffered the least amount of wear. The intensity of dust formation increased with an increase in cutting speed during turning and milling for all brittle materials (Gradus et Popov, 1984). The dust formed when machining iron, steel and brass at higher speeds contains a much larger percentage of particles below five microns in size. They has confirmed that using fluids can reduce dust formation by 40-50%.

Zaghbani *et al.* (2009) found that dust is related directly to the chip formation process zone and it decreases with the energy rate per area. They concluded that wet milling processes produce more particles in the submicron size range than dry milling. This conclusion is confirmed by experimental studies (Songmene *et al.*, 2004) investigating the fundamental causes of the production of dust during dry drilling processes. Light materials (aluminum and magnesium alloys) were drilled under different machining conditions, and the effects on fine dust generation were studied. Chip formation phenomenology was used to explain the observed results.

Khettabi *et al.* (2010) studied modeling for particle emission in the machining process. They found that tool geometry, workpiece material and cutting conditions have a significant influence on particle emission. On the other hand, generation of micronic and submicronic particles is less pronounced when a negative tool rake angle is used than a positive one during an orthogonal cutting process. Increasing the feed rate also reduced the amount of particles emitted due to the segmented chips produced.

Khettabi *et al.* (2013) studied micro and nanoparticle emissions during the machining of titanium. It was concluded that the investigation of the chip formation mode can be considered as an index for the mechanisms of particle emission. In addition, the disintegration of coarse particles during the machining of titanium alloys under certain conditions produced a number of fine and ultrafine particles. Under similar conditions, the machining of titanium alloys produced more micro and nanoparticles compared to aluminum alloys.

Kamguem *et al.* (2013) studied surface finish and metallic particle emissions during the machining of aluminum alloys. It was found that TiCN coating provided a better surface

finish with low metallic particle emissions compared to multilayer-coated tools for 6061-T6, 2024-T351, and 7075-T6 due to less BUE formation. They found it possible to choose the cutting process to improve surface finish and reduce dust generation, which is helpful for work environments.

Despite, some techniques having been suggested in the literature to decrease particle emissions in machining alloys, there is not sufficient knowledge to decrease dust emissions when machining metal matrix composites. Therefore, in this project, the behaviour of particle emissions during the machining of Al-20Mg<sub>2</sub>Si metal matrix composite was investigated. In addition, the best cutting condition was selected to minimize dust emissions during the machining process.

## **2.7. Adaptive network-based fuzzy inference system (ANFIS)**

There are several computing techniques (e.g., neural networks, support vector machines and the adaptive neuro-fuzzy inference system) proposed in many studies to estimate phenomena behaviour in real-life applications (Pourtousi *et al.*, 2015). Among these techniques, the adaptive network-based fuzzy inference system (ANFIS) has attracted researchers' attention because of its ability to learn complex relationships, and its vast application has been illustrated in numerous studies. The accuracy of the ANFIS approach can be altered by changing the prediction model structure and adapted on the basis of relationship complexity (Abdulshahed *et al.*, 2015).

The ANFIS method can use experimental results as training data to learn phenomena behaviour. An appropriate set of training data is required to successfully train the ANFIS

model. The membership function (MF) is an important portion of the ANFIS method that must be correctly defined in order to achieve an accurate relationship between inputs and output (Azwadi *et al.*, 2013). Figure 2.14 depicts an ANFIS structure.

The structure of the ANFIS model used has two different inputs (time and temperature) which are implemented with three membership functions (MFs) for time and two MFs for temperature. The first input, time, is divided into three spaces: low, medium and high and the second input, temperature, is divided into two spaces: low and high. The structure has six rules and the outputs show the prediction of Ra for this experiment.

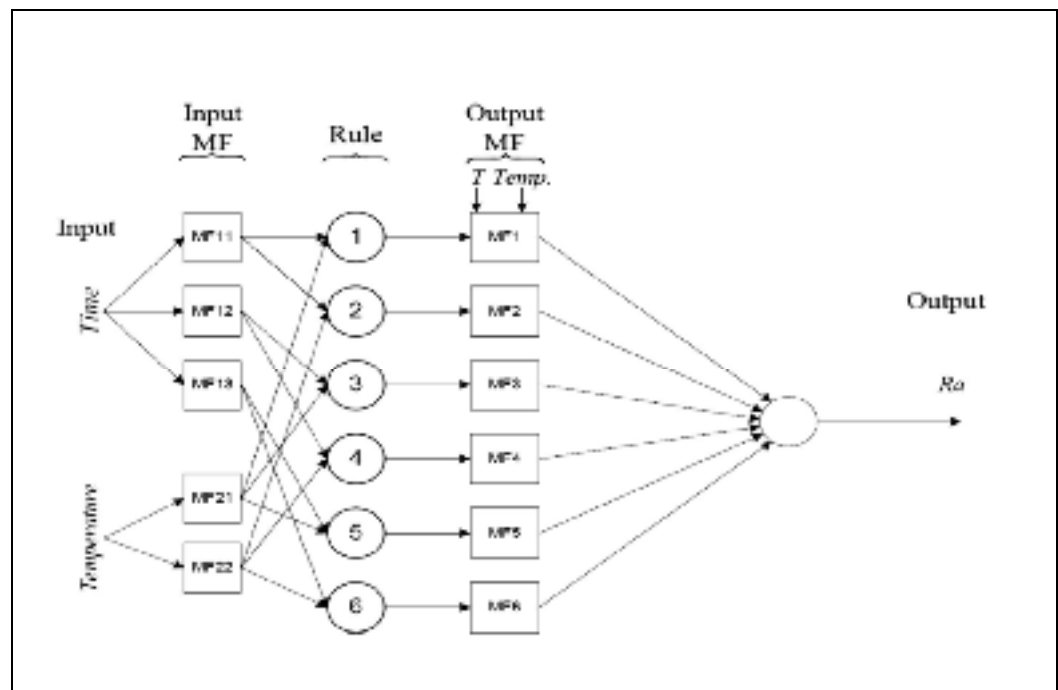


Figure 2.14 ANFIS structure (Mohammad *et al.*, 2015)

Ekici (2009) investigated an ANFIS model for wire electrical discharge machining (Wire-EDM). It was reported that ANFIS improved the process responses such as surface roughness

and white layer thickness in Wire-EDM. Maher *et al.* (2015) investigated the productivity of the wire-cut electrical discharge machine using ANFIS modeling. They reported that ANFIS was used to introduce technological knowledge base for the selection of machining parameters to achieve high productivity at the highest possible surface quality for sustainable production and lowering process cost.

Ho *et al.* (2009) reported on an ANFIS for predicting surface roughness in the end milling process. They concluded that the optimal prediction error was 4.6%, which was the lowest amount of error compared to other methods. Mohd et Habibollah (2015) used the ANFIS to model the relationship between surface roughness and milling parameters during the machining process. They reported that the optimum result for predicted surface roughness with a triangular membership function using ANFIS was 95.35%. In addition, the accuracy predicted by a trapezoidal membership function was 92.69%.

Dong et Wang (2011) studied an adaptive network-based fuzzy inference system with validation approach for predicting surface roughness. An improved approach is proposed to model surface roughness with and ANFIS and leave-one-out cross-validation (LOO-CV) approach. It was concluded that the ANFIS approach can achieve satisfactory performance. In addition, the rule-reduction approach based on LOO-CV was an effective method for modeling with ANFIS and provides an effective way to predict surface roughness in the end milling process. Ebtahaj *et al.* (2015) experimented with monitoring of tool wear based on machining forces and neuro-fuzzy modeling approaches during the machining of the composite. In fact, the ANFIS models were able to match the nonlinear relationship of tool wear and feed force data highly affected.

The ANFIS method has attracted researchers' attention because of its ability to learn complex relationships, and its vast application has been illustrated in numerous studies (Abdulshahed *et al.*, 2015). Therefore, in this research work, an ANFIS model will be used to predict the machinability of the composites.

## **2.8. Summary and conclusive remarks**

After the literature review, this section outlines the major findings related to this research work and the main issues that have not yet received sufficient attention and require further investigation:

- The machinability of metal matrix composite plays an important role when it is necessary to fabricate some cast industrial products. Therefore, there is a need to optimize the machining process based upon certain output variables, such as cutting forces, surface finish and chip morphology to improve the quality of products and reduce the cost of manufacturing.
- Cast Al-20Mg<sub>2</sub>Si metal matrix composites contain some primary Mg<sub>2</sub>Si particles that can have detrimental effects on the mechanical properties of the composite in terms of elongation and ductility. Therefore, these particles need to be modified to obtain the desired mechanical properties. Melt treatment with the addition of certain inoculation agents, known as modifier elements, can produce a very fine matrix structure. It is a more practical method since it keeps production costs low and is suitable for general engineering applications.

- The machining process produces liquid and solid particle aerosols that can be harmful to the operator and environment. It has also been noticed that metallic dust generated during the machining process can be associated with the nature of the material being machined and create hazardous dust. In fact, the protection of operators and the environment has become another machining performance variable to consider. Therefore, there is a need to reduce dust emission during the machining process to protect the operator's health and the industrial environment.
- Soft computing tools are widely used to model and control the machining processes. Artificial intelligence (AI) is the science and engineering of making intelligent machines, especially intelligent computer programs. An ANFIS is an artificial intelligence method in which the neural networks are utilized to elaborate the fuzzy rules of the fuzzy inference approach. There is insufficient knowledge about modeling Al-20 Mg<sub>2</sub>Si metal matrix composite machining using ANFIS, which is an important factor to predict the machinability of the composite to minimize fabrication cost during the process.

## **CHAPTER 3**

### **METHODOLOGY**

#### **3.1. Experimental details**

In this chapter, the experimental methods are outlined, namely casting, machining and metallographic analysis. A full factor experimental design with three parameters (cutting speed, feed rate, and workpiece materials) and three levels ( $3^3$ ) was selected for this study. The cutting tool and the depth of cut were constant. The experimental factors and their levels are shown in Table 3.1. Cutting tools and workpiece materials were treated as qualitative factors, while the other remaining factors were considered quantitative. Two furnaces were used together to cast three workpieces: Al-20Mg<sub>2</sub>Si (base composite), Al-20Mg<sub>2</sub>Si-0.4 Bi (Bi-containing composite) and Al-20Mg<sub>2</sub>Si-0.2Ba (Ba-containing composite) using a permanent mold.

#### **3.2. Casting process**

The first furnace was used to preheat the permanent mold, and the second furnace was used to melt the alloys. Figures 3.1a and b show the furnaces. The chemical composition of the fabricated workpiece is shown in Table 3.2. A commercial alloy, pure aluminum (99%) and pure magnesium (99%) were used as starting materials. The materials were melted to manufacture Al20Mg<sub>2</sub>Si ingot. An induction furnace was used to melt a 2-kg ingot in a silicon carbide crucible at a temperature of  $750 \pm 5$  °C. Two different elements, bismuth (Bi) and barium (Ba) in pure metallic form were added separately into the melt as agent elements.

Certain addition levels of 0.4 and 0.2 wt.% were introduced to the melt for Bi and Ba, respectively. Dissolution and homogenization were performed in 15min. In addition, the molten alloy was stirred and the surface was skimmed. A rectangular ceramic mold 30 mm long and 25mm wide was used as a workpiece for pouring the molten alloy. Figure 3.2 shows the cast workpieces.

Table 3. 1 Machining parameters

Factors	Levels		
A: Cutting speed (m/min)	300	700	1100
B: Feed rate (mm/tooth)	0.1	0.15	0.2
C: Depth of cut (mm)	1		
D:workpiece material	Al20Mg <sub>2</sub> Si	Al20Mg <sub>2</sub> Si 0.2% Bi	Al20Mg <sub>2</sub> Si 0.4%Ba
E :Cutting tool(Iscar)(HM90 E90A-D.75-3-W.75)	IC28		

Table 3. 2 Chemical composition of base aluminum alloy used

Element	Si	Fe	Cu	Mn	Mg	Cr	Zn	Al
Base Alloy (wt%)	7.07	0.64	2.034	0.217	12.710	0.034	0.614	Bal



(a)



(b)

Figure 3. 1 (a) Melting furnaces and (b) furnace for preheating the permanent mold (Université du Québec à Chicoutimi)

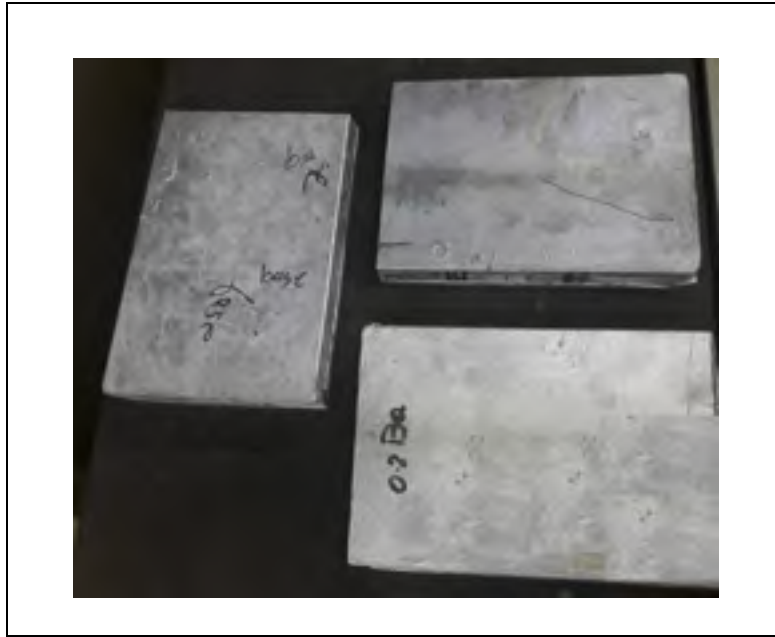


Figure 3. 2 Image of the workpiece specimens

As can be seen in figure 3.3(a, b, c and d)  $Mg_2Si$  particle ( $Mg_2Si_p$ ) in the unmodified composite as shown in Fig. 4.15a1 exists in a coarse skeleton shape and exhibits a bigger size. This kind of shape has high stress concentration at its sharp edges, which would increase the fracture surface of the structure and weaken the composite performance. Addition of Bi at 0.2wt% (Figure 3.3b) has shown positive result as the coarse particles start to refine to a polyhedral shape and decrease in size. However, some of them still appeared as coarse structure.

With further addition of 0.4wt% Bi, the particles changed into a better polygonal shape as well as continuing to decrease in size, as seen in Figure 3.3c. In fact,  $Mg_2Si_p$  was observed in most refined particles. With an increase of Bi content to 0.8wt%, the particles exhibit coarser morphology and their size increased again (figure 3.3c). Therefore, 0.4wt% Bi has been selected for casting the composite.

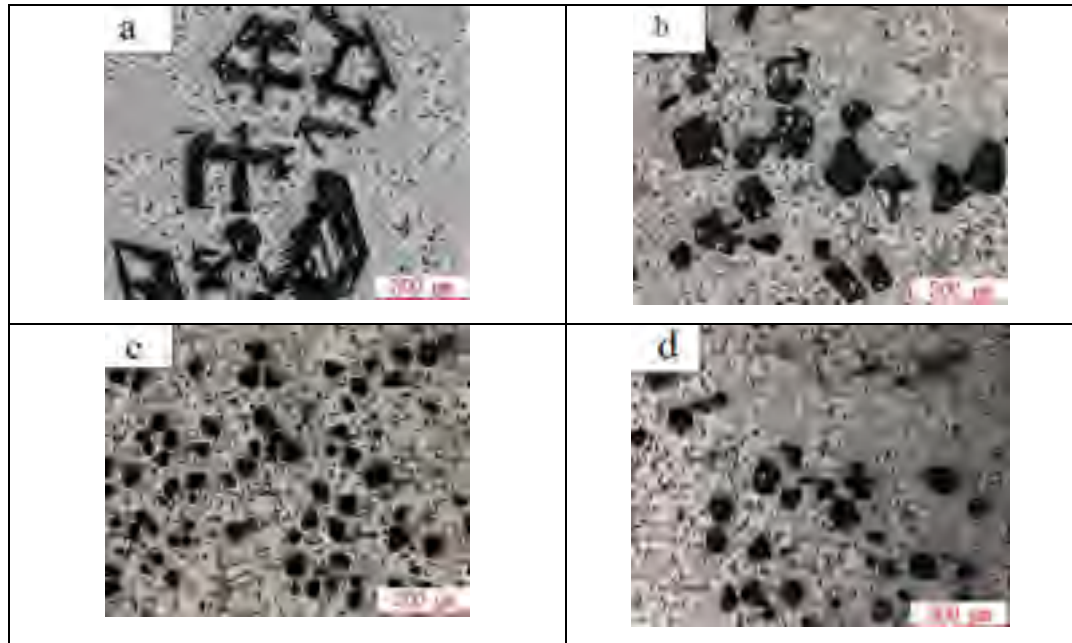


Figure 3. 3 Optical micrographs showing changes of morphologies for  $Mg_2Si$  with (a) 0.0wt% Bi, (b) 0.2 Bi, (c) 0.4wt% and (d) 0.8wt%Bi

Figure 3.4(a, b, c and d) illustrates the changes in microstructure of the composite corresponding to two phases  $Mg_2Si_P$  and  $Mg_2Si_E$  as a result of Ba addition. As observed in Figure 3.4a, the  $Mg_2Si_P$  particles in unmodified state exhibit coarse skeleton and dendritic structure. Introducing Ba element into the composite melt are shown to cause significant effects on  $Mg_2Si_P$  structure as the particles are transformed into polyhedral shape with changes in their average mean size. As can be seen in figure 3.4b, the addition of 0.2wt% Ba changed coarse shape  $Mg_2Si$  particles to the polygonal shape, while some particles still keeping their triangular and rectangular form. However, with further additions of Ba up to 0.4wt%, the refinement effect seems to disappear as the particles exhibit coarser morphology and their size increased again as illustrated in Figure 3.4c. This trend continued with increased Ba concentration up to 0.8 wt% Ba. In fact, 0.2wt% Ba is a turning point for  $Mg_2Si_P$  refinement as they are shown to have the most modified and refined structure.

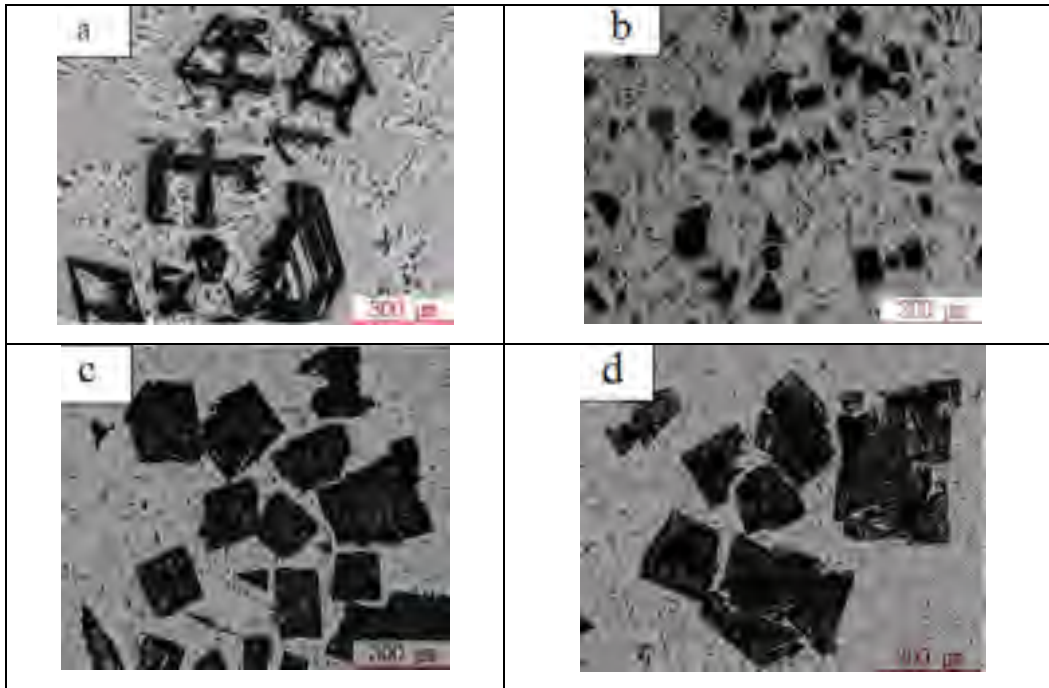


Figure 3. 4 Optical micrographs showing changes of morphologies for  $Mg_2Si$  with (a) 0.0wt% Ba, (b) 0.2 Ba, (c) 0.4wt% Ba and (d) 0.8wt%Ba

### 3.3. Machining process

In total, 81 experiments were performed (and repeated three times). The machining tests were carried out on a computer numerical control (CNC) HURON-K2X10 milling machine (spindle speed (N) 28000 rpm, power (P) 50 kW and Torque (T) 50 Nm) as shown in Figure 3.5. An Iscar uncoated carbide insert (IC28) was selected to contact the machining test. An Iscar tool holder (HM90 E90A-D.75-3-W.75) with three flutes ( $Z=3$ ), and diameter (D) 20 mm was also selected for this study. Figures 3.6a and b show the tool holder. A new insert was used after each cutting experiment. All cutting conditions were selected based on the tool manufacture's recommendations for the machining of aluminum metal matrix composite.



Figure 3.5 CNC machine tool used

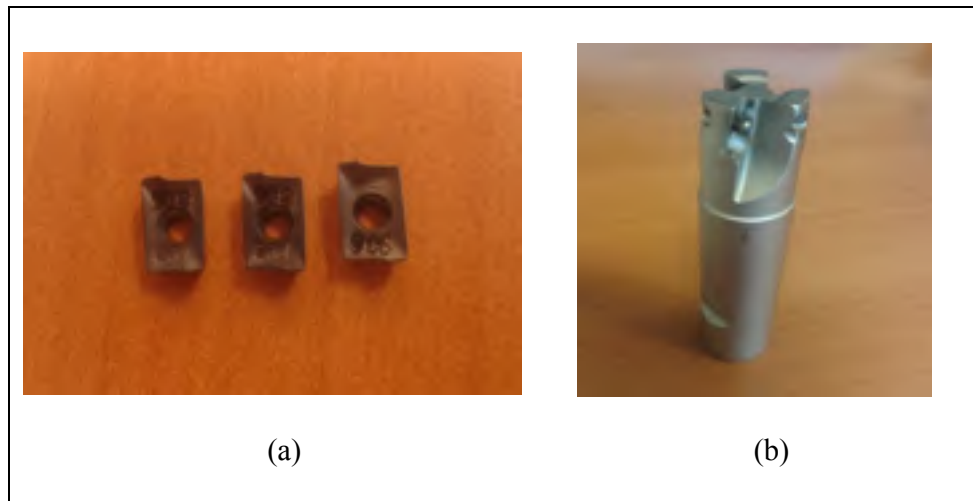


Figure 3.6 (a) Cutting inserts and (b) tool holder

### 3.4. Metallography

Metallographic specimens were mounted, ground and polished using standard routine techniques (Figure 3.7). Microstructures were analyzed (Figure 3.8) using an optical microscope and a scanning electron microscope (SEM) equipped with energy dispersive spectroscopy (EDS) (Figure 3.8-3.9). Mechanical tests Samples for mechanical property testing were produced using gravity permanent mold casting technique.

The mechanical properties of the alloys along with the examination of the corresponding fracture surfaces were experimentally determined using universal mechanical tensile testing machine, hardness tester, and Zwick impact testing machine, respectively (Figure 3.10- 3.12). For tensile tests, an ASTM-B77 size specimen (Figure 3.13) was used. A computerized testing machine was used for tensile tests at a strain rate of 1 mm/min at room temperature. The impact test (Figure 3.14) was conducted based on charpy type using Zwick impact testing machine (D-7900) using a 15J hammer to measure the total absorbed energy.



Figure 3.7 Mounted specimens

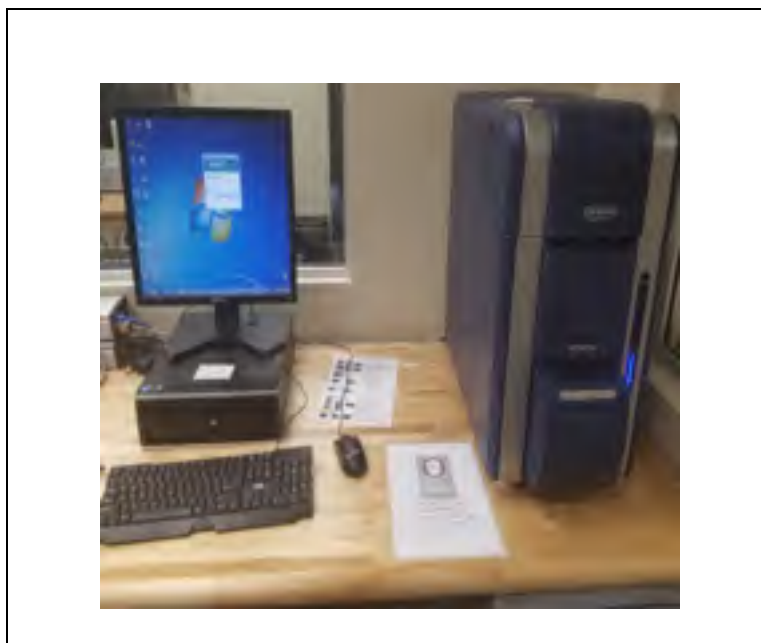


Figure 3.8 Scanning electron microscopy (SEM)



Figure 3.9 Optical microscope



Figure 3.10 Universal mechanical tensile testing machine



Figure 3.11 Hardness machine testing



Figure 3.12 Zwick impact testing machine (Courtesy of Ecole Polytechnique de Montréal)



Figure 3.13 Tensile samples



Figure 3.14 Impact test samples

### 3.5. Surface roughness and cutting force

A surface roughness tester (Mitutoyo SJ-400) was used to measure the roughness of the machined surface (Figure 3.15). The cutting force was measured with a three-component piezoelectric dynamometer (KISTLER, 9255B). The dynamometer has several quartz-base piezoelectric force transducers in a steel housing. When force is applied on the dynamometer, each transducer produces a charge proportional to the force component that is sensitive to axis. The Kistler was connected to the charge amplifiers (type 5010). All signals were independently monitored, digitized and recorded into a LabView where Cut Pro 8.0 software was used in order to force measurements. The cutting force signals were exported to Matlab for further analysis.



Figure 3.15 Surface roughness tester

### 3.6. Dust emission

Dust sampling (Figure 3.16) was performed by suctioning of air from the cutting area during the machining process using an aerodynamic particle sizer (APS model 3321, TSI, Inc.) and a scanning mobility particle sizer (SMPS model #3080, TSI, Inc). Particle concentration, specific area concentration and mass concentration were measured as a function of particle aerodynamic diameters by the above mentioned instruments. Figure 3.17 shows a summary of the overall methodology.



Figure 3.16 Aerodynamic particle sizer (APS) and scanning mobility particle size (SMPS)

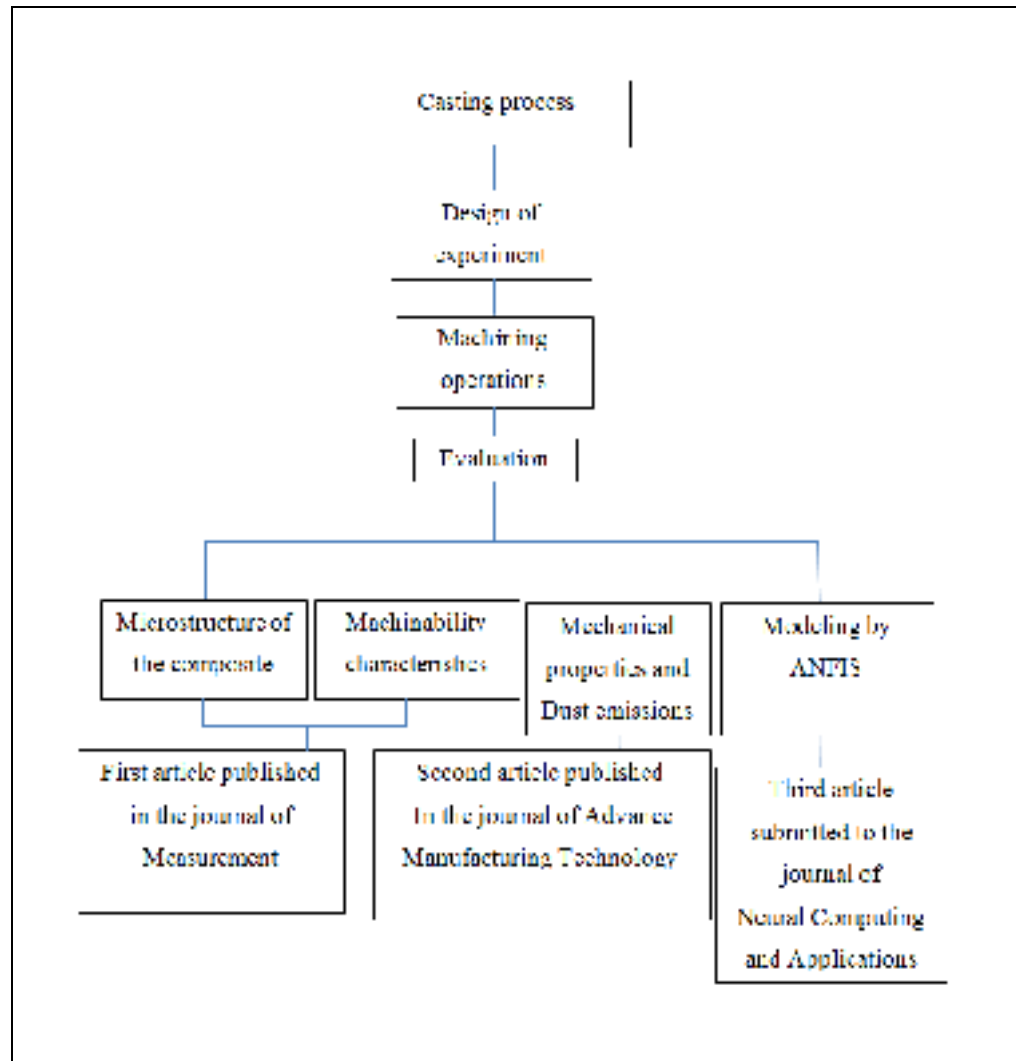


Figure 3.17 Summary of the overall methodology



## CHAPTER 4

# MACHINABILITY CHARACTERISTICS AND MECHANICAL PROPERTIES OF Al-Mg<sub>2</sub>Si-Cu METAL MATRIX COMPOSITE WITH BISMUTH

Mohsen Marani Barzani<sup>1</sup>, Seed Farahany<sup>2</sup>, Victor Songmene<sup>3</sup>

<sup>1,3</sup>Department of Mechanical Engineering, École de Technologie Supérieure, 1100 rue Notre-Dame West, Montréal, Québec, Canada

<sup>2</sup> Department of Materials and Mechanical Engineering, Buein Zahra Technical University, 3451745346, Gazvin, Iran

Paper published in the journal of Measurement 110 (June, 2017): 263-274, Elsevier.

### 4.1. Abstract

In the present work, the effect of Bi addition on machinability, microstructure and mechanical properties of Al-20Mg<sub>2</sub>Si metal matrix composite is investigated. The structure of the primary Mg<sub>2</sub>Si reinforcement particle changed from coarse to fine polygonal accompanied with a decrease in size and increase in density. The addition of Bi improved the ultimate tensile strength (UTS), elongation (El %), impact toughness and hardness values. Dry turning tests for various cutting conditions and feed rates were carried out with a cemented carbide tool. The result indicated that surface roughness and cutting force improved with the addition of 0.4wt% Bi due to changing Mg<sub>2</sub>Si particle size and less built-up edge during the machining process.

**Keywords:** Machinability, metal matrix composite, surface roughness, bismuth

## 4.2. Introduction

The Al and Mg-based composites, reinforced with particulates of  $Mg_2Si$ , have recently been introduced as a new group of particulate metal matrix composites (PMMCs) that offer attractive advantages such as low density, good wear resistance, and good castability (Fadavi *et al.*, 2015; Hadian *et al.*, 2008). The advantages of  $Mg_2Si$  reinforcement particles make them a potential candidate in aerospace and engine applications ( Li *et al.*, 2009; Sun et Ahlatci, 2011). Despite the advantages of the  $Mg_2Si$  particles, such as high melting temperature, low density, and high hardness, their coarse and rough morphology in the Al matrix has been thought to lead to the low ductility observed in these materials. Therefore, it is necessary to control the primary  $Mg_2Si$  phase to improve the mechanical properties of the composites ( Sun et Ahlatci, 2011).

Different reinforcement particles such as strontium (Sr), copper (Cu) and bismuth (Bi), have been used to modify the primary and eutectic  $Mg_2Si$  phase (Emamy *et al.*, 2010; Hadian *et al.*, 2008). It has been concluded that the addition of modifier elements improve the microstructure and mechanical properties of Al- $Mg_2Si$  metal matrix composites (Farahany, Nordin, *et al.*, 2014). Using modifier elements is more cost effective and practical compared to the other methods (Farahany, Nordin, *et al.*, 2014).

The mechanical properties of composites have a direct effect on the machinability of the composites. It is known that metal matrix composites (MMC) are more difficult to machine compared to the other alloys. Emamy *et al.* (2010) studied the effect of Cu addition on the microstructure and hardness of Al-15 $Mg_2Si$  composite. It was found that the Cu addition has a marginal effect on both primary and secondary  $Mg_2Si$  particles. Guo *et al.* (2008) reported

that adding an optimum concentration of Bi improved the mechanical properties of Mg-Si alloy.

Azmah *et al.* (2013) investigated the refinement of Mg<sub>2</sub>Si in a commercial Al-Mg<sub>2</sub>Si metal matrix composite containing bismuth and antimony. A continuous decrease in the nucleation and growth temperatures of Mg<sub>2</sub>Si particles was found to be a consequence of these additive elements. In the study of machinability, parameters such as cutting conditions, tool geometry and workpiece material are important factors. It was reported that using a certain type of reinforcement particle in casting processes can be helpful in the machining process. In fact, reinforcement particles lead to a change in the microstructure of workpieces, which may affect the resulting machinability characteristics. Certain free-machining elements, such as tin (Sn), lead (Pb), copper (Cu) and bismuth (Bi) have been used to improve machinability (Ozben *et al.*, 2008).

Koch (2016) reported that Sn concentration in Al-Cu-Mg alloy led to the formation of continuous chips and improved the machined surface during the machining process. It was also found that increasing the formation of the Sn-rich phase improved machinability due to a homogeneous distribution of the Sn-containing phase. Koch (2008) investigated the effect of Ti and Zr on Al-Cu-Mg-Sn alloy for machining purpose. It was found that the machinability of Al-Cu-Mg-Sn alloy improved with the addition of Zr. In addition, Zr promoted the formation of short-broken chips and consequently improved surface roughness in the machining process.

Koch et Antrekowitsch (2011) considered the behavior of Cu within the range of 1.6 to 4.7% in Al-Cu for free machining. The results showed that the alloy with the highest range of Cu provided the shortest chip size and improved the surface roughness value. Songmene et

Balazinski (1999) investigated the machinability of metal matrix composite containing graphite particles. It was found that the addition of graphite improved chip breakability and the machinability of the composite.

Kannan et Kishawy (2006) studied surface characteristics when machining MMC. They reported that particle fracture provided some geometrical defects such as pits, voids, and microcracks. It was also found that the percentage of defects increased when cutting speed increased. It has been reported that adding Bi into Al-Si alloy improved the surface roughness value and decreased the cutting force, while the addition of antimony and strontium had a negative effect on composite machinability (Barzani *et al.*, 2013; Barzani *et al.*, 2015). Most work on MMC machinability has involved Al-SiC<sub>P</sub>, while only a few studies have dealt with Al-20Mg<sub>2</sub>Si metal matrix composite. There is still a lack of understanding about the machinability of the composite when using modifier elements that have not been clarified. Therefore, the aim of this research is to study the machinability and mechanical properties of Al-20Mg<sub>2</sub>Si metal matrix composite using Bi as a modifier element.

### **4.3. Experimental work**

#### **4.3.1. Material**

Industrial pure Al-Si-Cu die-cast alloy, pure aluminum (99.8%) and pure magnesium (99.8%) were used to adjust the chemical composition. The materials were melted to fabricate Al-Mg<sub>2</sub>Si ingot. A resistance furnace with a melt temperature of  $750 \pm 5$  °C was used to melt a 2-kg ingot in a silicon carbide crucible. The element of Bi in the form of pure

metallic shots (99.9%) was added into the melt after melting was completed. The authors concluded that the optimal concentration for refining the Al-20Mg<sub>2</sub>Si metal matrix composite with Bi was 0.4 wt.%.

The molten alloy was stirred and skimmed after 15 min to allow for dissolution and homogenization. A cylindrical ceramic mold with a 40 mm outer diameter and a 40 mm height was used to cast the molten alloy. The cylindrical mold was preheated to 750°C for 15 min. The samples were sectioned for metallography and standard grinding procedures.

A Vickers scale was used to measure the hardness of samples, and an average of five readings were taken to report the samples. An ASTM-B77 size specimen (Figure 4.1) was used for the tensile test. A computerized testing machine was used for tensile tests at a strain rate of 1 mm/min at room temperature. A scanning electron microscope (SEM; Hitachi table microscope TM3000) equipped with EDS and a laser scanning digital microscope (LEXT OLS4100) were used to analyze the microstructures. Emphasis was given to the influence of Bi additions on the morphology of the Mg<sub>2</sub>Si particles. Table 4.1 illustrates the workpiece's composition.

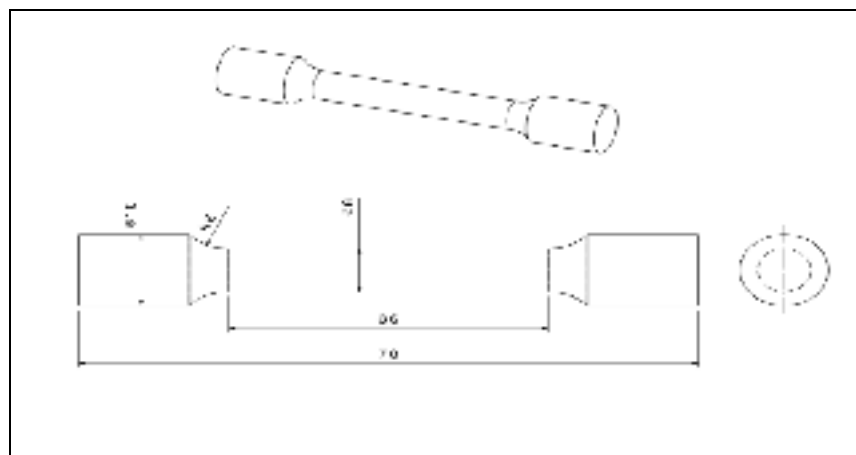


Figure 4.1 Tensile sample dimension (mm)

Table 4. 1 Chemical composition of Al-20Mg<sub>2</sub>Si metal matrix composite

	Si	Fe	Cu	Mn	Mg	Cr	Zn	Al
Wt%	7.07	0.64	2.034	0.217	12.710	0.034	0.614	Bal

### 4.3.2. Machining test

The experiments were conducted on a three-axis CNC turning machine HURON- 1350S (power drive, 8.5 kW; speed, 7500 rpm) using a TiN-coated carbide tool under dry conditions. Table 4.2 shows information about the tool and tool holder. A three-component piezoelectric dynamometer was used to record cutting forces during the machining process. Different cutting speeds and feed rates were used with a constant depth of cut. The cutting conditions were selected based on the tool manufacturing's recommendations.

In order to ensure the accuracy of the surface roughness value, the experiments were repeated twice. The surface roughness was measured at different locations using a surface roughness tester ( $\pm 0.01\mu\text{m}$  accuracy). In addition, a new cutting insert was used for each set of conditions. Chip morphology and the machined surface were characterized using a scanning electron microscope (SEM) and an optical microscope.

Table 4. 2 Cutting tool and tool holder

Tools grade	Coating	ISO Catalogue number	Nose radius	Tool holder
KU10	TiN	VBGT110302F	0.2mm	SVJBL-1616H1

#### 4.4. Results and discussion

##### 4.4.1. Microstructure

Figures 4.2a and b show the microstructure of Al-20Mg<sub>2</sub>Si metal matrix composite. The primary Mg<sub>2</sub>Si coarse particles and eutectic Al-Mg<sub>2</sub>Si phases were observed in the microstructure of the composite. Figures 4c and d show optical micrographs of the composite with the addition of Bi. As can be seen, the irregularly shaped Mg<sub>2</sub>Si coarse particles became fine polygonal shaped. The mean particle size reduced from 180.1 μm (base composite) to 113.5 μm (Bi-containing) with the addition of Bi. Additionally, the flake-like morphology of eutectic Al-Mg<sub>2</sub>Si assumed a more lamellar shape following the addition of Bi.

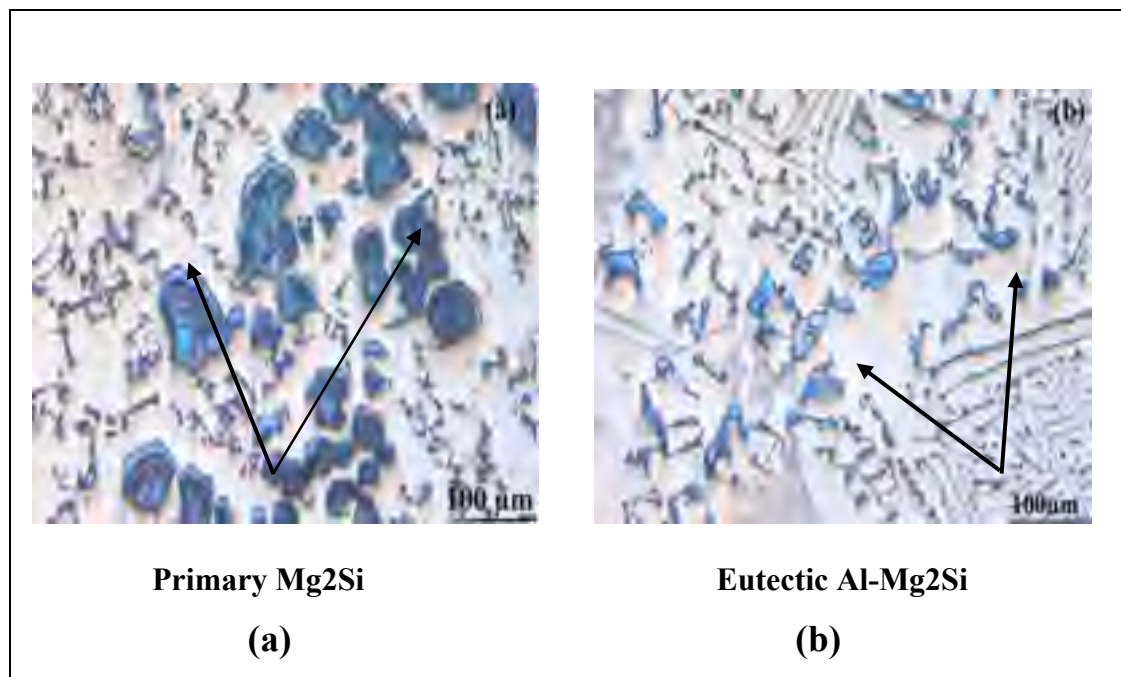


Figure 4.2

Optical micrographs of Al-20Mg<sub>2</sub> metal matrix composite (a,b) without Bi and (c,d) with 0.4 wt.% Bi additions

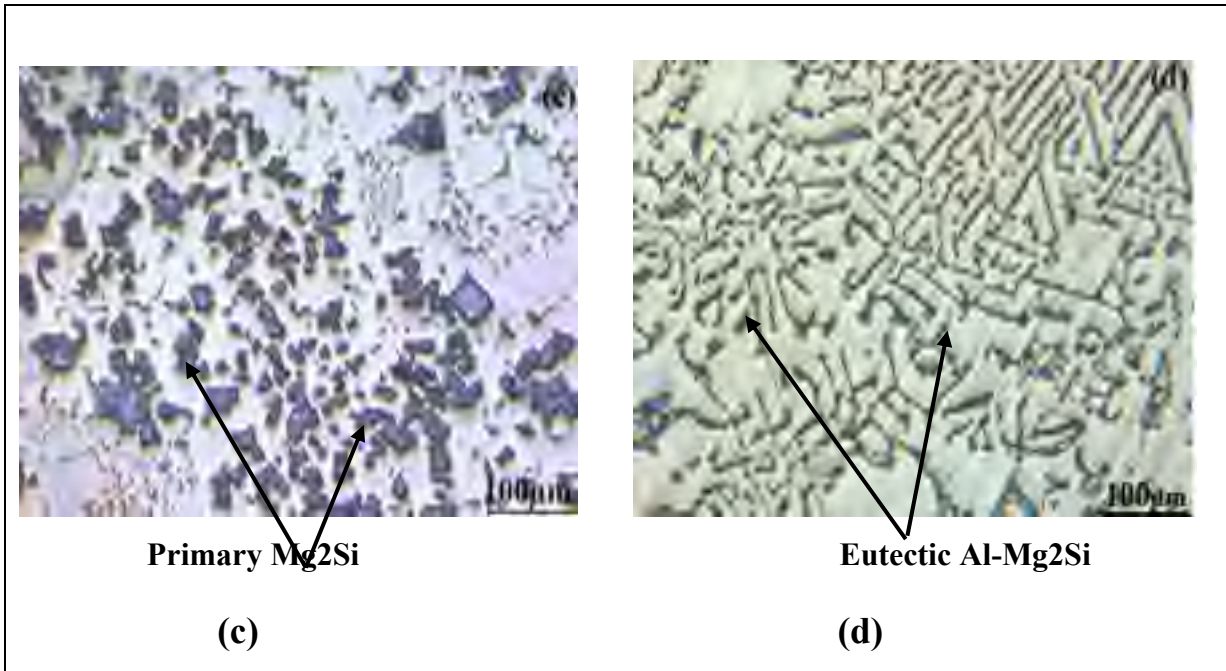


Figure 4.2 (Continued)

#### 4.4.2. Mechanical properties

Figure 4.3a shows the engineering stress-elongation curves for Al-20Mg<sub>2</sub>Si metal matrix composite. The UTS value increased from 103.4±5 MPa for the base composite to 116.1±10.6 MPa for the Bi-containing composite. Figure 4.3a also shows 1.1±0.1 El% for the Bi-containing composite, which is approximately two times more than that of the base composite (0.6±0.1).

Figure 4.3b shows variations in impact toughness and hardness values following the addition of Bi. The impact value of the Al-Mg<sub>2</sub>Si composite increased from 0.8±0.1 to 1.4±0.1 J. In addition, the hardness value increased from 65±3 to 80±4 HV with the addition of Bi. The improvement in hardness can be related to the fine primary Mg<sub>2</sub>Si particles providing more

obstacles for grain boundary sliding. The results obtained show that the mechanical properties of the composite samples were affected by the addition of 0.4 wt.% Bi.

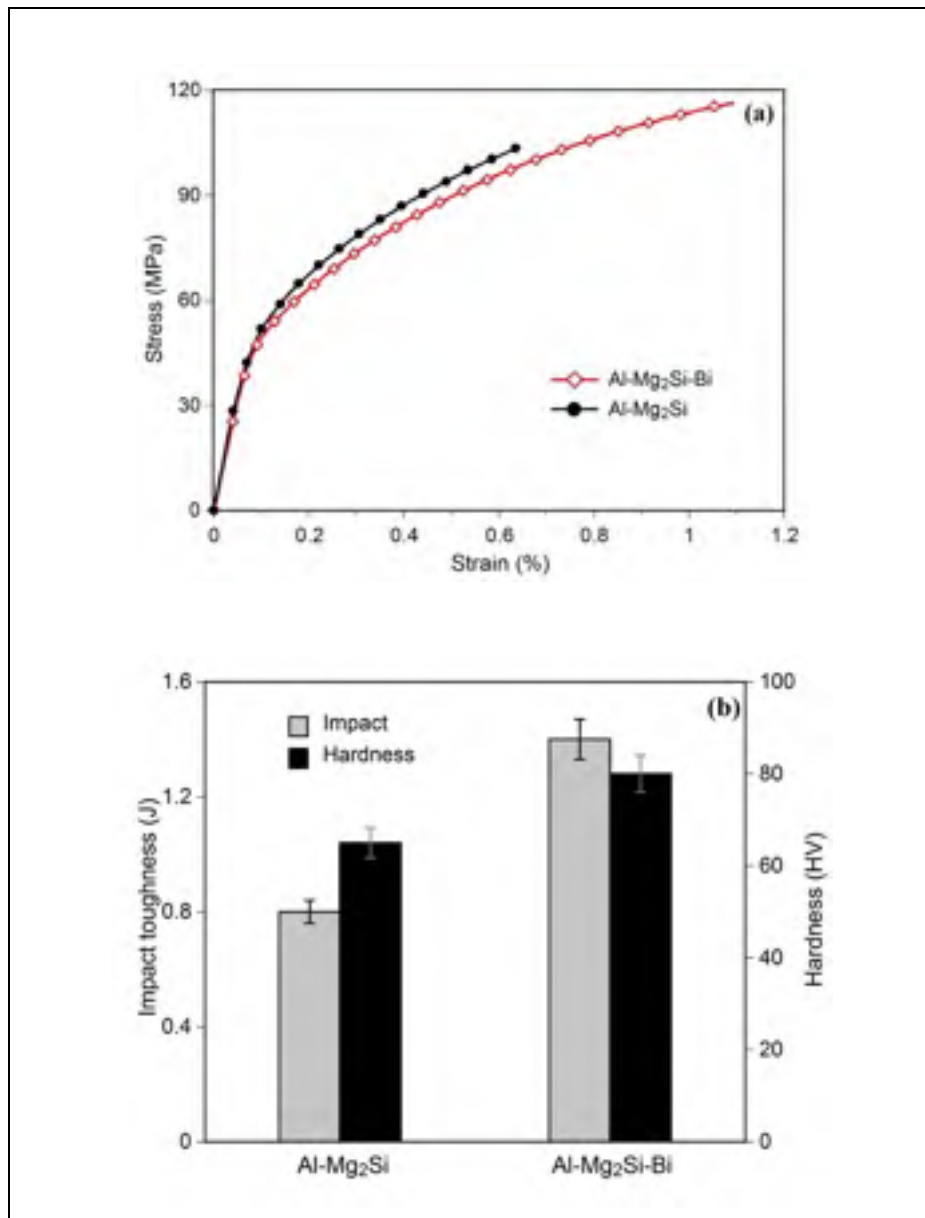


Figure 4.3 (a) Stress-strain curve and (b) variation of impact toughness with hardness value for Al-20Mg<sub>2</sub>Si (MMC), and Bi-containing composite

#### 4.4.3. Fracture surface

The fracture surface of failed tensile samples was investigated to determine the type of failure in Figures 4.4a, b, c and d. The micrographs show cracks in the coarse dendritic  $Mg_2Si$  particles due to the intrinsic brittleness of the particles. Basically, when stress is applied, the matrix plastically deforms and gradually transfers stress to the particles. Moreover, the fracture of the eutectic Al-20 $Mg_2Si$  phase was observed around primary  $Mg_2Si$  particles (Azmah *et al.*, 2013).

It has been found that  $Mg_2Si$  has more intrinsic defects and greater potential for cracking, and therefore rapid fracture (Hadian *et al.*, 2008). Therefore, both particle decohesion and particle cracking are observed in the fracture faces of Bi-free composite (Figures 4a and b). Figure 4.4c demonstrates the fracture surface of Bi-containing composite. As can be seen, fracturing occurs more often in the particles. In addition, Bi (white points) is observed on the fracture surface, and the surface exhibits more fine dimples with fewer decohered particles (Figure 4.4d). It has been concluded that primary and eutectic  $Mg_2Si$  particles are able to change fracture behaviour. They also have a direct effect on the ductility of MMCs (Hadian *et al.*, 2008).

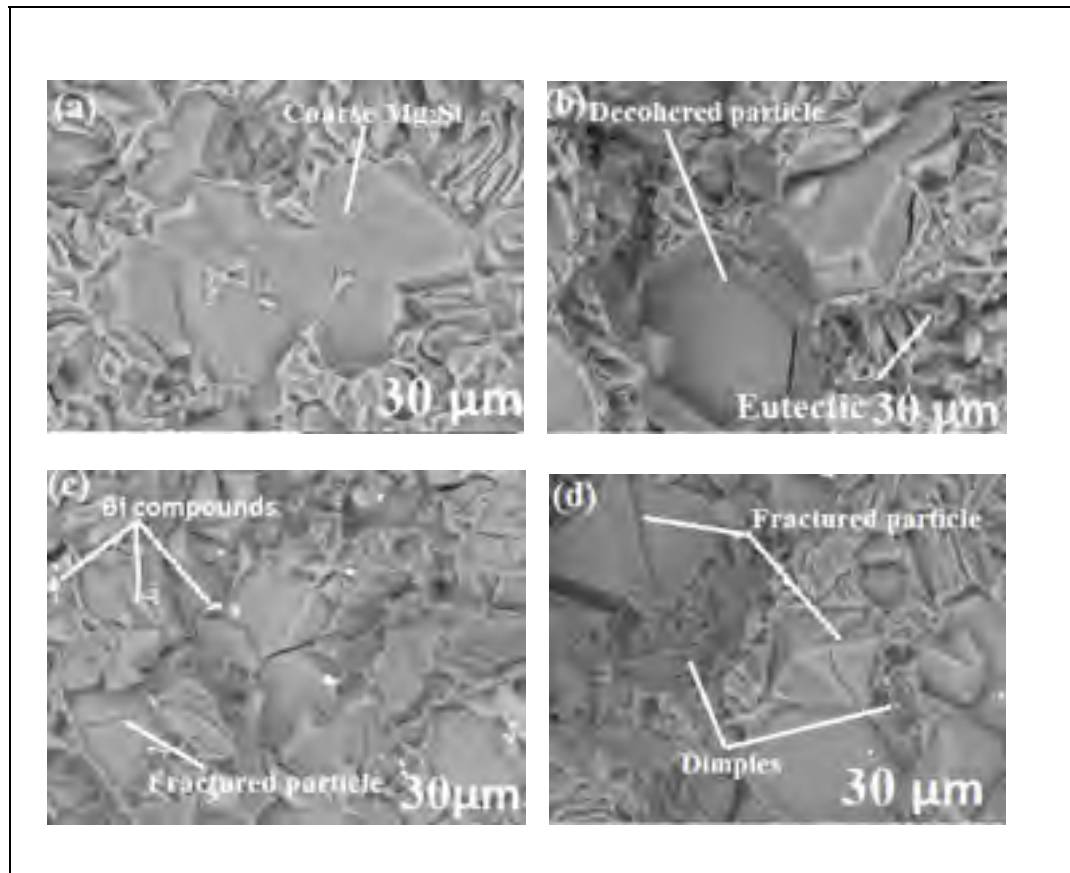


Figure 4.4 SEM micrographs of tensile samples for (a,b) Base composite (c,d) Bi-containing composite

## 4.5. Machinability of metal matrix composite

### 4.5.1. Cutting force

Cutting force plays an important role in the machinability of metal matrix composite. It has been reported that higher cutting force caused higher stress on the tool, which may cause wear and vibration when machining and consequently deteriorate the machined surface (Palanikumar et Muniaraj, 2014). Figure 4.5 shows that the cutting force increased when the

feed rate increased from 0.1 to 0.2 mm/rev and decreased when the cutting speed was increased from 90 to 270 m/min.

The lowest cutting force was around 10 N at a cutting speed of 270 m/min and a feed rate of 0.1 mm/rev for Bi-containing composite, while it was around 35 N at a cutting speed of 180 m/min and a feed rate of 0.2 m/rev for the base composite. It has been found that the friction between the tool and the machined material increases the cutting temperature in the cutting zone and ultimately increases cutting force value when machining metal matrix composite (Davim, 2012). Barzani *et al.* (2013) reported that the addition of Bi decreased the cutting force by having a lamellar silicon structure when machining Al-Si alloy. In fact, the lower cutting force improved dimensional accuracy of the machined surface.

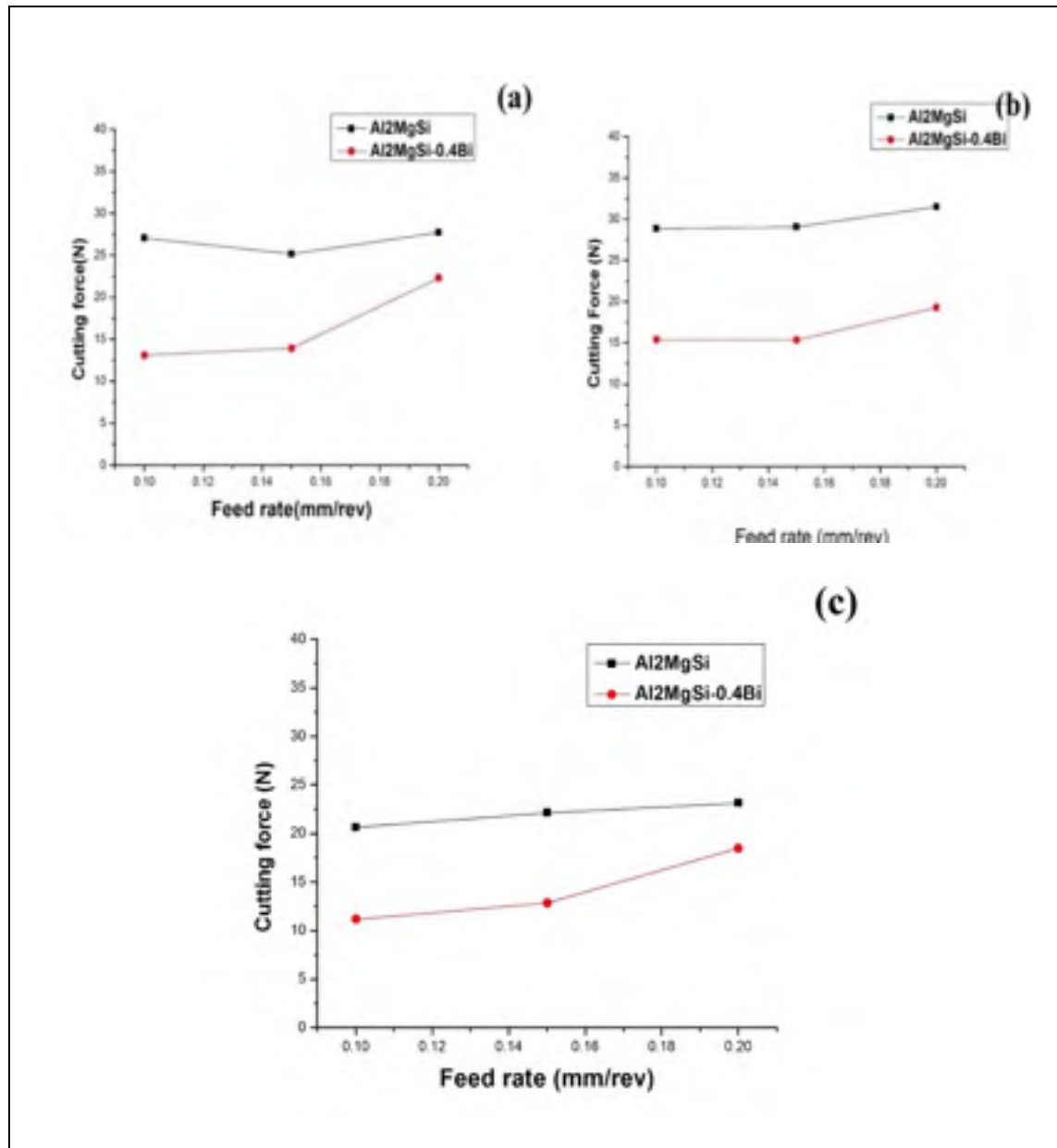


Figure 4.5 Variation of forces at cutting speed of (a) 90 mm/min (b) 180 m/min and (c) 270 m/min

Figure 4.6 illustrates the shape of the built-up edge (BUE) during the machining process. Figures 4.6a and b show that the BUE formation covered the flank face of the insert when machining the base composite at both feed rates (0.1 and 0.2 mm/rev), while there was no

tendency to have BUE when machining the Bi-containing composite Figures 4.6c and d. On the other hand, the Bi-containing composite showed a reduction in the cutting force value due to a low tendency of BUE formation.

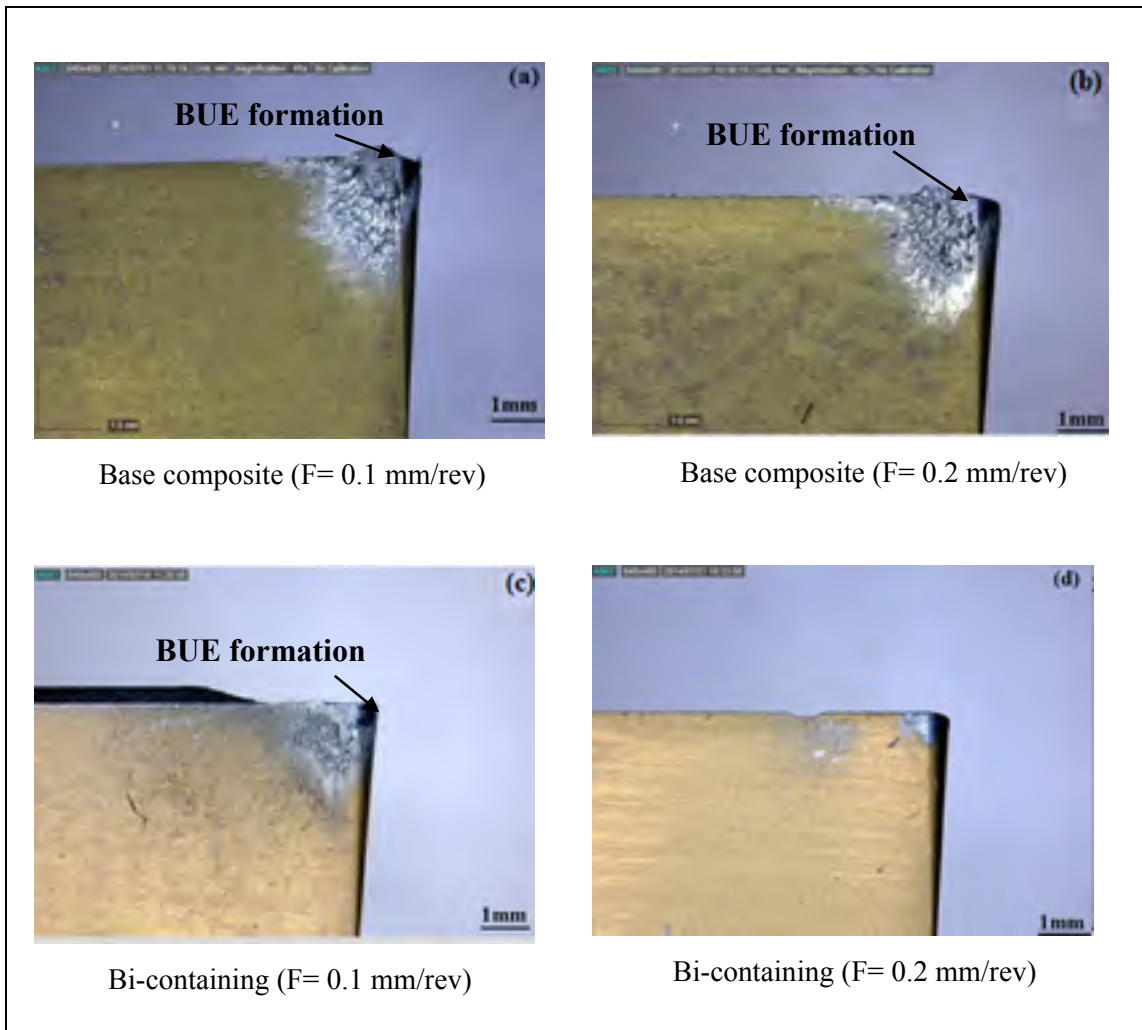


Figure 4.6 Images of inserts (BUE formation) at cutting speed of 270 m/min for (a,b) base composite, and (c,d) Bi-containing composite

Figures 4.7 and 4.8 show backscattered electrons (BSE) and elemental mapping for both composites. The existence of Bi distributed in the microstructure (white particle) was

observed in Figure 4.8. BSE microscopy revealed that Bi particles appear as precipitation due to the low solubility of the Bi in aluminum, which is around 0.3 wt.% at 658 °C. Therefore, the Bi particles are melted due to their low melting point and act as a kind of lubricant when machining composite. Bismuth has also been introduced as a free-machining element (FME) to improve the machinability of aluminum alloys (Ozcatlbas, 2003).

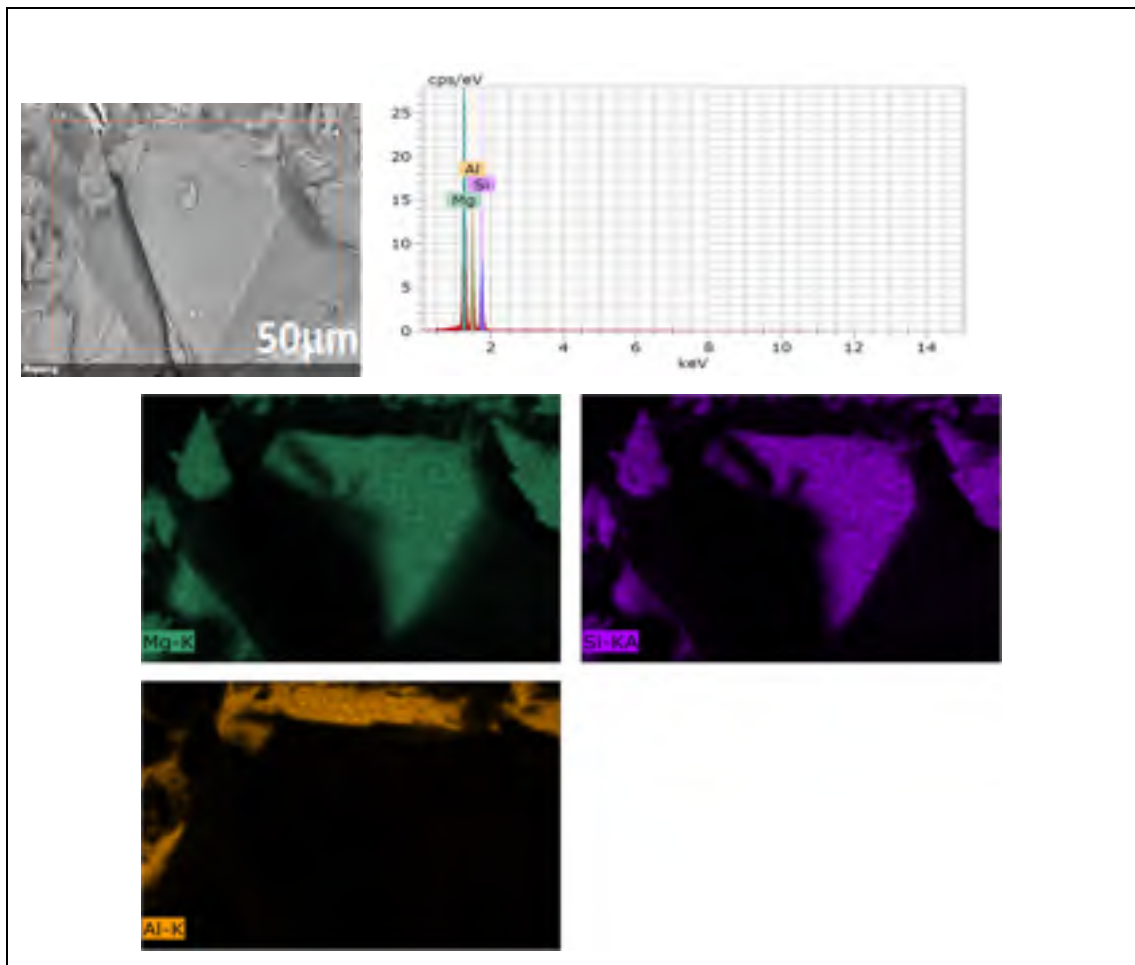


Figure 4.7 BSE image of Al-20Mg<sub>2</sub>Si and elemental mapping

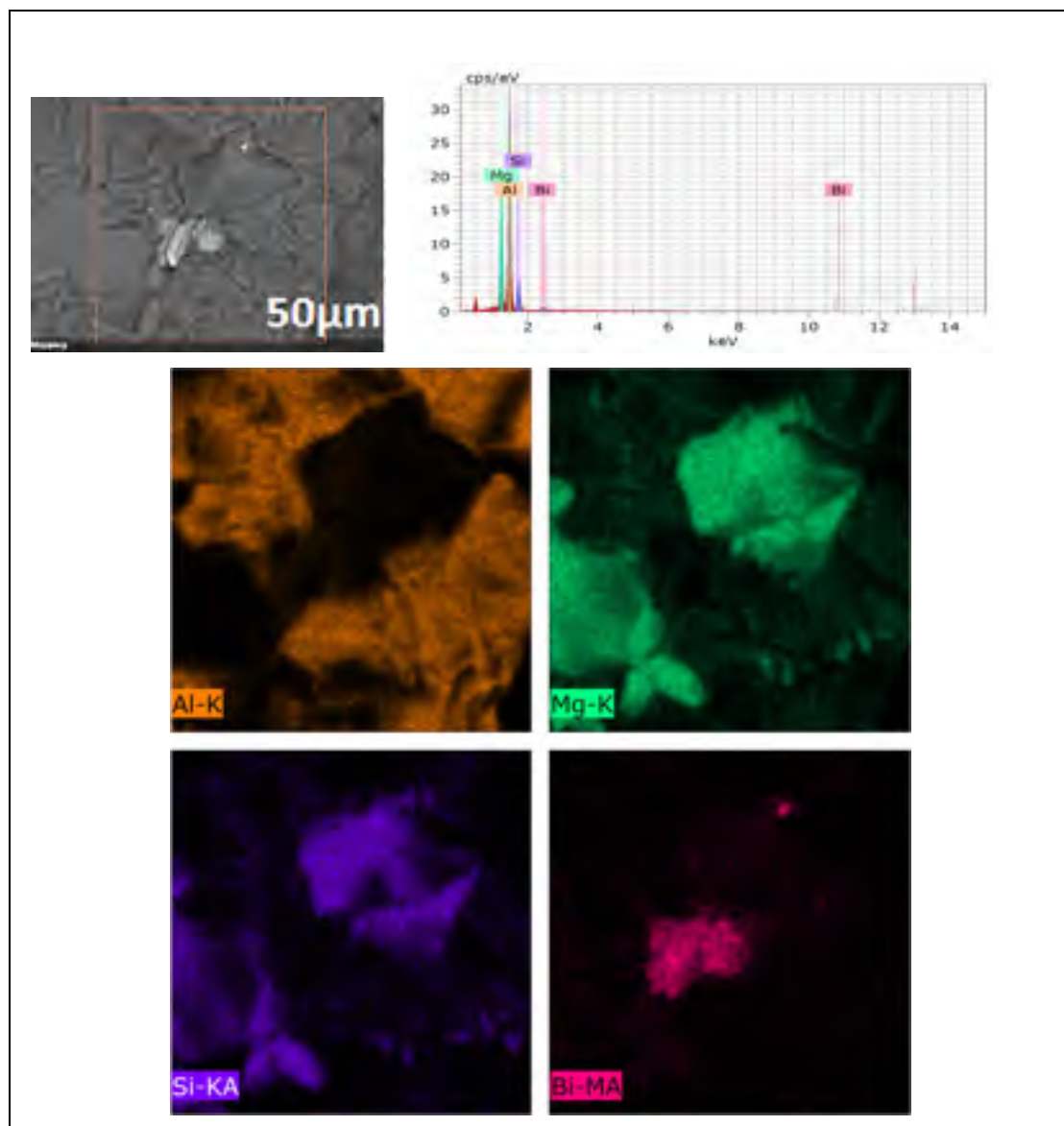


Figure 4.8 BSE image of Al-20Mg<sub>2</sub>Si and elemental mapping indicating Bi white compound

#### 4.5.2. Surface roughness

Figures 4.9a and b show the influence of cutting speed and feed rate on arithmetic average surface roughness. The surface roughness (Ra) is the most common index for determining surface quality in machining process. In addition, roughness average (Ra) is more common than the Rt and Rz values because it is considered the averages of peaks and valleys on the surface.

As expected, the best surface roughness value obtained was just below 2  $\mu\text{m}$  for Bi-containing composite at highest cutting speed (270 m/min) and lowest feed rate (0.1 mm/rev). The surface roughness value increased when the feed rate increased from 0.1 to 0.2 mm/rev for both workpieces, as is usually observed in machining. It was due to a distance between the peak and valley of the machined surface that had been made by the domination of feed mark at higher feed rates.

On the other hand, most irregular shape of  $\text{Mg}_2\text{Si}$  particles come to the machined surface during machining of the base composite and high energy is required to pull them out from the surface after connecting the particles to the insert tool, consequently increasing the cutting force and surface roughness values.

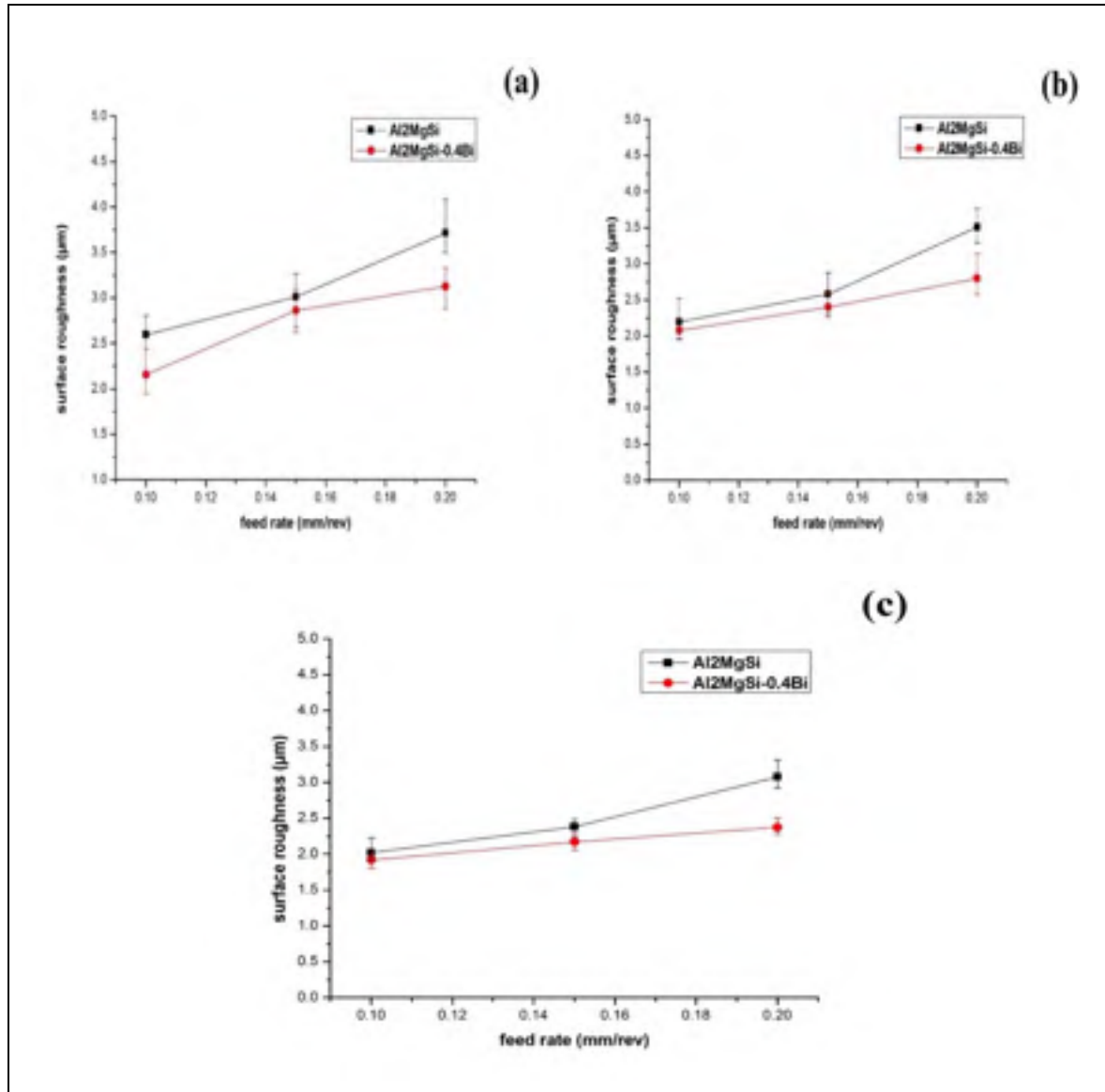


Figure 4.9 Surface roughness value with feed rate at cutting speed of (a) 90 mm/min (b) 180 m/min and (c) 270 m/min.

An infinite Focus (optical 3D micro coordinate measurement system) was used to acquire a deeper understanding of surface roughness in machining process (Figures 4.10a and b). As

can be seen in Figure 4.10a that the distance between peak and valley is higher for the base composite than for the Bi-containing composite (Figure 4.10b) which leads to voids on the machined surface and deteriorates the surface roughness value.

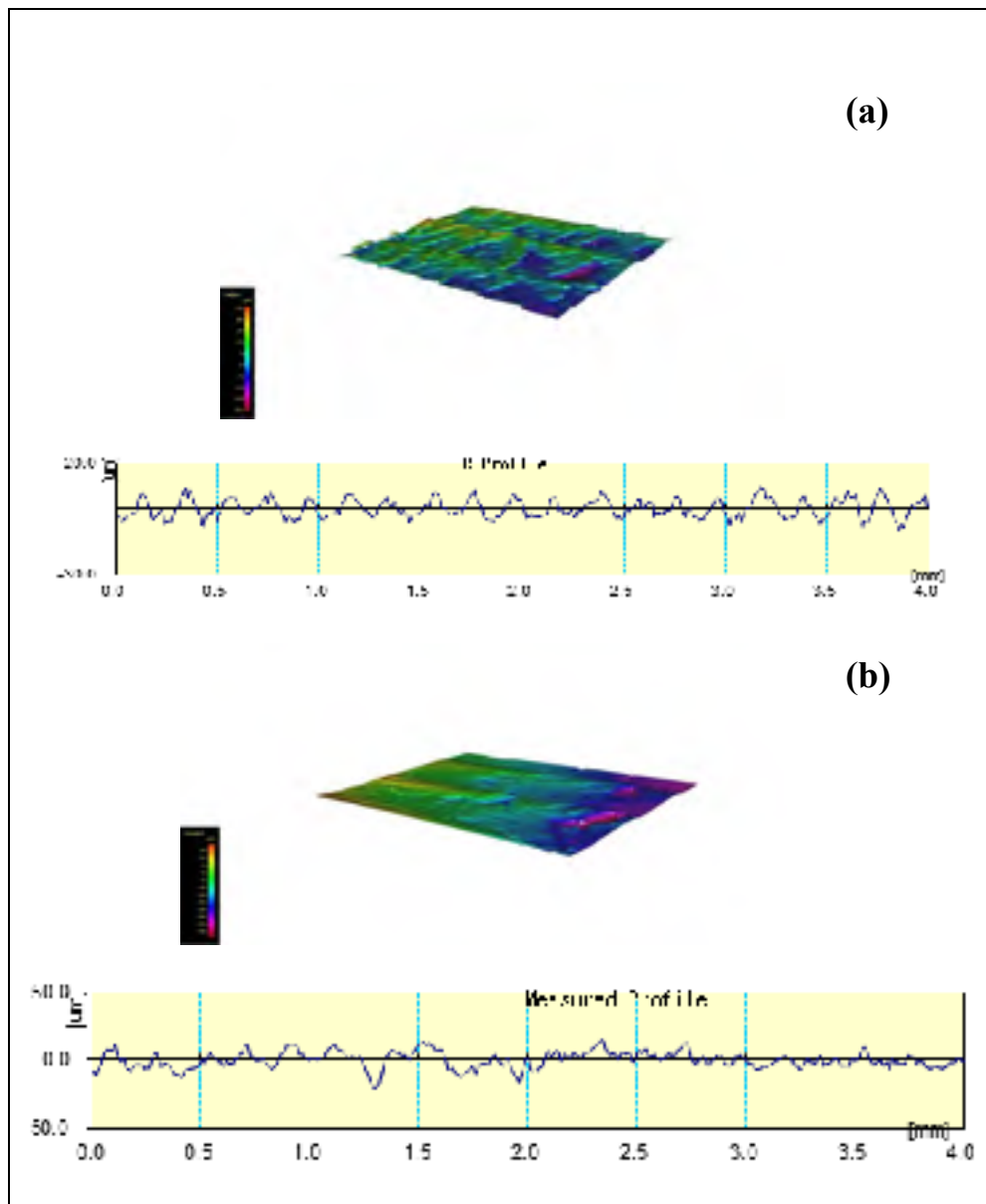


Figure 4.10 Optical 3D micro coordinate system (a) base composite (b) Bi-containing composite.

Figures 4.11a, b, c, and d show the SEM of the machined surface for both workpieces at the lowest and highest cutting speeds. More surface tearing is observed on the machined surface for the base composite (Figures 4.11a and b) than for the Bi-containing composite at different cutting speeds. It can be related to the coarse primary  $Mg_2Si$  particles that are in the microstructure of the workpieces. In fact, machining hard  $Mg_2Si$  particles was associated with stress relaxation of tool cutting edge ( Farahany *et al.*, 2014), which increased the surface roughness value due to the pull-out of primary  $Mg_2Si$  particles. In addition, some cavities and depths were formed on the machining surface, leading to poor surface finish.

In contrast, Bi particles decreased friction between the chip and the tool (with melting in cutting zone) to improve the surface roughness value during the machining process. Less surface tearing is evident at both cutting speeds in Figures 4.11c and d. The addition of Bi into the composite decreased the built-up edge (BUE) by increasing particle density in the matrix. It has been found that reinforcements have a direct effect on the quality of surface roughness through the size, shape and volume fraction in the microstructure of workpieces (Gaitonde *et al.*, 2012).

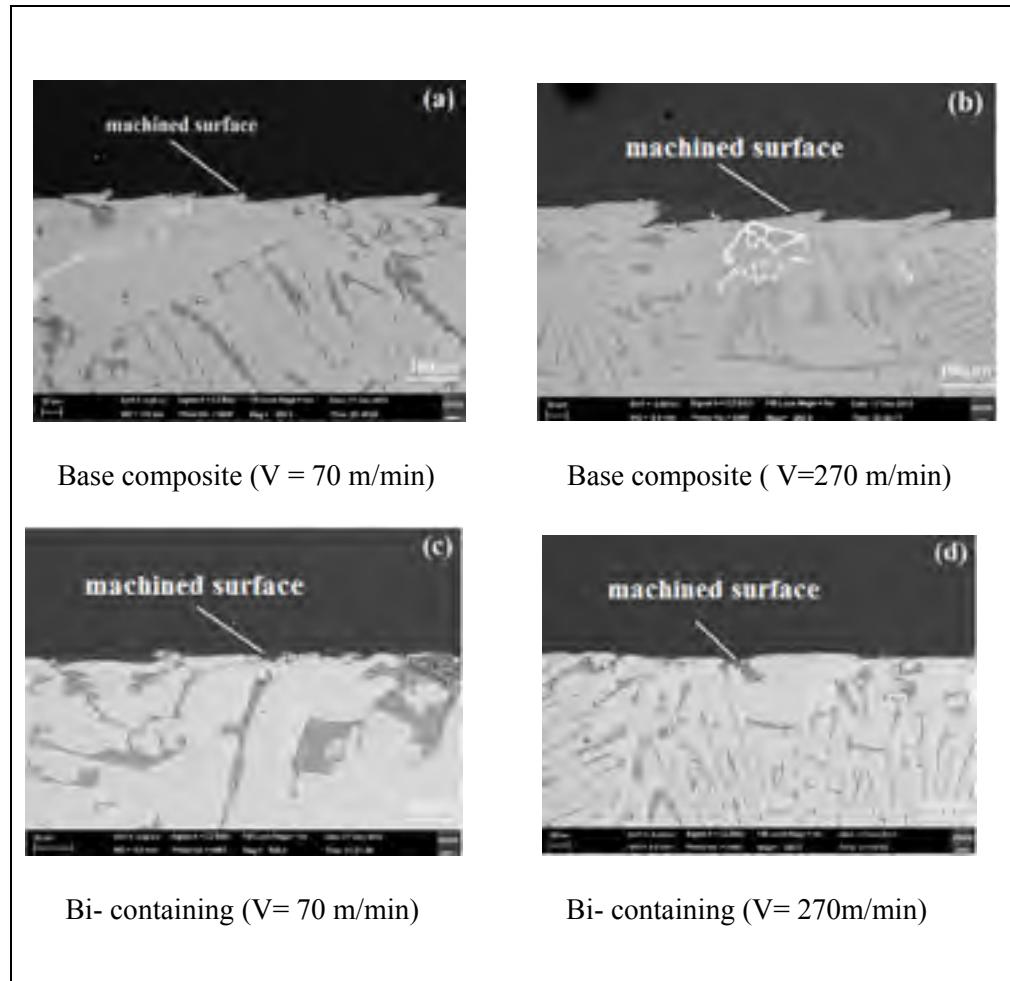


Figure 4.11 Scanning electron image of machined surface (a) and (b) for Base composite, (c) and (d) for Bi-containing composite

#### 4.5.3. Chip morphology

It has been concluded that ductility, thermal conductivity, and microstructure of workpiece influence chip formation. Figures 4.12a to f illustrate the chip shapes formed when machining the base composite and the modified composite at a cutting speed of 270 m/min and feed rates of 0.1, 0.15 and 0.2 mm/rev. It is observed that very short and irregular chips

formed at 0.1 mm (the lowest feed rate) and long chip formed at higher feed rates (from 0.1 to 0.2 mm/rev) for both workpieces. It has been reported that continuous chips are forced to curl due to unequal strain in the plastic zone (Kumar et Satsangi, 2013).

As can be seen in Figures 4.12a, b and c, the base composite produced a large chip with no tendency to curl due to the brittle nature of the primary  $Mg_2Si$  particles. It is worth mentioning that MMC has high strain while passing through the primary and secondary zone (Rai, Datta, Chakraborty, & Chattopadhyay, 2006). Segmented chips were produced when machining the Bi-containing composite (Figures 4.12d, e, and f). It can be related to the constraints imposed on the uniform plastic deformation of the ductile aluminum matrix by the small brittle  $Mg_2Si$  particles along the shear zones. These segmented chips increase chip breakability and improve the machinability of the composite. In fact, Bi acts as a lubricant by making a boundary layer between the tool and workpiece and improves the machinability of the composite. Rabinovich *et al.* (2011) found that elements with low melting points are able to provide wettability during the machining process, consequently improving the machinability of the composite (Figure 4.13).

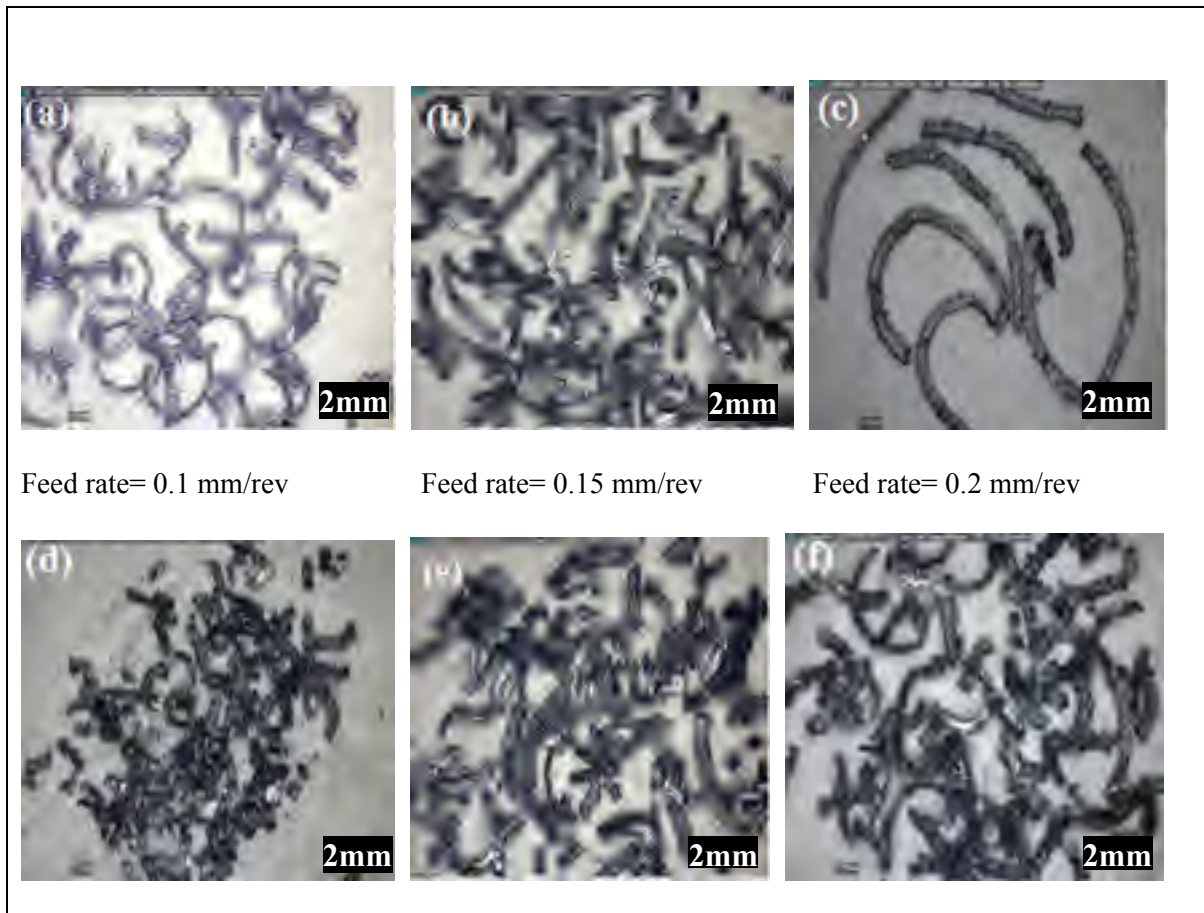


Figure 4.12 Optical images of the chip formed (a, b, c) for base composite and (d, e, f) Bi-containing composite

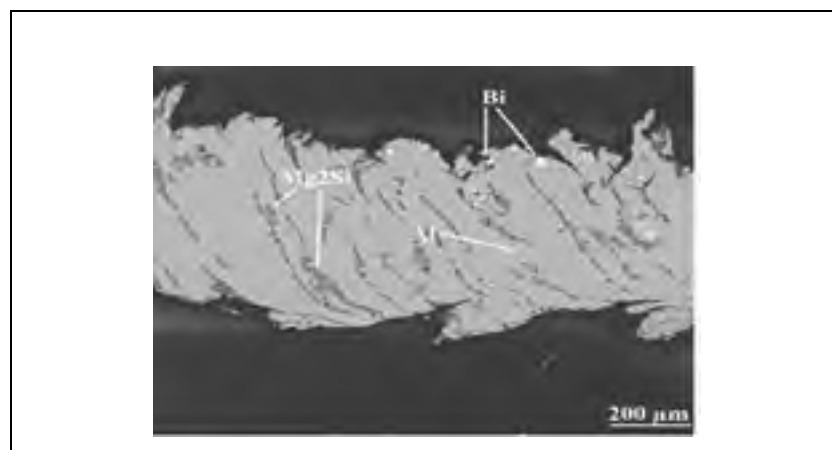


Figure 4.13 SEM micrograph of chip formation for Bi-containing composite

#### 4.6. Conclusion

This paper presents machinability and mechanical properties of Al-20Mg<sub>2</sub>Si metal matrix composites (one containing Bi). The following conclusions can be made:

- The structure of primary Mg<sub>2</sub>Si changed from a coarse to a fine shape with the addition of Bi. Moreover, the flake-like eutectic morphology became lamellar-shape. The addition of Bi decreased the average particle size from 180.1 μm to 113.5 μm.
- A number of decohered particles were observed on fracture surfaces, thereby increasing the composite's ductility (EI%), and hardness by 75%, and 23% respectively with the addition of Bi.
- The addition of Bi improved the machinability of the composite. Bi acted like a lubricant by making a boundary layer between the tool and workpiece and improved chip breakability and surface roughness values. Bi decreased BUE formation and cutting force during the machining process.

## CHAPTER 5

# EXPERIMENTAL INVESTIGATION ON MICROSTRUCTURE, MECHANICAL PROPERTIES AND DUST EMISSION WHEN MILLING Al-20Mg<sub>2</sub>Si-Cu METAL MATRIX COMPOSITE WITH MODIFIER ELEMENTS

Mohsen Marani<sup>1</sup>, Victor Songmene<sup>1</sup>, Jules Kouam<sup>1</sup>, Yasser Zedan<sup>1</sup>,

<sup>1</sup>École de Technologie Supérieure (ÉTS), 1100 Notre-Dame Street West, Montréal (QC)  
H3C1K3, Canada

Paper published in the journal of Advanced Manufacturing Technology, 99.1-4 (August, 2018): 789-802, Springer

### 5.1. Abstract

Sustainable manufacturing regulations are pushing manufacturing towards decreasing of manufacturing hazards including micro particles and ultrafine particles. Machining process such as milling produces dust that can be harmful for operators' health. The emission of this dust depends on workpiece materials (microstructure, mechanical properties) and machining conditions. The aim of this paper is to determine the effect of the microstructure and machining conditions on dust emission during dry milling of Al-20Mg<sub>2</sub>Si-2Cu metal matrix composite with addition of bismuth (Bi) and barium (Ba). Experiments were carried out using dry CNC milling by uncoated carbide tools. An aerodynamic particle sizer (APS) and a scanning mobility particle sizer (SMPS) were used to measure micro particles and ultrafine particles emission, respectively. It was found that the addition of 0.4%wt Bi and 0.2%wt Ba changed Mg<sub>2</sub>Si particle size and improved the hardness of composite. In addition, ultrafine particles number concentration, specific area concentration and mass concentration decreased

with the addition of modifiers. It was confirmed that cutting conditions and microstructure of workpieces have a direct effect on dust emission during the milling process.

**Key words:** composite, microstructure, bismuth, barium, fine particles, ultrafine particles.

## 5.2. Introduction

In recent years, sustainable manufacturing has been considered as an important goal in different industrial fields due to its financial and environmental benefits. In fact, sustainable manufacturing is able to play a linking role between the driven economy and the technology together by the main goal of a green world (Bordin *et al.*, 2017) . From the sustainability performance and machining points of view, some factors such as economic, environmental, and social impacts have been mainly considered for evaluation (Goindi et Sarkar, 2017).

It has been confirmed that there is a high demand to switch over to green manufacturing techniques (Cai *et al.*, 2017). There are some suitable methods for converting materials into finished products such as reducing environmental emissions and contamination, reducing the consumption of earth's natural resources energy (Schultheiss *et al.*, 2017). The mentioned methods are considered as aims of sustainable manufacturing and need to be developed (Schultheiss *et al.*, 2013).

Zaghbani *et al.* (2009) investigated fine and ultrafine particle characterization in high-speed Milling 6061-T6 Aluminum alloy. They found that shearing zone is the main source of dust emission during machining. It was concluded that wet milling process produced more aerosols than dry milling for the submicron size range. They reported that machinability of alloys has produced fine and ultrafine particle emission which is harmful to operators.

Kamguem *et al.* (2013) studied surface finish and metallic particle emission during machining of aluminum alloys. They found that TiCN-coated tool generated fewer respirable airborne particles than multilayers (TiCN+Al<sub>2</sub>O<sub>3</sub>) and reduced dust generation during machining .

Particle emission is an important issue during machining metal matrix composite. It has been reported that nanoparticles can be harmful when absorbed by body cell (Zhang, *et al.*, 2000). Oberdorster *et al.* (2005) found that some inert particles could become biologically active when their dimensions are reduced to the nanometre scale. Ostiguy *et al.* (2006) reported that the first particularity of nanoparticles is their pulmonary deposition modes which are more dangerous than the deposition modes of microparticles.

Elder *et al.* (2004) found that nanoparticle toxicity is in direct relation to their number and specific surface and mass concentration. With the recent results published on nanoparticles and how harmful they are, it is, therefore, necessary to know all size ranges particles produces during machining metal matrix composites. However, in the case of open machining which is related to large-scale parts, there are still some risks on particle emission during the machining process.

Development of high-speed machining of die casting materials improved capabilities in the forming industries. In fact, machining of casting alloy is known as a highly efficient machining method due to higher demands for the use of the casting materials (Fadavi *et al.*, 2015). Minimizing waste streams in machining industries is necessary due to the enforcing governmental laws related to pollution, preventing initiatives and norms (Mulyana *et al.*, 2017).

Some machining environments such as cryogenic cooling (Bordin *et al.*, 2017), minimal quantity of lubrication (MQL) (Deiab *et al.*, 2014), flood technology (Shokrani *et al.*, 2016), and dry machining (Kaynak *et al.*, 2014) have been considered to minimize dust emission in machining process. From the ecological aspects of cutting fluids, the release of harmful substances into the environment and hazardous working conditions has been considered a major cause of diseases for industrial workers. Inhalation of cutting fluids loaded with biocides and toxic metal particles would be a major cause of cancer (Songmene *et al.*, 2018). In this regards, respiratory conditions such as a cough, bronchitis, and asthma are common illnesses.

A significant amount of energy and machining cost is needed for the equipment which works with cutting fluids (Kadam et Pawade, 2017). Therefore, researchers have considered machining components without cutting fluids. In today's modern manufacturing system dry machining is becoming popular. Dry machining is also classified as an environmentally friendly technique (Debnath *et al.*, 2014).

Al-20Mg<sub>2</sub>Si metal matrix composites are widely employed in the aerospace and automotive industries due to high wear resistance, low specific weight and low thermal expansion (Marani *et al.*, 2017). The composite stands out recently to be commonly used material instead of aluminum. However, the mechanical properties of the composite need to improve due to the brittle of Mg<sub>2</sub>Si particles by controlling the primary Mg<sub>2</sub>Si particles (Azmah *et al.*, 2013).

Modification of microstructure by the addition of some modifier elements improved mechanical properties of the Al-20Mg<sub>2</sub>Si composite (Kadam et Pawade, 2017; Debnath *et al.*, 2014). The mentioned method also has a direct effect on the machinability of the

composites. Lee et Yoon (2014) investigated properties of alumina matrix composite reinforced with SiC whisker. They found that the addition of SiC whisker to  $Al_2O_3$  improved the mechanical properties of Inconel 718 significantly, and flexural strength improved more than 60% compared to unmodified composite.

Azarbarmas *et al.* (2011) reported that the addition of 0.3% boron to Al15%Mg<sub>2</sub>Si decreased the average size of primary particles from 23  $\mu\text{m}$  to 5  $\mu\text{m}$ . It was found that ultimate tensile strength and elongation value increased by the addition of 0.3% boron from 252 to 273 MPa and 2.2% to 3.7%, respectively. Barzani *et al.* (2015) studied the machinability of Al-Si-Cu cast alloy containing bismuth and antimony. It was found that Bi-containing composite improved surface roughness and decreased cutting force compared to Sb-containing composite. Wright, (2000) reported that addition of lead in bras reduced the cutting forces and made shorter chips and decreased the tool wear. This could be related to the role of lead as an internal lubricant during the machining process.

Farahany *et al.*, (2015) reported a potential improvement for using Bi-containing alloy. On the basis of these considerations, dry milling can be implemented as clean production to the machining of Al-20Mg<sub>2</sub>Si metal matrix composite. No dedicated study has been conducted on microstructure evaluation and particle emission during the milling process. Therefore, the presented research is aimed to study the microstructure, mechanical properties, and particles emission when Al-20Mg<sub>2</sub>Si metal matrix composite containing bismuth or barium as modifier elements.

### **5.3. Experimental setup**

#### **5.3.1. Work material and tooling**

A commercial alloy, pure aluminum (99%) and pure magnesium (99%) were used as starting materials. The materials were melted to manufacture Al20%Mg<sub>2</sub>Si ingot. A resistant furnace was used in order to melt a 2 kg ingot in a silicon carbide crucible at a temperature of 750±5 °C. Two different elements including bismuth (Bi) and barium (Ba) in the form of pure metallic were added separately into the melt as agent elements. The addition levels were 0.4wt% and 0.2 wt%, respectively. Dissolution and homogenization were performed in 15 min. In addition, the molten alloy was stirred and the surface was skimmed. For pouring the molten alloy, a rectangular ceramic mold with 30 mm length and 25 mm wide was used. For tensile tests, an ASTM-B77 size specimen was used. A computerized testing machine was used for tensile tests at a strain rate of 1 mm/min at room temperature.

#### **5.3.2. Machining tests**

Table .51 shows the chemical composition of Al-20Mg<sub>2</sub>Si metal matrix composite used for the present study. The experiments were carried out on a computer numerical control (CNC) HURON-K2X10 milling machine (spindle speed (N): 28000 rpm, power (P): 50 kW and Torque (T): 50 Nm) using uncoated insert (Iscar IC28). Table .52 is shown details of the cutting tool and tool holder. Different cutting speeds and feed rates were used with 1 mm depth of cut. Table .53 shows the cutting conditions and parameters used during the experiments.

A three-component piezoelectric dynamometer (KISTLER, 9255B) was used to recorded cutting forces during machining. The Kistler was connected to the charge amplifiers (type 5010). All signals were independently monitored, digitized and recorded into a LabView where Cut Pro 8.0 software was used in order to force measurements. The cutting force signals were exported to Matlab for further analysis. All cutting conditions were selected based on the tool factory's recommendations for the metal matrix composite. Metallographic specimens were ground and polished using standard routine techniques. Microstructures were analyzed using a laser scanning digital microscope (LEXT OLS4100) and scanning electron microscope (SEM) equipped with energy dispersive spectroscopy (EDS).

Table 5. 1            Composition of Al20%Mg<sub>2</sub>Si composite

Al	Si	Fe	Cu	Mn	Mg	Cr	Zn
Wt%	7.07	0.64	2.034	0.217	12.710	0.034	0.614
Bal							

Table 5. 2            Cutting tool and tool holder

Nose radius	Relief angle	Rake angle	Tool type	Tool holder
0.5mm	0.2°	0°	Uncoated	HM90 E90A-D75-3W.75

Dust sampling was performed by suction of air from the cutting area during machining process using an aerodynamic particle sizer (APS- model 3321, TSI, Inc) with particle size ranging from 0.5 to 20 µm and a scanning mobility particle sizer (SMPS- model #3080 TSI, Inc) to measure ultrafine particles from 7 to 100 nm during machining process. The SMPS was connected to lumps of collection using a suction pipe at a flow rate of 1.5 l/min from the cutting area. Particle number concentration, specific area concentration, and mass

concentration were measured as the function of particle aerodynamic diameters by mentioned instruments. The experimental scheme is illustrated in Figure 5.1.

Table 5.3 Cutting conditions and parameters

Cutting speed $V_c$ (m/min)	300	700	1100
Feed rate $V_f$ (mm/tooth)	0.1	0.15	0.2
Depth of cut $D$ (mm)	1		
Workpiece materials	Al-20Mg <sub>2</sub> Si-2Cu Al-20Mg <sub>2</sub> Si-2Cu + 0.4Bi Al-20Mg <sub>2</sub> Si-2Cu+ 0.2 Ba		

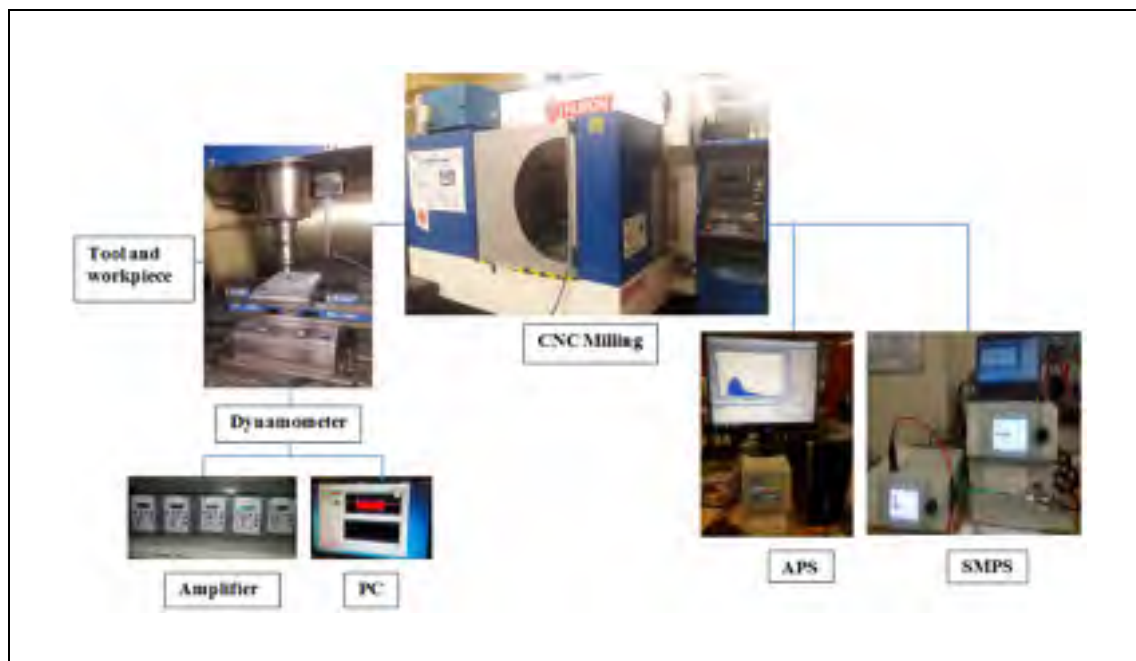


Figure 5.1 Schematic representation of machining and dust sampling system

## 5.4. Results and discussion

### 5.4.1. Microstructure and mechanical properties

Figure 5.2 shows a typical microstructure of cast Al20%Mg<sub>2</sub>Si-2Cu composite. Figure 5.2 (c, f, i) shows the electronic diffusion spectroscopy (EDS) of the composite to find out the elements in the microstructure of workpieces. As can be seen in Figure 5.2 (a, b), the microstructure shows coarse primary Mg<sub>2</sub>Si particles and eutectic Mg<sub>2</sub>Si flake-like shapes, respectively. Three parameters such as size, density, and aspect ratio were measured to evaluate the effect of Bi and Ba concentrations. Three mentioned factors were calculated as follows:

$$\text{Mean size} = \frac{1}{m} \sum_{j=1}^m \left( \frac{1}{n} \sum_{i=1}^n L_i \right)_j \quad (1)$$

$$\text{Mean density} = \frac{1}{m} \sum_{j=1}^m \left( \frac{1}{n} \sum_{i=1}^n D_i \right)_j \quad (2)$$

$$\text{Mean aspect ratio} = \frac{1}{m} \sum_{j=1}^m \left( \frac{1}{n} \sum_{i=1}^n \frac{a_i}{b_i} \right)_j \quad (3)$$

where  $L_i$ ,  $D_i$ ,  $a_i$  and  $b_i$  are the size, density, longest and shortest dimensions of single Mg<sub>2</sub>Si particle, respectively. In addition,  $n$  and  $m$  are the number of Mg<sub>2</sub>Si particles measured in a single field ( $1055800\mu\text{m}^2$ ), and the number of the evaluated fields, respectively.

The primary Mg<sub>2</sub>Si particles have been analyzed by an image analyzer and an optical microscope which might be useful for predicting material properties (Figure 5.3). The addition of 0.4%wt Bi decreased the average size of primary Mg<sub>2</sub>Si particles in Al-20%Mg<sub>2</sub>Si composite from 180.1 to 113.5  $\mu\text{m}$ . It is also found that the morphology of primary Mg<sub>2</sub>Si particles changed from a coarse shape to a fine polygonal shape (Figure 5.2e).

An increase in the number of  $Mg_2Si$  particles can reduce the size of  $Mg_2Si$  particles (Yusof *et al.*, 2016).

In addition, the mean aspect ratio decreased from 1.30 for the unmodified species to 1.15 after treatment. In fact, 0.4wt% Bi caused the highest number of particles (mean density) formed from 13 to 40 particle/ $mm^2$ . In a similar work, It has been reported that the addition of Bi changed the nucleation of  $Mg_2Si$  particles and improved the mechanical properties of composite (Nordin *et al.*, 2014).

The value of hardness increased from  $62\pm 2$  HV to about  $80\pm 3$  HV (Figure 5.4). The addition of 0.4% Bi provides more obstacles to grain boundary sliding and finally changed the morphology of eutectic Al- $Mg_2Si$  from flake like to lamellar shape (Marani *et al.*, 2017). According to Figure 5.2 (g and h), it is noticeable that the addition of 0.2%wt Ba changed  $Mg_2Si$  particles from coarse to polyhedral shape. The addition of Ba changed size, aspect ratio, and density of the particles. The average size of primary  $Mg_2Si$  particles decreased from 180.1  $\mu m$  in unmodified composite to 102.20  $\mu m$  after treatment. The particle size decreased about 43%. Aspect ratio also decreased around 8% from 1.30 to 1.20, while the number of particles density increased from 13 to 35 particle/ $mm^2$ .

However, the shape of primary  $Mg_2Si$  particles changed to polygonal shape, some particles still kept their rectangular form. In addition, structure of the eutectic  $Mg_2Si$  changed from flake-like in unmodified composite to fibrous form with the addition of 0.2%wt Bi which improved properties of the composite.

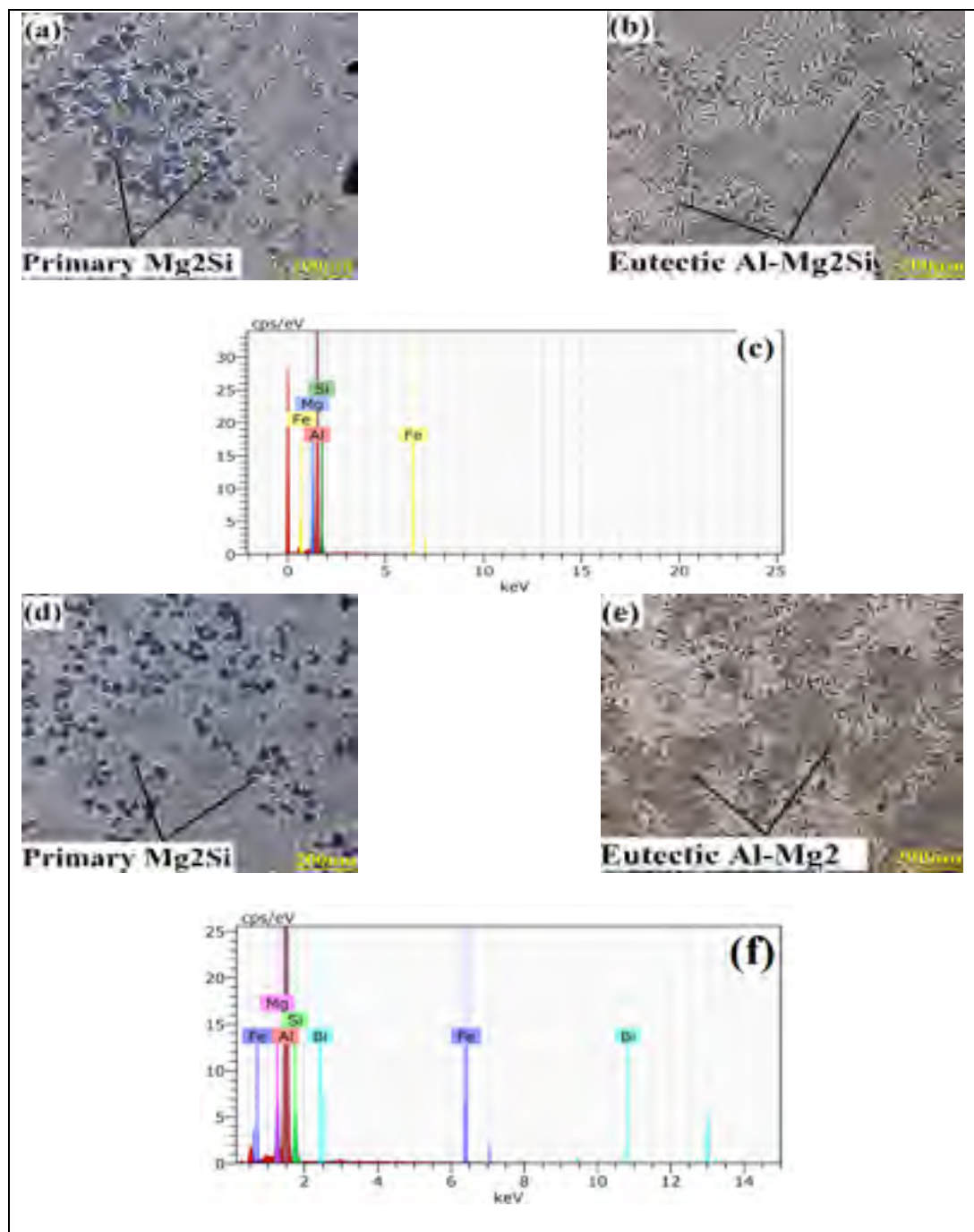


Figure 5. 2 Optical micrographs and EDS showing primary and secondary  $Mg_2Si$  for (a, b, c) Base composite, (d, e, f) Bi-containing, and (g, h, i) Ba-containing

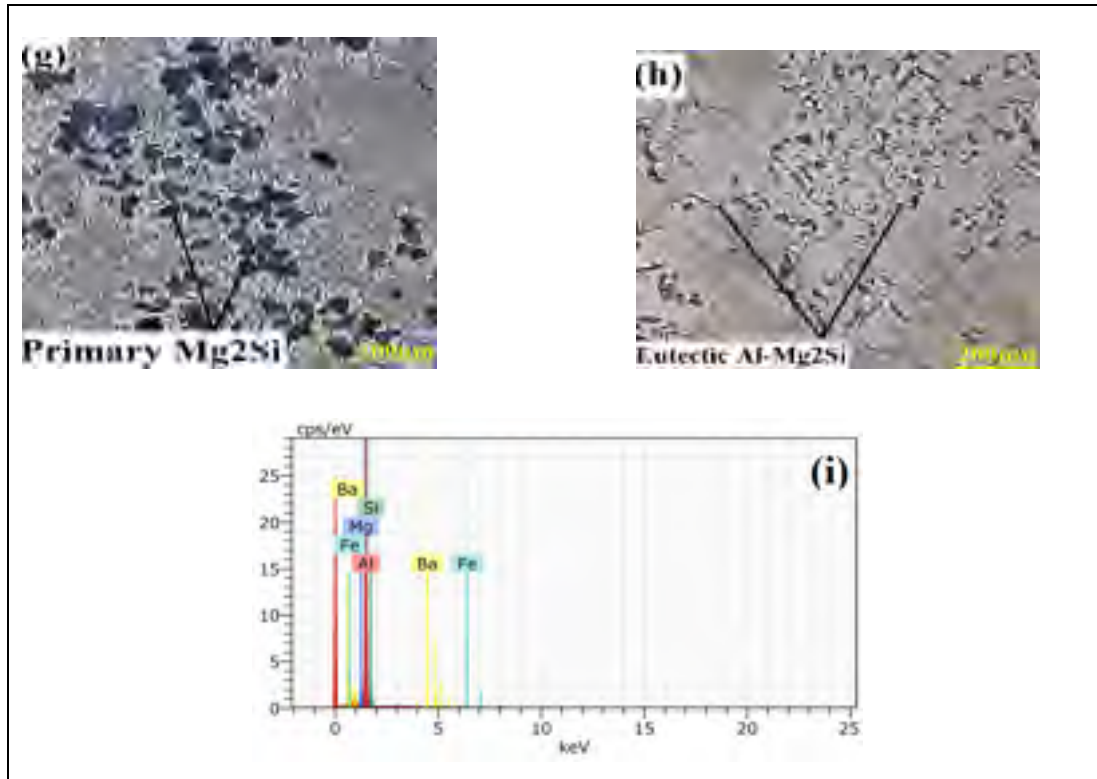


Figure 5.2 Continued

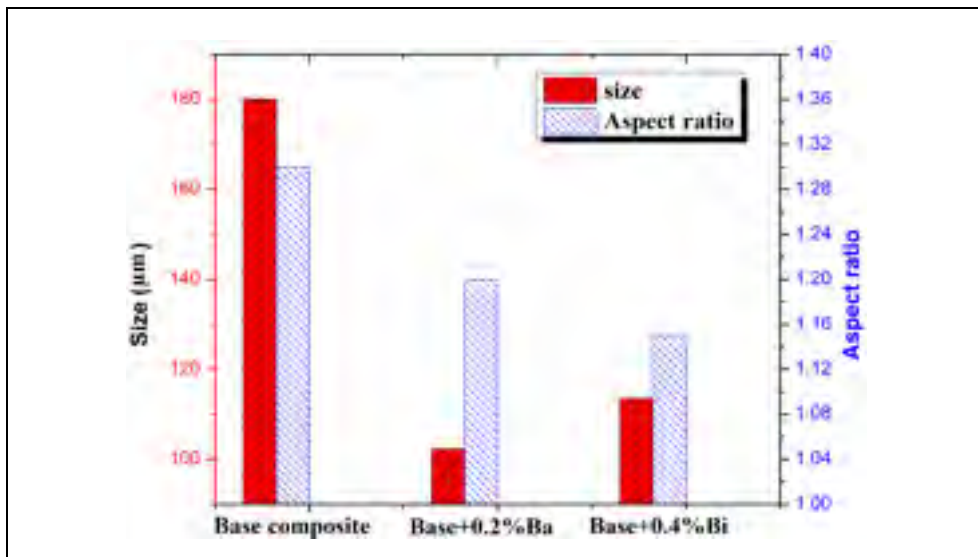


Figure 5.3 Comparison of size and aspect ratio of primary  $Mg_2Si$  for the base composite, Bi and Ba-containing

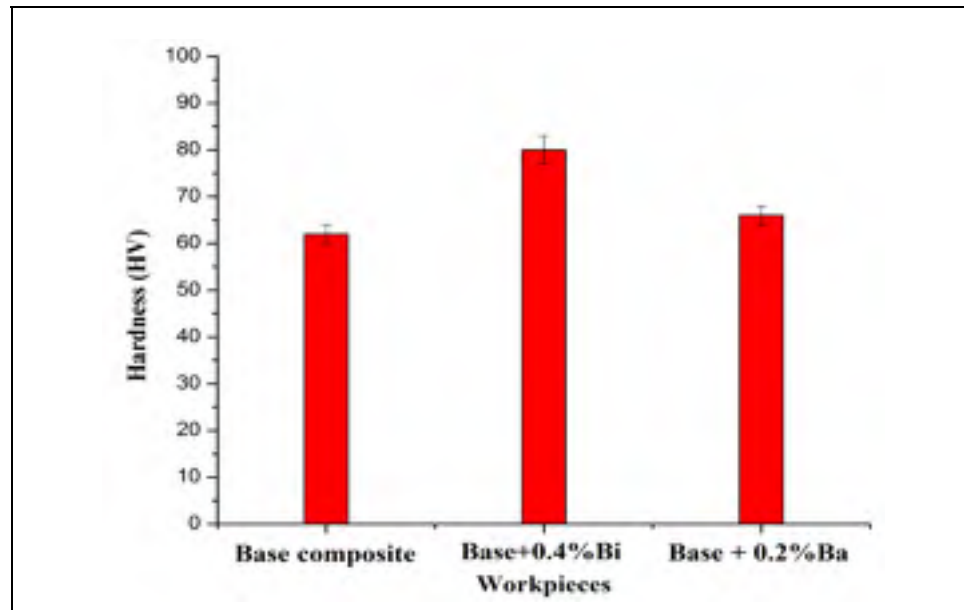


Figure 5.4 Vickers hardness values of base composite as a function of Bi and Ba-containing.

#### 5.4.2. Fractography

Figure 5.5 illustrates the variation of ultimate tensile test (UTS) and elongation (El) values for base composite, Bi-containing, and Ba-containing composite. As can be seen, the addition of 0.4% Bi and 0.2% Ba improved UTS and Elongation values. The UTS value for base composite was about 90.2 MPa which increased to 110.2 and 106.4 MPa with the addition of Bi and Ba, respectively. The base composite (Al-20Mg<sub>2</sub>Si) showed an El 62% and increased to 1.1% with the addition of Bi. The addition of 0.2%Ba also increased value of El from 62% (for base composite) to 0.95%. Farahany *et al.* (2016) reported that ductility increased when Mg<sub>2</sub>Si particles provide sites for fracture initiation by particle fracture and reduced local stress concentration for particle fracture by reduce local stress concentration.

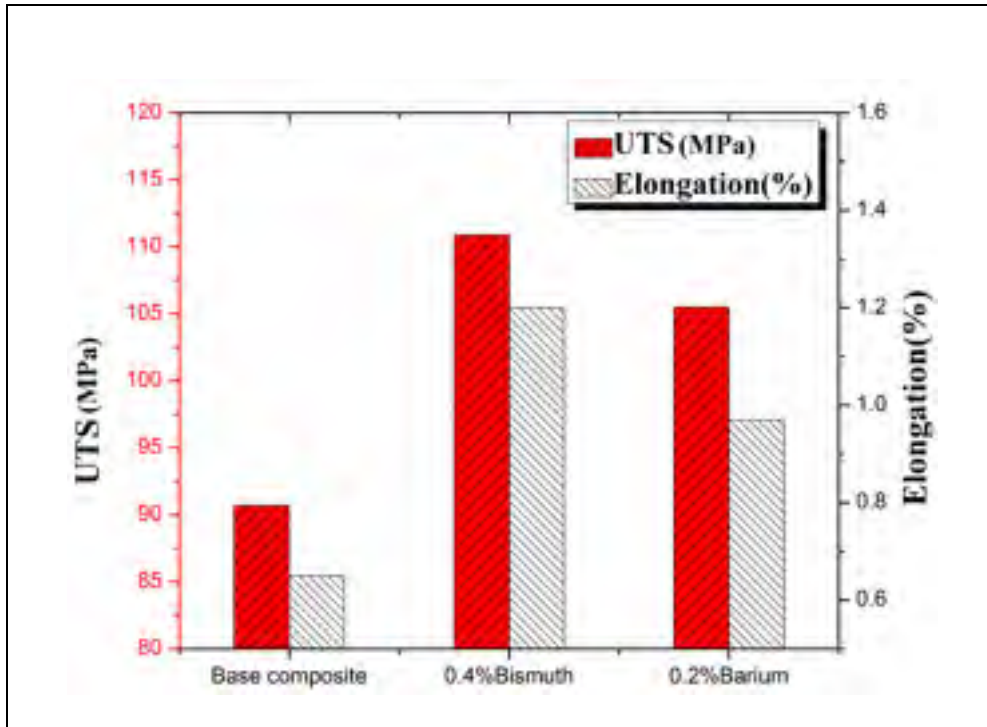


Figure 5.5 Variations of UTS and El values as a function of Bi and Ba-containing.

Figure 5.6 shows the fracture characteristics of tensile test samples for three workpieces under the SEM. As can be seen in figure 5.6a, the microstructure of specimen shows more decohered primary  $Mg_2Si$  particles which made microstructure more brittle. On the other hand, in brittle fracture most coarse  $Mg_2Si$  particles illustrate flat surface (cleavage facets). They are formed by the fracture of flake  $Mg_2Si$  eutectic structure and subsequently created a rapid fracture which derived from their intrinsic brittleness (Emamy *et al.*, 2013).

Specimens with Bi and Ba show a higher density of dimples on their fracture faces (Figure 5.6b and 5.6c). The modified composite contains several cracked particles and a few decohered primary  $Mg_2Si$  particles with less flat surface compared to base composite (Figure 5.6a). Indeed, there is a mixed fracture mode comprising of brittle and ductile fracture. The

microstructure of specimens illustrates more ductile mode of fracture. It has been reported that ductile fracture rupture initiates in material whereas voids generate and grow while stress regularly transferring to the particles and finally cavities unify by an internal necking mechanism to provide the dimple mode surface in ductile fracture (Nasiri *et al.*, 2012). It is also reported that Bi and Li addition into the composite changed the structure from brittle to ductile by convert cleavage fracture surface to fine dimples (Yusof *et al.*, 2016).

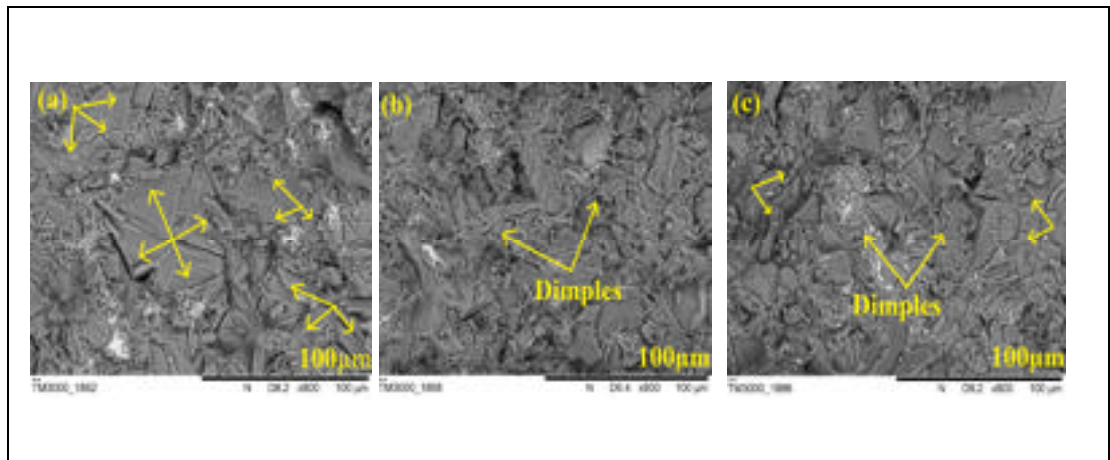


Figure 5.6 Fracture surface for (a) base composite (b) Bi-containing and (c) Ba-containing.

## 5.5. Dust emission

### 5.5.1. Fine particle emission during milling

Figure 5.7 presents the results of particle emission for the particle number, the specific area concentration, and mass concentration of fine particles as a function of aerodynamic diameter using an APS particle size ranging from, 0.5 to 10  $\mu\text{m}$  for all workpieces. In general, the results show that base composite produced particles with less specific surface and mass

concentration compared to modified composites. As can be seen in Figure 5.7a, the most emitted particles have an aerodynamic diameter around 1  $\mu\text{m}$ . It has been found that the particle sizes below 2.5  $\mu\text{m}$  would be harmful to human health (Kouam *et al.*, 2013).

Figure 5.7 (b and c) shows the particle emission for the specific area and the mass concentration, respectively. A high concentration (around 4  $\mu\text{m}$ ) is found for all workpieces. Therefore, it would be less harmful to human health compared to particles with a concentration less than 2.5  $\mu\text{m}$  which is considering a dangerous factor in the machining process (Kamguem *et al.*, 2013). The distribution of brittle  $\text{Mg}_2\text{Si}$  particles in the microstructure of workpieces is an important factor during the milling process (Azmah *et al.*, 2013). In fact, the high density of  $\text{Mg}_2\text{Si}$  particles provides a large contact surface between the tool and brittle  $\text{Mg}_2\text{Si}$  particles for modified composite during machining which lead to generating more particle emission. This result is in accordance with that found by Saidi *et al.* (2015).

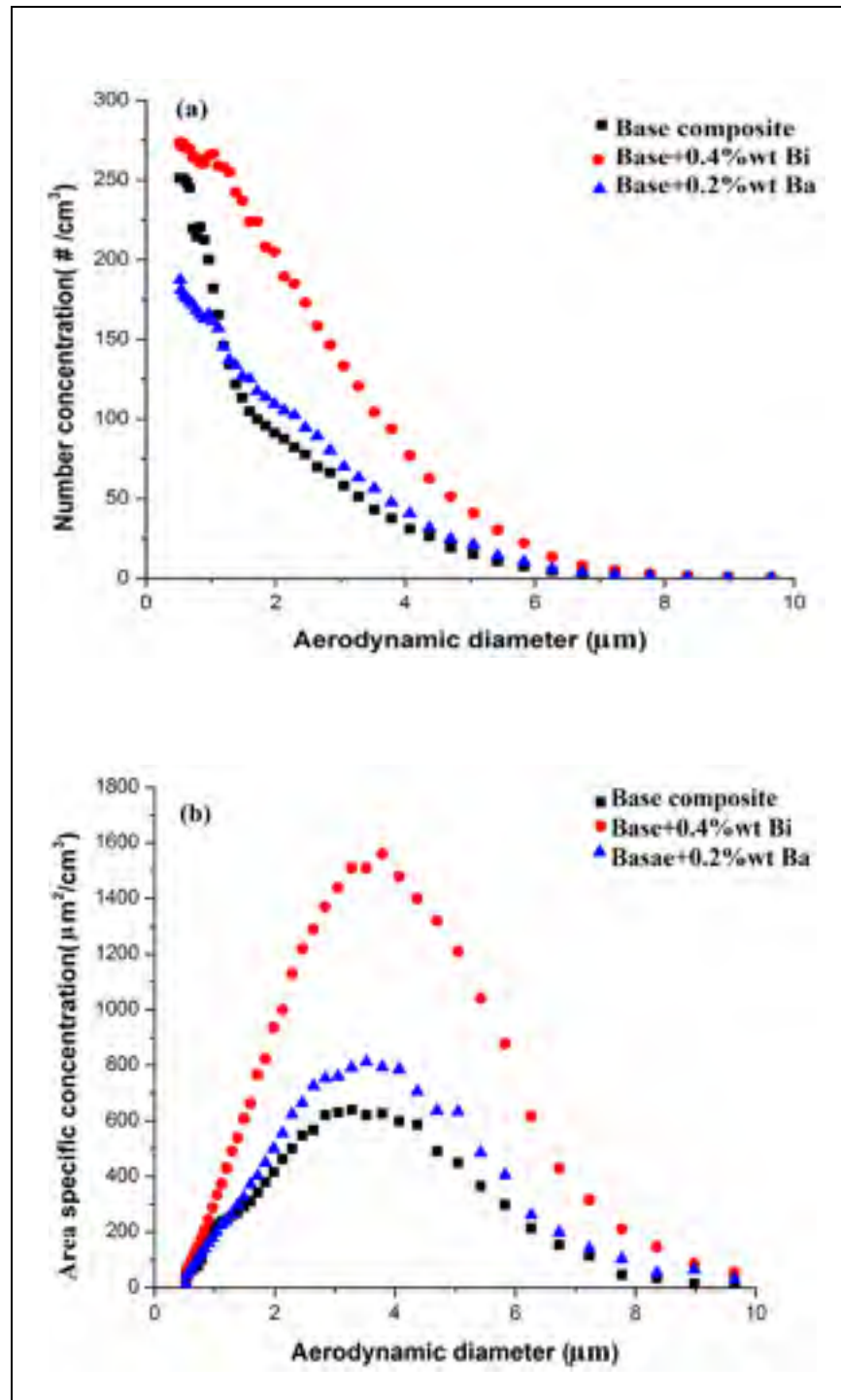


Figure 5.7

Comparison of (a) fine particle number concentration (b) specific area concentration and (c) mass concentration as function of diameter of particles at cutting speed of 700 m/min and feed rate of 0.2 mm/tooth

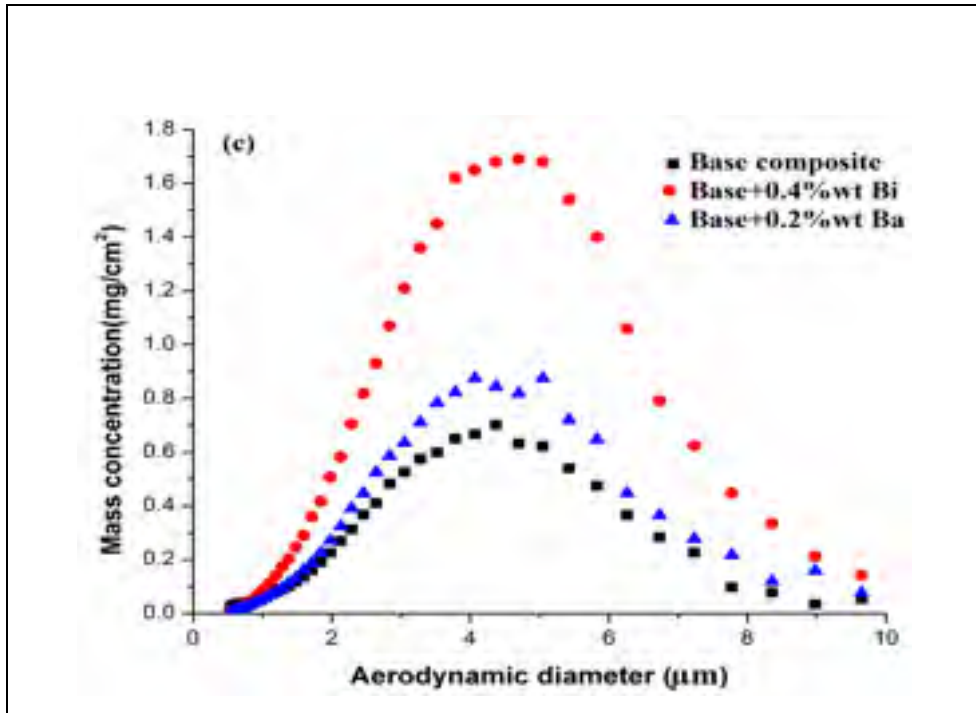


Figure 5.7 Continued

Figure 5.8 shows the distribution of the total fine particle number concentration, specific area concentration, and mass concentration as a function of cutting speed during the milling process. The amount of emitted particle (number concentration) is low at low cutting speed (300 m/min) for all workpieces and it then increased and reached the maximum value at cutting speed of 700 m/min and eventually decreased with increasing cutting speed (Figure 5.8a). In a similar work on the friction test, it was found that particle emission increased with increasing the speed and then eventually decreased (Nasiri *et al.*, 2012).

Two-speed regimes are observed for emitted particles. The first regime is between cutting speed of 300 to 700 m/min and the second regime is between cutting speed of 700 to 1100 m/min. As can be seen in Figure 5.8 (b, and c), the same trend is observed with the specific area concentration and mass concentration, respectively. When the cutting speed increased,

the temperature in the primary and secondary shear zones increase as well, after which the mechanical properties fall when a critical speed is reached. This situation applies in the case of ductile materials ( Khettabi *et al.*, 2010).

Songmene *et al.* (2004) reported two different zones corresponding to low and high cutting ranges, respectively, in which the dust emission is low, at low and high cutting speed and high dust emission seen between the two zones. This tendency was also confirmed by Khettabi *et al.* (2007) in turning of aluminum alloys. The result was also confirmed in this work during the dry milling metal matrix composite (Figure 5.8).

It has been concluded that particle production is a phenomenon which is related to chip formation mode. In fact, the friction in the chip shearing zone, which produce a lot of particles, taking place in the chip (Khettabi *et al.*, 2010). At low cutting speeds, the chip crack is controlled by its brittleness (Dabade et Joshi, 2009). Therefore, there is no contact and friction between its lips due to the crack opens. At intermediate speeds, the slip planes are localized, and their density increase as well as friction between the lips (Shahrom et Yusoff, 2014).

At high cutting speeds, the generation of fine particles tends to decrease due to the low density of segmentation and delocalized of plastic deformation as reported by Zaghbani *et al.* (2009) during the machining of 6061-T6 aluminum alloy at cutting speed ranging from 300 to 900 m/min. Therefore, machining of the composite is recommended at high cutting speed due to decrease dust emission, which is suitable for the environment and worker health.

Untreated composite generated less fine particle emission compared to treated composites. It can be explained based on the microstructure of the workpieces. It was found that hardness of

workpiece has a direct effect on the particle emission during the machining process as well as deformability the matrix and shape of particles (Djebara *et al.*, 2013). The addition of Bi and Ba into the composite improved hardness value from  $62\pm 2$  HV to  $80\pm 3$ , and  $66\pm 2$  HV, respectively (Figure 5.4). Increasing hardness provides an abrasive action on the tool cutting edge (between the tool, and  $Mg_2Si$  particles) and there is a high level of dust emission level during machining process. This action was achieved by Kamguem *et al.* (Kamguem *et al.*, 2013) when milling of aluminum alloys. Balout *et al.* (2007) found that ductile materials generate more fine dust than brittle materials.

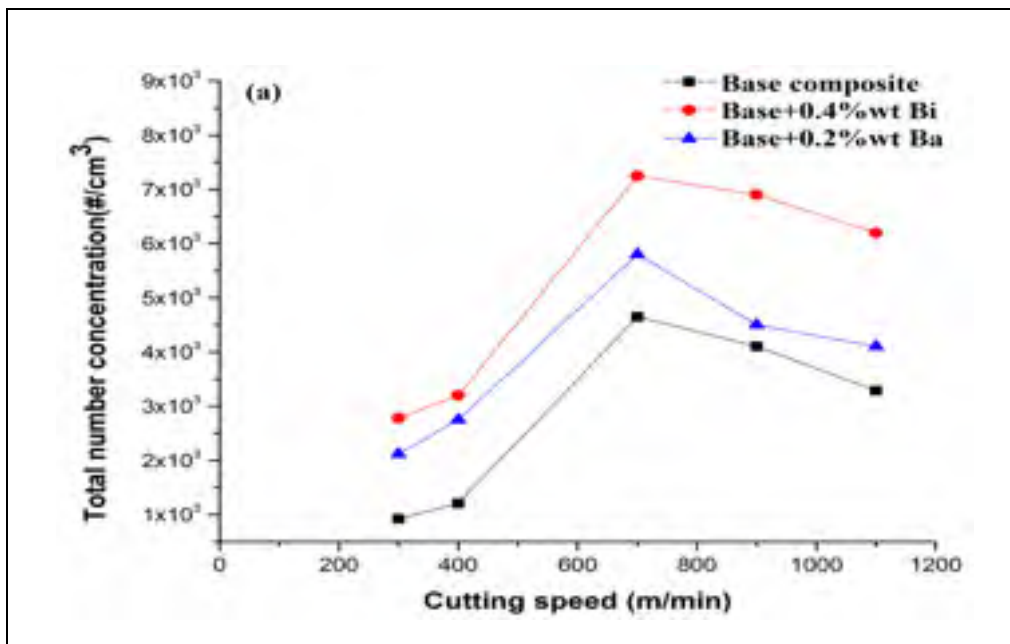


Figure 5.8 Total fine particle number concentration (b) surface concentration and (c) mass concentration as function of cutting speed for all workpieces at feed rate of 0.2 mm/tooth

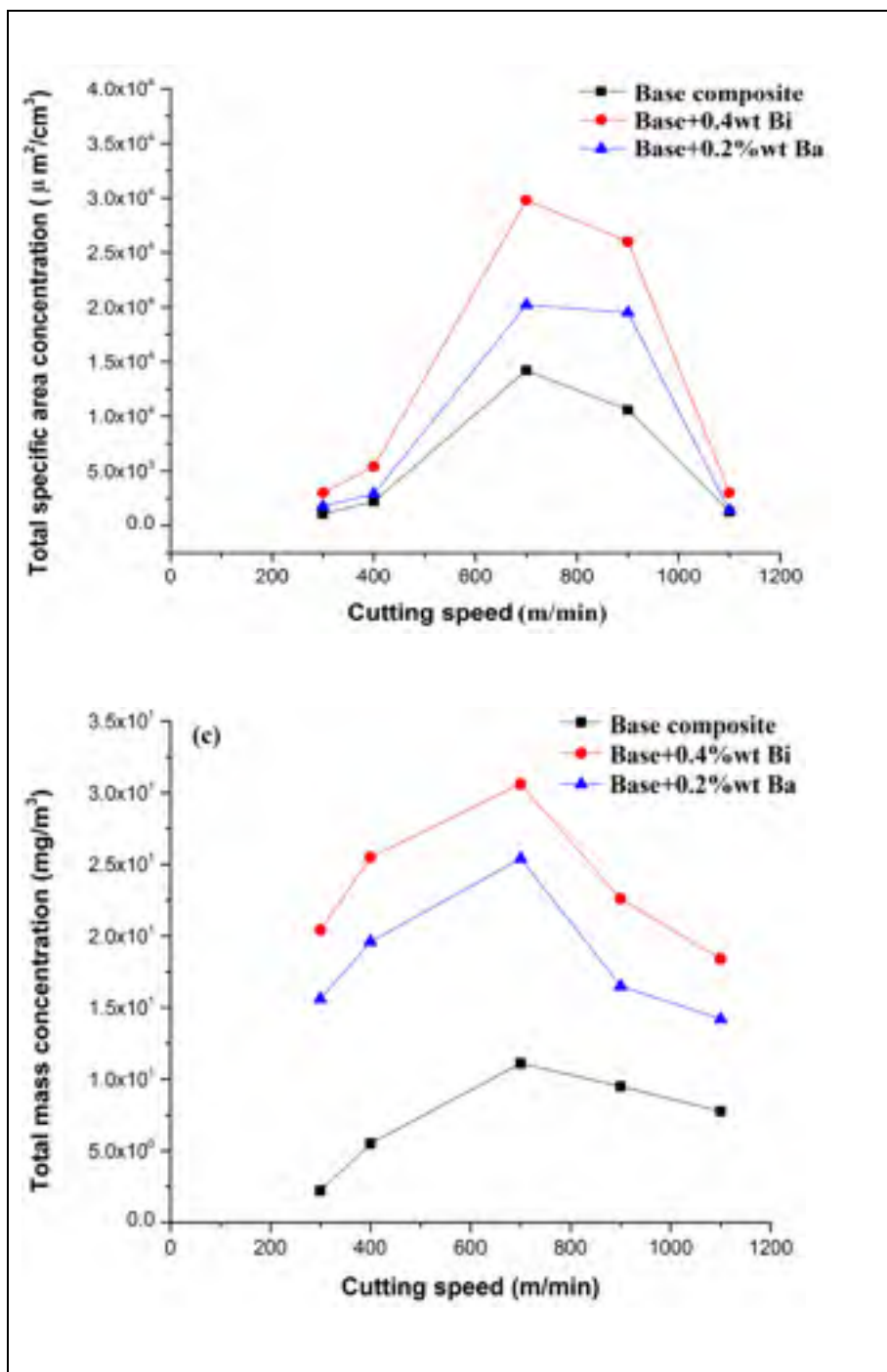


Figure 5.8 Continue

### 5.5.2. Ultrafine particle emission during milling

Figure 5.9 illustrates ultrafine particle emission results as a function of the particle diameters for number concentration, specific area concentration, and mass concentration. It is observed that the particle number for Al-20Mg<sub>2</sub>Si-2Cu metal matrix composite (base composite) is higher than treated composites. In fact, the addition of Bi and Ba decreased the generation of particle numbers concentration compared to the base composite (Figure 5.9a). Figure 5.9b shows surface concentration for all metal matrix composites. A similar trend is observed for the surface concentration which is helpful for human health during the machining process.

Figure 5.9c illustrates particle emission as a mass concentration for all workpieces. The addition of Bi and Ba decreased particle emission (mass concentration) about 4 times compared to the base composite. This observation can be explained by the fact that both machining parameters and microstructures play an important role in generating particle emission. Khettabi *et al.* (2007) observed that machining of the Ti6Al4V titanium alloy produced more ultrafine particles emission than aluminum alloy. They found that machining parameters have a direct effect on dust emission during machining (Kouam *et al.*, 2013). It is observed that Al-20Mg<sub>2</sub>Si-2Cu metal matrix composite produced more ultrafine particles compared to Bi-treated and Ba-treated composite (with a ductile fracture) because the compos has more brittle Mg<sub>2</sub>Si particles.

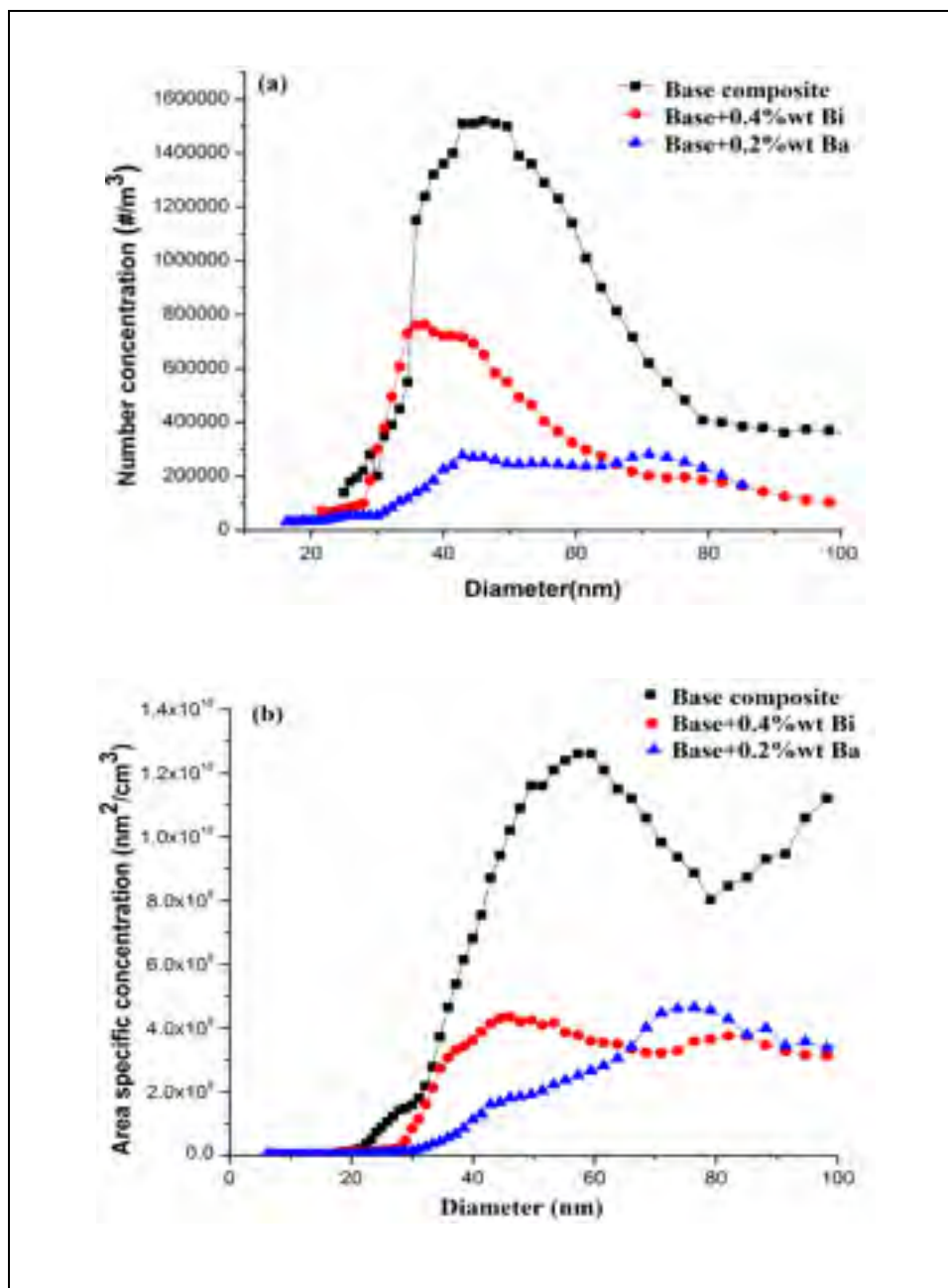


Figure 5.9 Comparison of (a) ultrafine particle number concentration (b) specific area concentration and (c) mass concentration as function of diameter of particles at cutting speed of 700 m/min and feed rate of 0.2 mm/tooth

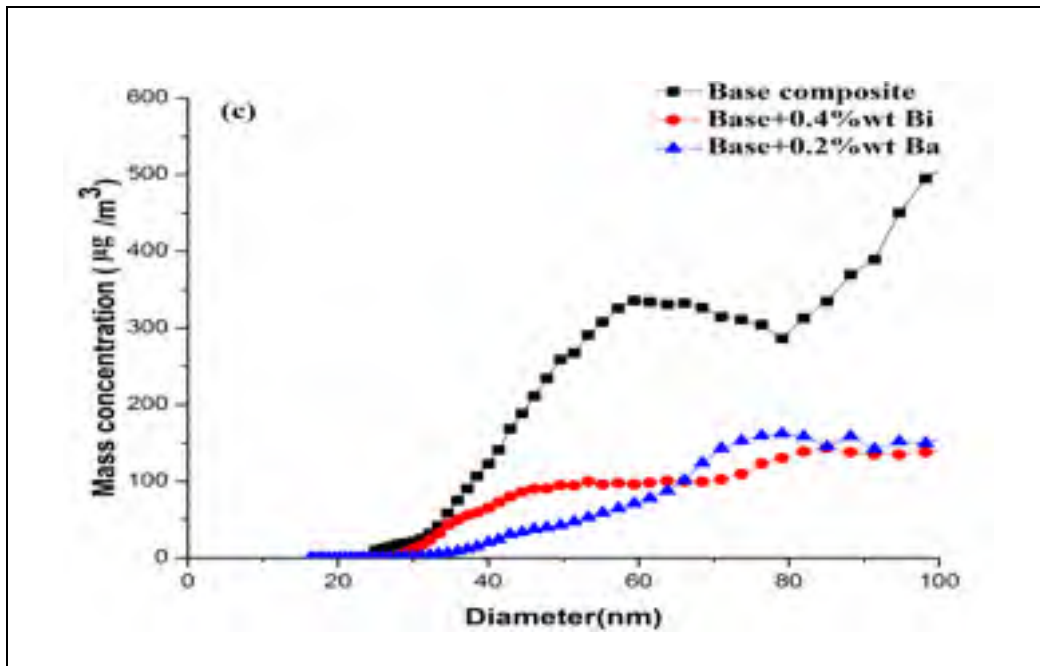


Figure 5.9 continue

Figure 5.10 shows the effect of cutting speed on the machining forces generated during milling Al-20Mg<sub>2</sub>Si metal matrix composite. As can be seen (Figure 5.10), the force component shows a decreasing trend with an increase in cutting speed for all workpieces. It can be attributed to the softening of the composite with increasing speeds. The trend in the changing forces as a result of increasing or decreasing speed is highly dependent on the properties of workpieces (Barzani *et al.*, 2015).

Figure 5.10 also illustrates that cutting force increased when feed rate increased from 0.1 to 0.2 mm/tooth. The lowest cutting force is just below 20 N at highest cutting speed (1100 m/min) and highest feed rate (0.2 mm/tooth) for composite contained Bi and Ba while it was around 55 N for base composite at cutting speed of 300 m/min and the same feed rate. For the base composite, high energy was required to pull out the coarse shape of primary Mg<sub>2</sub>Si from the machined surface (Barzani *et al.*, 2015). On the other hand, the addition of Bi and

Ba decreased cutting force by decreasing the size of primary  $Mg_2Si$  particles in the microstructure of workpieces. It has been reported that the coefficient friction plays an important role between the tool and machined material (Barzani *et al.*, 2013).

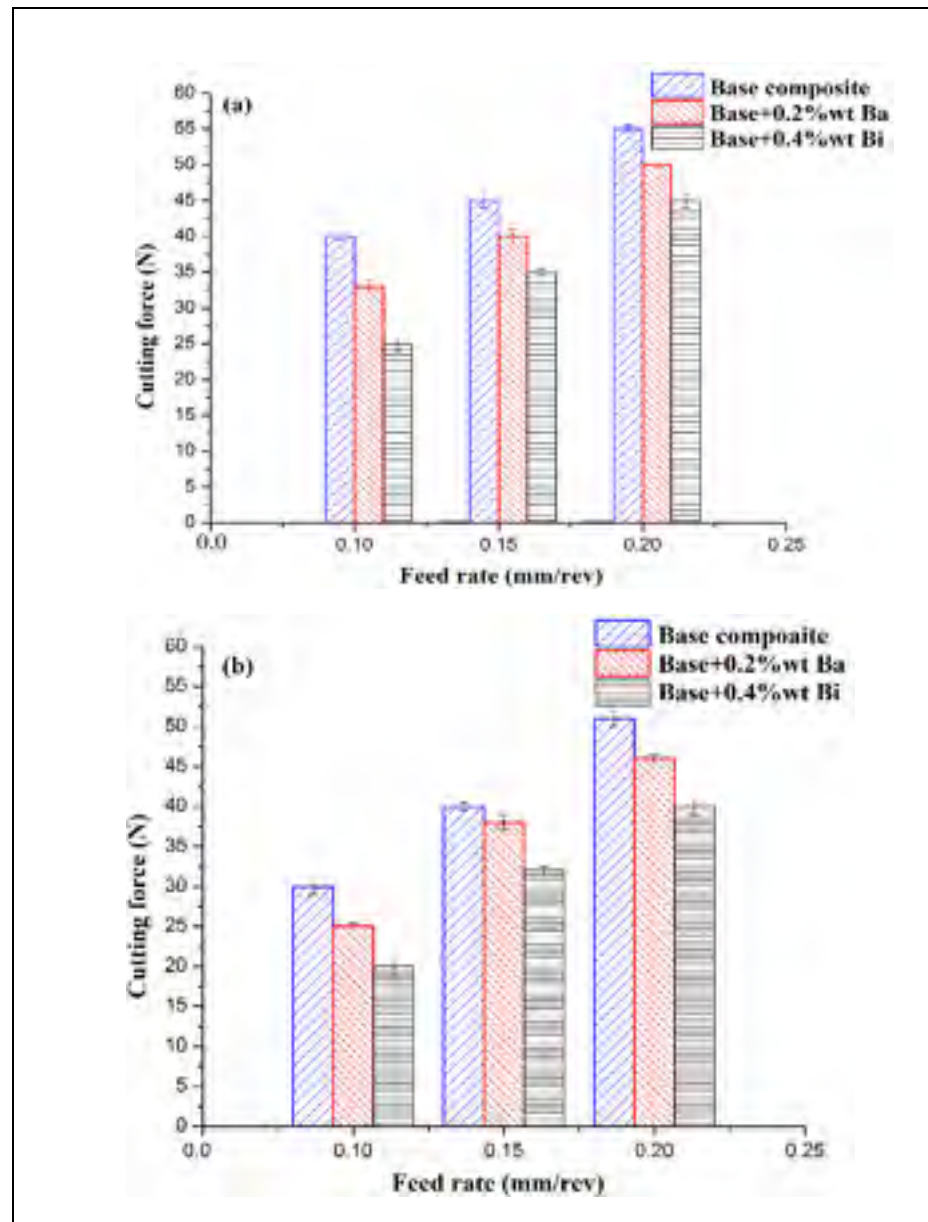


Figure 5.10 Variation of forces with feed rate at cutting speed of (a) 300 (b) 700 and (c) 1100 m/min

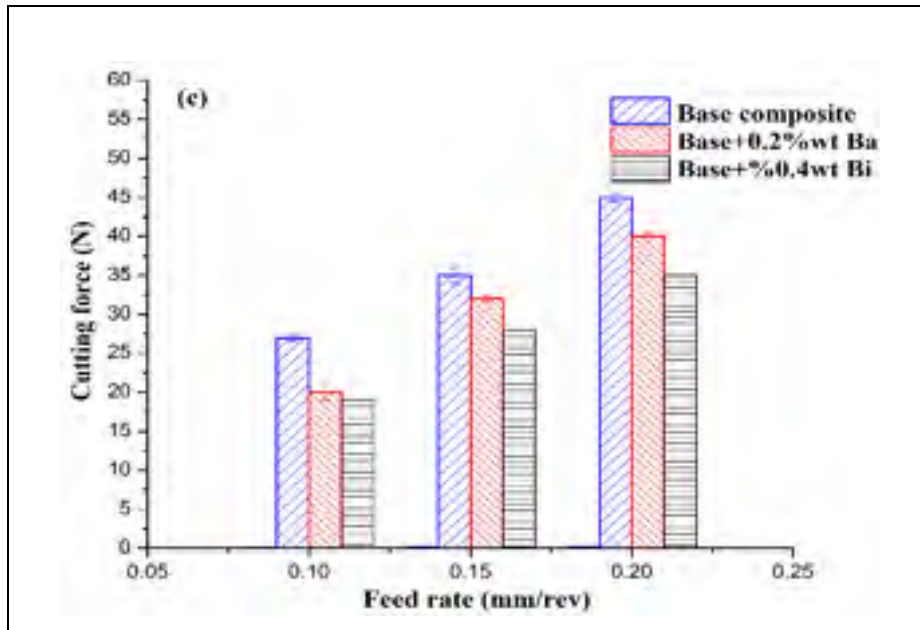


Figure 5.10 Continued

Figure 5.11 displays a comparative example of total dust emission for ultrafine particles using three criteria: number concentration, surface concentration and mass concentration as a function of the cutting speed. In general, for ultrafine particle emission, the amount of dust emission is low at lowest cutting speed 300 m/min for all workpieces. As can be seen in Figure 5.11a, for number concentration, the particle emission increased with increasing cutting speed from 300 to 700 m/min. The particle emission decreased with increasing cutting speed from 700 to 1100 m/min. The same trend was found in high-speed milling of 6061-t6 aluminum alloy (Khettabi *et al.*, 2007).

Figure 5.11b shows total surface concentration for all workpieces. It is observed that Al-20Mg<sub>2</sub>Si metal matrix composite produced a high level of particle emission about 3 times more than other workpieces which might be related to the big size of brittle Mg<sub>2</sub>Si particles in the matrix. In fact, particle emission increased with increasing the cutting speed at about 700 m/min (critical cutting speed) and decreased steadily at highest cutting speed (1100 m/min). There is evidence of the existence of a critical speed for the tested metal matrix composites at which both the fine and ultrafine particle emissions are high. This critical speed was found to be independent of the composite treatments (for all workpieces). This result is consistent with Songmene *et al.* (2015) during drilling of two cast aluminum alloys (A356-T0 and A319-T0).

For mass concentration (Figure 5.11c), the highest concentration of particles are shown at cutting speed of 700 m/min while it is low at lowest and highest cutting speed, respectively. The addition of Bi and Ba produced the lowest amount of dust emission compared to the base composite at 700 m/min. It can be explained by the small size Mg<sub>2</sub>Si particles in the microstructure which provided more ductility in the composite (Figure 5.6). In general, in the ductile fracture, there is a small contact surface between abrasive Mg<sub>2</sub>Si particles and the tool which leads to producing less particle emission compared to the base composite with brittle fracture (Djebara *et al.*, 2013).

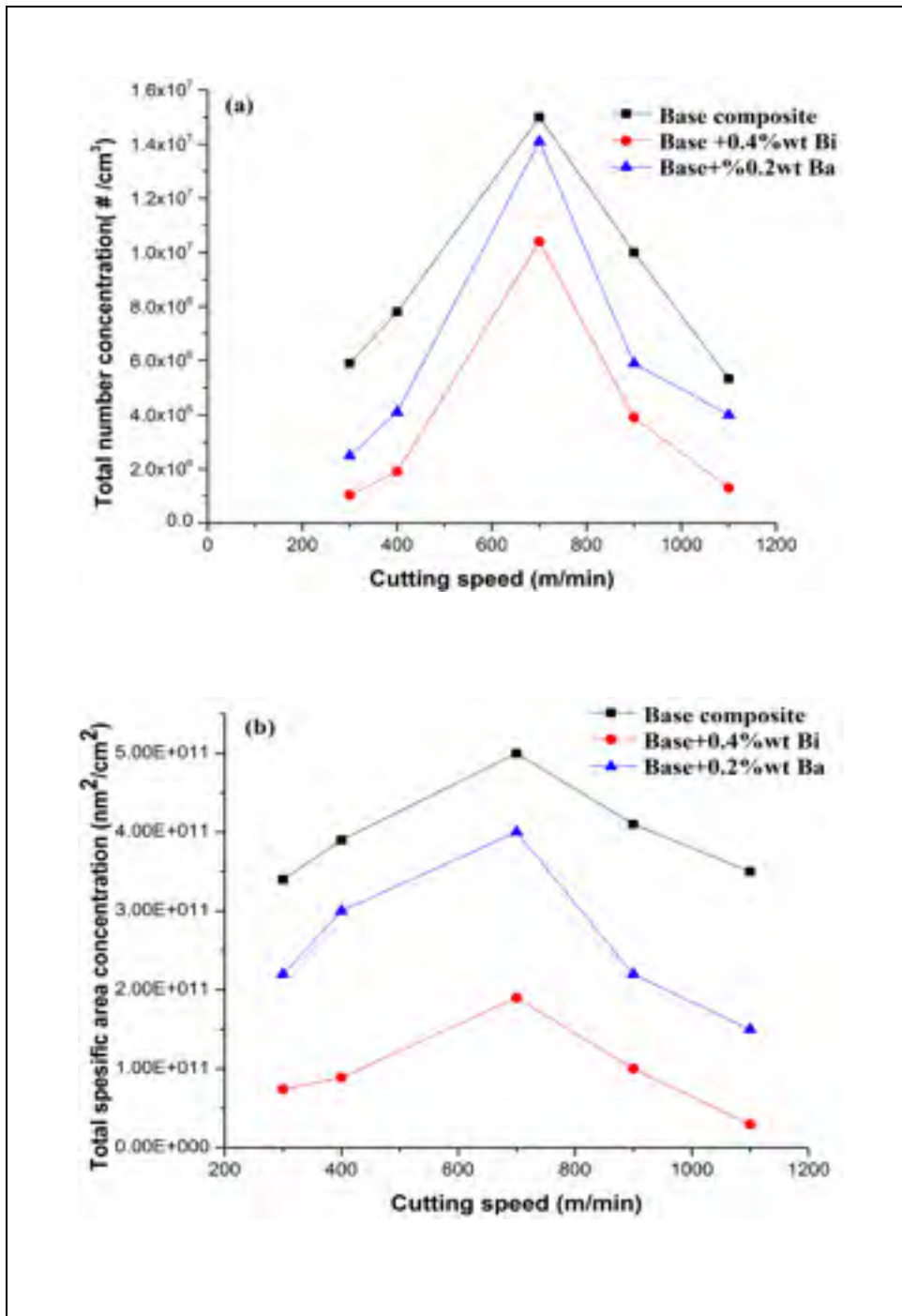


Figure 5.11 Total ultrafine particle number concentration (b) surface concentration and (c) mass concentration as function of cutting speed for all workpieces at feed rate of 0.2 mm/tooth.

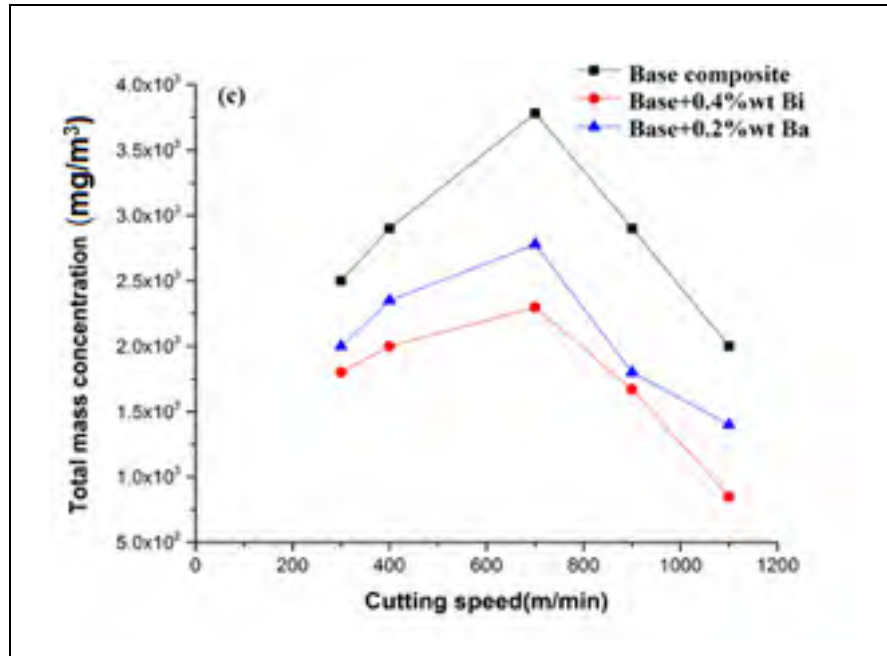


Figure 5.11 Continued

## 5.6. Conclusion

The effect of cutting conditions and reinforcement on particle emission when milling Al-20Mg<sub>2</sub>Si-2Cu metal matrix composite was investigated. The main findings of this investigation can be summarised as follows:

- 1- The morphology of primary Mg<sub>2</sub>Si particles changed from coarse shape to fine polygonal structure by the addition of Bi. The mean size and the mean aspect ratio of Mg<sub>2</sub>Si particles decreased by 37% and 11%, respectively. The addition of Ba to the composite decreased the mean size and aspect ratio by 43% and 8%, respectively. In addition, Bi and Ba changed the morphology of primary Mg<sub>2</sub>Si particles from the coarse shape to the fine polygonal and polyhedral shape, respectively.

- 2- It was found that metal matrix composites containing 0.4.%wt Bi and 0.2.%wt Ba have a higher density of dimples on their fracture faces with a few decohered primary  $Mg_2Si$  particles as a ductile fracture. The value of hardness also increased from  $62\pm 2$  to  $80\pm 3$  HV and  $66\pm 2$  HV by the addition of Bi and Ba, respectively.
- 3- It was found that microstructure and cutting condition have a direct effect on dust emission during the milling process. Particle emission increased with increasing cutting speeds from 300 to 700 m/min and then decreased with increasing cutting speed to 1100 m/min. It could be related to the role of temperature in the primary and secondary shear zones. Machining of this composite is recommended at high cutting speed due to decrease dust emission, which is suitable for the environment and worker health. In addition, cutting force decreased with increasing cutting speed. The addition of modifiers decreased cutting force due to decreasing in size of primary  $Mg_2Si$  particles.
- 4- Modification of the composite by Bi and Ba decreased ultrafine particle emission (number concentration, surface and mass concentration) compared to the base composite by a factor of 4 and 8, respectively. It can be related to the ductility of metal matrix composite which strongly controlled the dust emission level during the machining processes.

## CHAPTER 6

### NEURO-FUZZY PREDICTIVE MODLE FOR SURFACE ROUGHNESS AND CUTTING FORCE OF MACHINED Al-20Mg<sub>2</sub>Si-Cu METAL MATRIX COMPOSITE USING ADITIVES

Mohsen Marani<sup>1</sup>, Victor Songmene<sup>1</sup>, Mohammadjavad Zeinali<sup>2</sup>, Jules Kouam<sup>1</sup>, Yasser Zedan<sup>1</sup>

<sup>1</sup>École de Technologie Supérieure (ÉTS), 1100 Notre-Dame Street West, Montreal, QC H3C 1K3, Canada

<sup>2</sup>VSE Research Laboratory, Malaysia–Japan International Institute of Technology (MJIT), Universiti Teknologi Malaysia (UTM), 54100 Kuala Lumpur, Malaysia

Paper submitted in the journal of Neural Computing and Applications, (January, 2019) Springer.

#### 6.1. Abstract

Today's, metal matrix composites are widely used due to their excellent properties, which are useful for high performance applications in the automotive and aerospace industries. Furthermore, improving the machinability of these composites is vital for improving product quality in the manufacturing process. In this research, various adaptive network-based fuzzy inference systems (ANFIS) were introduced to evaluate the effect of the feed rate, the cutting speed and the particle size on the machinability of Al-20Mg<sub>2</sub>Si metal matrix composite. Two ANFIS models were selected as the most precise models for predicting surface roughness and cutting force, and two mathematical models were obtained based on these models. Results show that the proposed mathematical models have an adequate accuracy in predicting the machinability of metal matrix composites.

Keywords: Machinability, Metal matrix composite, ANFIS, Additives

## 6.2. Introduction

Today's fast changing manufacturing environment requires the application of optimization techniques to machining processes in order to react to market changes, involving factors such as the quantity and quality of products. Maximum productivity and high quality at a minimum production cost is now a must (Hwang *et al.*, 2009). In this regard, information on the mechanical properties of these materials is required when selecting optimum machinability parameters (cutting speed, feed rate and depth of cut) (Gupta *et al.*, 2011). Cutting force and surface roughness are reportedly the most commonly used criteria in assessing machinability (Palanikumar et Karthikeyan, 2007).

Machinability can be improved when the cutting force decreases for specific cutting conditions. In fact, a lower cutting force leads to better dimensional accuracy and lower tool wear rates in the machining process (Hwang *et al.*, 2009). Furthermore, machining processes require specific attention to guarantee the quality of final products. Composite materials are important engineering materials due to their outstanding mechanical properties.

Owing to its beneficial material properties, Al-Mg<sub>2</sub>Si metal matrix composites have recently received wide attention and application in the production of various industrial products (Farahany *et al.*, 2014). These composites in fact been chosen for casting high-temperature applications such as cylinder heads and pistons for automotive components (Farahany *et al.*, 2016). Although these metal matrix composites are widely used, their mechanical properties still need improvement as they contains brittle Mg<sub>2</sub>Si particles. To this end, a modification

method involving melt treatment has been recommended over other methods as it is an easier technique, with a low-cost process and is very practical (Azmah *et al.*, 2013).

From a machinability perspective, the development of free-cutting aluminum alloys is the most common metallurgical technique used to improve the machinability of these types of alloys (Seeman *et al.*, 2010). Pb, Bi, Sn, Sr, and In have been used as free-cutting elements (Barzani *et al.*, 2015; Ozben *et al.*, 2008). It has been found that these additives produce short chips which flow freely from the cutting zone and improve the machinability of the composite. In fact, these elements decrease the friction between the chip and the tool, which leads to a decrease in built-up edge (BUE) formation, a lower cutting force, and to a smooth surface finish (Marani *et al.*, 2018).

Barzani *et al.* (2013) considered the machinability of Al-Si cast alloy using additives, and found that the alloy's machinability was improved with the addition of a certain inoculation agent material due to a decreased BUE formation on the tool rake face during the machining process. Recently, soft computing tools are widely used for modeling and controlling the machining processes. Artificial Intelligence (AI) is the science and engineering of making intelligent machines, especially intelligent computer programs. AI branches include Genetic algorithm (GA), fuzzy logic (FL), and artificial neural networks (ANN) ( Adnan *et al.*, 2013).

The adaptive network-based fuzzy inference system (ANFIS) is another artificial intelligence method in which neural networks are utilized to elaborate the fuzzy rules on fuzzy inference approach (Zeinali et Mazlan, 2013). The membership function (MF) is an important portion of the ANFIS method, and must be correctly defined in order to allow an

accurate relationship between inputs and outputs (Pourtousi *et al.*, 2015). Thus, various types and numbers of MFs are applied to obtain the best configuration of the ANFIS method with the highest accuracy.

Dong et Wang (2011) proposed a method for modeling surface roughness with ANFIS in the milling process. Horng *et al.* (2009) reported a surface reconstruction model based on a methodology developed for predicting machinability in a milling process. Ekici, (2009) investigated an ANFIS model for wire-cut electrical discharge machine (EDM). It was found that the ANFIS model developed surface roughness achieved as a function of the process parameters and improved the machining performances.

Maher *et al.* (2015) studied increasing the productivity of the Wire-cutting EDM using Neuro fuzzy modeling. They concluded that ANFIS introduced a technological knowledge base in the selection of machining parameters in order to obtain high productivity and satisfactory surface quality. This technique is used to reduce costs and total experiment time.

However, some investigations have been carried out with respect to the machinability of metal matrix composites, there is still a general lack of knowledge when it comes to predicting the machining results for Al-20Mg<sub>2</sub>Si metal matrix composites by ANFIS; this prediction is a vital factor in improving the machinability of the composite. Therefore, the present work investigates an ANFIS model to accurately predict the amount of surface roughness and cutting forces when milling the Al-20Mg<sub>2</sub>Si metal matrix composite using modifier elements. In addition, ANFIS introduces two models for machinability of the composite.

### **6.3. Experimental procedure**

#### **6.3.1. Workpiece fabrication**

A commercial Al–Si alloy, pure magnesium (99.8%) and pure aluminum (99.8%) were used to fabricate Al-20 Mg<sub>2</sub>Si ingots. A 2 kg ingot was then melted using a resistance furnace with a melt temperature of 750±5°C. Once melted, elements of Bi and Ba in the form of pure metallic shots were introduced separately into the melt. The nominal addition levels were 0.4 wt% Bi and 0.2 wt% Ba, respectively (Marani *et al.*, 2018). A rectangular ceramic mold (25×30 mm) was used for pouring the molten alloy. Samples for metallography were cut and prepared by a standard grinding and polishing procedure. Quantitative data on the microstructure were determined using an optical microscope equipped with an image analysis tool. The measuring length after each condition was 5 mm and the cut-off length was fixed at 0.8 mm. An average of three readings for each condition was considered as the final surface roughness value.

#### **6.3.2. Machining tests**

A computer numerical control (CNC) milling machine (28,000 rpm) was used to run experimental tests with uncoated carbide inserts (Iscar, IC28). To record the cutting force, a three-component piezoelectric dynamometer connected to charge amplifiers was used during machining. A LabView was used to monitor and record all signals independently. Then, Matlab software was used to export the cutting force signals for further analysis. Different cutting speeds (300, 700 and 1100 m/min) and feed rates (0.1, 0.15, 0.2 mm/

tooth) were used, while the depth of cut was kept at 1 mm.

### **6.3.3. Adaptive network-based fuzzy inference system (ANFIS)**

ANFIS is a neuro-fuzzy approach, in which a fuzzy inference system is employed in the framework of an adaptive neural network. On the other hand, ANFIS is able to build an input- output mapping on fuzzy if-then rules. ANFIS is used to optimize the factors of the equivalent fuzzy inference system by using learning algorithm (Brevern *et al.*, 2009). ANFIS uses five network layers to complete the following fuzzy inference steps: (1) input parameters, (2) fuzzy set database layer, (3) fuzzy rule base construction, (4) decision making, and (5) output defuzzification (Maher *et al.*, 2015). Table 6.1 illustrates the experimental results used as training data sets for the ANFIS approach.

Table 6. 1 Experimental results used as training data for ANFIS structure

<i>Experiment No.</i>	<i>Feed Rate (mm/rev)</i>	<i>Cutting Speed (m/min)</i>	<i>Work Piece</i>	<i>Particle Size (<math>\mu\text{m}</math>)</i>	<i>Surface Roughness</i>	<i>Cutting Force (N)</i>
<i>1</i>	<i>0.1</i>	<i>300</i>	<i>Ba</i>	<i>102.2</i>	<i>2.6</i>	<i>31</i>
<i>2</i>	<i>0.1</i>	<i>300</i>	<i>Bi</i>	<i>113.5</i>	<i>2</i>	<i>28</i>
<i>3</i>	<i>0.1</i>	<i>300</i>	<i>Base</i>	<i>180.1</i>	<i>3</i>	<i>36</i>
<i>4</i>	<i>0.15</i>	<i>300</i>	<i>Ba</i>	<i>102.2</i>	<i>2.9</i>	<i>42</i>
<i>5</i>	<i>0.15</i>	<i>300</i>	<i>Bi</i>	<i>113.5</i>	<i>2.2</i>	<i>36</i>
<i>6</i>	<i>0.15</i>	<i>300</i>	<i>Base</i>	<i>180.1</i>	<i>3.3</i>	<i>48</i>
<i>7</i>	<i>0.2</i>	<i>300</i>	<i>Ba</i>	<i>102.2</i>	<i>3.2</i>	<i>47</i>
<i>8</i>	<i>0.2</i>	<i>300</i>	<i>Bi</i>	<i>113.5</i>	<i>2.9</i>	<i>43</i>
<i>8</i>	<i>0.2</i>	<i>300</i>	<i>Base</i>	<i>180.1</i>	<i>3.6</i>	<i>55</i>
<i>10</i>	<i>0.1</i>	<i>700</i>	<i>Ba</i>	<i>102.2</i>	<i>2.5</i>	<i>27</i>
<i>11</i>	<i>0.1</i>	<i>700</i>	<i>Bi</i>	<i>113.5</i>	<i>1.8</i>	<i>22</i>
<i>12</i>	<i>0.1</i>	<i>700</i>	<i>Base</i>	<i>180.1</i>	<i>2.7</i>	<i>30</i>
<i>13</i>	<i>0.15</i>	<i>700</i>	<i>Ba</i>	<i>102.2</i>	<i>2.7</i>	<i>37</i>
<i>14</i>	<i>0.15</i>	<i>700</i>	<i>Bi</i>	<i>113.5</i>	<i>2</i>	<i>33</i>
<i>15</i>	<i>0.15</i>	<i>700</i>	<i>Base</i>	<i>180.1</i>	<i>3.1</i>	<i>40</i>
<i>16</i>	<i>0.2</i>	<i>700</i>	<i>Ba</i>	<i>102.2</i>	<i>3.1</i>	<i>43</i>
<i>17</i>	<i>0.2</i>	<i>700</i>	<i>Bi</i>	<i>113.5</i>	<i>2.2</i>	<i>39</i>
<i>18</i>	<i>0.2</i>	<i>700</i>	<i>Base</i>	<i>180.1</i>	<i>3.3</i>	<i>52</i>
<i>19</i>	<i>0.1</i>	<i>1100</i>	<i>Ba</i>	<i>102.2</i>	<i>2.1</i>	<i>20</i>
<i>20</i>	<i>0.1</i>	<i>1100</i>	<i>Bi</i>	<i>113.5</i>	<i>1.7</i>	<i>18</i>
<i>21</i>	<i>0.1</i>	<i>1100</i>	<i>Base</i>	<i>180.1</i>	<i>2.3</i>	<i>24</i>
<i>22</i>	<i>0.15</i>	<i>1100</i>	<i>Ba</i>	<i>102.2</i>	<i>2.3</i>	<i>33</i>
<i>23</i>	<i>0.15</i>	<i>1100</i>	<i>Bi</i>	<i>113.5</i>	<i>1.9</i>	<i>27</i>
<i>24</i>	<i>0.15</i>	<i>1100</i>	<i>Base</i>	<i>180.1</i>	<i>2.6</i>	<i>37</i>
<i>25</i>	<i>0.2</i>	<i>1100</i>	<i>Ba</i>	<i>102.2</i>	<i>2.7</i>	<i>38</i>
<i>26</i>	<i>0.2</i>	<i>1100</i>	<i>Bi</i>	<i>113.5</i>	<i>2</i>	<i>35</i>
<i>27</i>	<i>0.2</i>	<i>1100</i>	<i>Base</i>	<i>180.1</i>	<i>3</i>	<i>42</i>

6.4. Result and discussion

6.4.1. ANFIS structure and membership function selection

Figure 6.1 shows the structure of the ANFIS model used in this paper, in which three different inputs (cutting speed, feed rate and workpiece) are implemented with three membership functions (MFs) for feed rate, two for cutting speed, and three for workpieces. Table 6.2 describes the function of each layer.

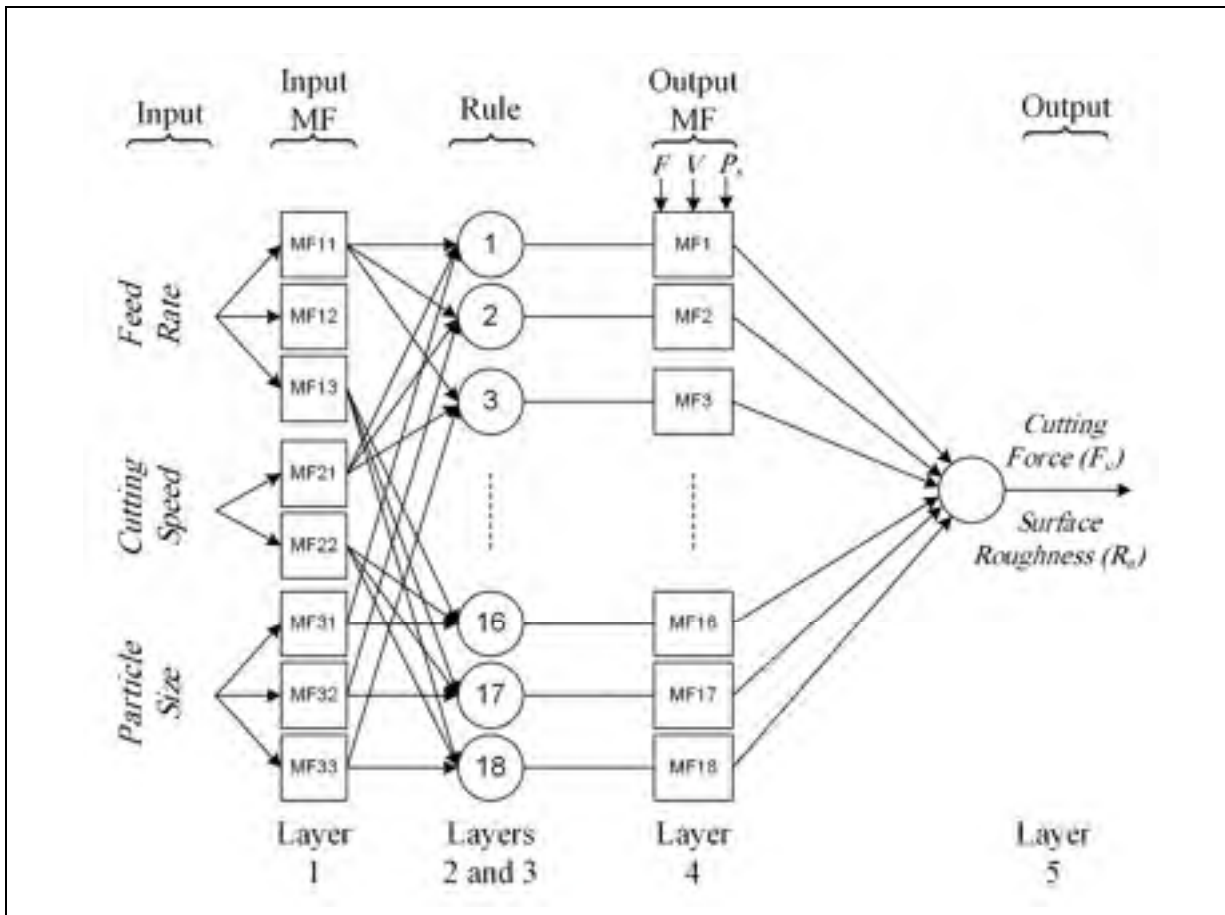


Figure 6.1 The structure of proposed ANFIS model

In this structure, three inputs, namely, feed rate ( $F$ ), cutting speed ( $V$ ) and particle size ( $P_s$ ), are acquired to predict the cutting force ( $F_c$ ) and surface roughness ( $R_a$ ) as outputs. As presented in Tables 6. 2 and 6.3, inputs are split into different numbers of spaces in the first layer using three different membership functions (MFs). An AND rule is applied in the second layer to produce the incoming signals of the first layer. Then, the value of the relative weight is obtained in the third layer using the equation described in Table 6.3. In the fourth layer, the outgoing signal of the third layer is multiplied by a linear function of inputs and the outgoing signals of the fourth layer are aggregated in the fifth layer to obtain the predicted surface roughness and cutting force as the outputs of the ANFIS model.

Table 6. 2 Applied equation of each layer.

Layer number	Equation	Layer number	Equation
1	$\mu_{1i}(F), \mu_{2j}(V), \mu_{3k}(P_s)$	4	$\bar{w}_r f_r = \bar{w}_r (p_r F + q_r V + r_r P_s + s_r)$
2	$w_r = \mu_{1i}(F) \times \mu_{2j}(V) \times \mu_{3k}(P_s)$	5	$F_c \text{ or } R_a = \sum_{r=1}^n \bar{w}_r f_r$
3	$\bar{w}_r = \frac{w_r}{\sum_{r=1}^n (w_r)}$		

Two evaluation tests are performed to obtain the most accurate model. At the first step, 78 different ANFIS structures are constructed and examined using the root mean square error (RMSE) value of approximated data. Working to find the best type and number of MFs for all inputs in terms of the Root Mean Square Error (RMSE) is an important aim of this

research work. Table 6.3 portrays three types of MFs that were applied in the ANFIS model for the first evaluation test. The equation of the RMSE is as follows (Sidik *et al.*, 2013).

$$RMSE = \sqrt{\frac{\sum_{i=1}^N (Actual\ Value - Predicted\ Value)^2}{N}} \quad (1)$$

where N is the number of testing sets. It can be noted that similar MF was implemented for all inputs, while the number of MFs could vary at this stage. Twenty-six combinations of the number of the MFs are utilized in the ANFIS model, and the RMSE values of all proposed structures are presented in Table 6.4. Among all these proposed structures, the ANFIS model constructed using a Bell-shaped MF (three MFs for feed rate, two for cutting speed ( $V$ ), and three for particle size ( $P_s$ ), respectively).

Table 6.3 Specifications of MFs employed in ANFIS model

<i>Membership Function</i>	<i>Equation</i>
Bell-shaped	$\frac{1}{1 + \left  \frac{x - c}{a} \right ^{2b}}$
Gaussian-shaped	$e^{-\frac{(x-c)^2}{2\sigma^2}}$
Sigmoidal-shaped	$\frac{1}{1 + e^{-a_1(x-c_1)}} - \frac{1}{1 + e^{-a_2(x-c_2)}}$

where  $a$ ,  $a_i$ ,  $b$ ,  $c$ ,  $c_i$  and  $\sigma$  are the MF parameters. On the other hand, there are three premise parameters for the Bell-shaped MF ( $a$ ,  $b$ ,  $c$ ), two for the Gaussian MF ( $\sigma$  and  $c$ ), and four for the Sigmoidal MF ( $a_1$ ,  $a_2$ ,  $c_1$ , and  $c_2$ ).

Table 6. 4 RMSE values of different structures of the ANFIS model

<i>Number of MF for</i>			<i>RMSE</i>					
			<i>Bell-Shaped</i>		<i>Gaussian-Shaped</i>		<i>Sigmoidal-Shaped</i>	
<i>F</i>	<i>V</i>	<i>Ps</i>	<i>Ra</i>	<i>Fc</i>	<i>Ra</i>	<i>Fc</i>	<i>Ra</i>	<i>Fc</i>
1	1	2	9.59E-02	1.33E+00	9.57E-02	1.33E+00	9.57E-02	1.33E+00
1	1	3	9.49E-02	1.32E+00	9.49E-02	1.32E+00	9.49E-02	1.32E+00
1	2	1	2.96E-01	2.56E+00	2.96E-01	2.56E+00	2.96E-01	2.56E+00
1	2	2	8.48E-02	1.28E+00	8.39E-02	1.28E+00	8.39E-02	1.28E+00
1	2	3	5.42E-02	1.28E+00	4.98E-02	1.26E+00	5.47E-02	1.28E+00
1	3	1	2.96E-01	2.56E+00	2.96E-01	2.56E+00	2.96E-01	2.56E+00
1	3	2	6.75E-02	1.22E+00	6.67E-02	1.22E+00	6.67E-02	1.22E+00
1	3	3	4.91E-02	1.21E+00	4.91E-02	1.21E+00	4.98E-02	1.21E+00
2	1	1	2.97E-01	2.37E+00	2.97E-01	2.37E+00	2.97E-01	2.37E+00
2	1	2	8.20E-02	8.86E-01	8.12E-02	8.59E-01	8.13E-02	8.84E-01
2	1	3	7.01E-02	8.03E-01	6.11E-02	8.03E-01	7.01E-02	8.10E-01
2	2	1	2.94E-01	2.28E+00	2.93E-01	2.27E+00	2.94E-01	2.28E+00
2	2	2	4.73E-02	4.35E-01	5.52E-02	5.81E-01	4.68E-02	5.69E-01
2	2	3	1.24E-02	4.51E-01	1.24E-02	4.51E-01	1.24E-02	4.16E-01
2	3	1	2.93E-01	2.24E+00	2.93E-01	2.21E+00	2.93E-01	2.24E+00
2	3	2	9.89E-03	3.51E-01	1.01E-02	3.54E-01	9.65E-03	3.47E-01
2	3	3	7.00E-04	3.28E-02	3.38E-04	1.93E-02	3.96E-04	1.24E-02
3	1	1	2.96E-01	2.36E+00	2.96E-01	2.36E+00	2.96E-01	2.36E+00
3	1	2	8.05E-02	7.93E-01	8.10E-02	7.96E-01	7.96E-02	7.90E-01
3	1	3	6.03E-02	7.78E-01	6.03E-02	7.78E-01	6.03E-02	7.78E-01
3	2	1	2.93E-01	2.26E+00	2.93E-01	2.26E+00	2.93E-01	2.26E+00
3	2	2	4.70E-02	3.29E-01	5.30E-02	3.79E-01	5.24E-02	3.60E-01
3	2	3	5.68E-06	1.24E-04	1.66E-05	2.68E-04	8.69E-06	9.67E-05
3	3	1	2.92E-01	2.19E+00	2.92E-01	2.19E+00	2.92E-01	2.19E+00
3	3	2	4.03E-05	2.74E-04	1.88E-05	1.97E-04	5.18E-05	5.36E-04
3	3	3	2.57E-05	5.58E-04	1.24E-04	4.31E-04	7.19E-05	8.48E-04

As can be seen in Table 6.4, the ANFIS structures with a combination of two and three MFs have a better accuracy than the others. Therefore, the second evaluation test is performed to realize the most appropriate MF type for each input with two or three MFs. In this stage, 3584 ANFIS structures are constructed, in which 7 MF arrangements for 512 MF type combinations are evaluated. Tables 6.5 and 6.6 depict the MF arrangements and types for the model inputs. The main difference between this step and the previous step is in the implemented MF types. Here, each input can have a different MF type, while in the previous

step, all inputs have a similar MF type. Therefore, the combination of 8 MF types for 3 inputs will produce 512 diverse ANFIS models.

Table 6. 5 MF arrangements for each input

<i>Arrangements of MF for</i>			<i>Total number of arrangements</i>
<i>F</i>	<i>V</i>	<i>Ps</i>	
2	3	3	8
3	2	3	
3	3	2	
3	2	2	
2	3	2	
2	2	3	
3	3	3	

Table 6. 6 Utilized MF types

Utilized MF types for			Total number of combinations
<i>F</i>	<i>V</i>	<i>P<sub>s</sub></i>	
Bell-shaped	Bell-shaped	Bell-shaped	512
Gaussian-shaped	Gaussian-shaped	Gaussian-shaped	
Sigmoidal-shaped	Sigmoidal-shaped	Sigmoidal-shaped	
Triangular-shaped	Triangular-shaped	Triangular-shaped	
Gaussian-shaped 2nd type	Gaussian-shaped 2nd type	Gaussian-shaped 2nd type	
Sigmoidal-shaped 2nd type	Sigmoidal-shaped 2nd type	Sigmoidal-shaped 2nd type	
Π-shaped	Π-shaped	Π-shaped	
Trapezoidal-shaped	Trapezoidal-shaped	Trapezoidal-shaped	

## 6.5. ANFIS prediction result

### 6.5.1. Surface roughness prediction

After evaluating all ANFIS structures (in section 6.2) based on their accuracy, it was seen that the ANFIS models for predicting the surface roughness were those with the following characteristics: Gaussian-shaped MF with three MFs for feed rate ( $F$ ), Triangular-shaped MF with two MFs for cutting speed ( $V$ ) and Triangular-shaped MF with three MFs for particle size ( $P_s$ ). Figure 6.2 shows the plots of MFs for ( $F$ ), ( $V$ ), and ( $P_s$ ) inputs in the surface roughness prediction model. The equations of MF inputs for surface roughness modeling are shown in Table 6.7.

Table 6. 7 ANFIS model for surface roughness prediction

ANFIS model for surface roughness prediction	
Input	MF Equation
$F$	$\mu_{1i} = e^{-\frac{(x-c)^2}{2\sigma^2}}$
$V$	$\mu_{2j} = \max\left(\min\left(\frac{x-a}{b-a}, 1, \frac{c-x}{c-b}\right), 0\right)$
$P_s$	$\mu_{3k} = \max\left(\min\left(\frac{x-a}{b-a}, 1, \frac{c-x}{c-b}\right), 0\right)$

where  $a$ ,  $b$ ,  $c$  and  $\sigma$  are the MFs parameters.

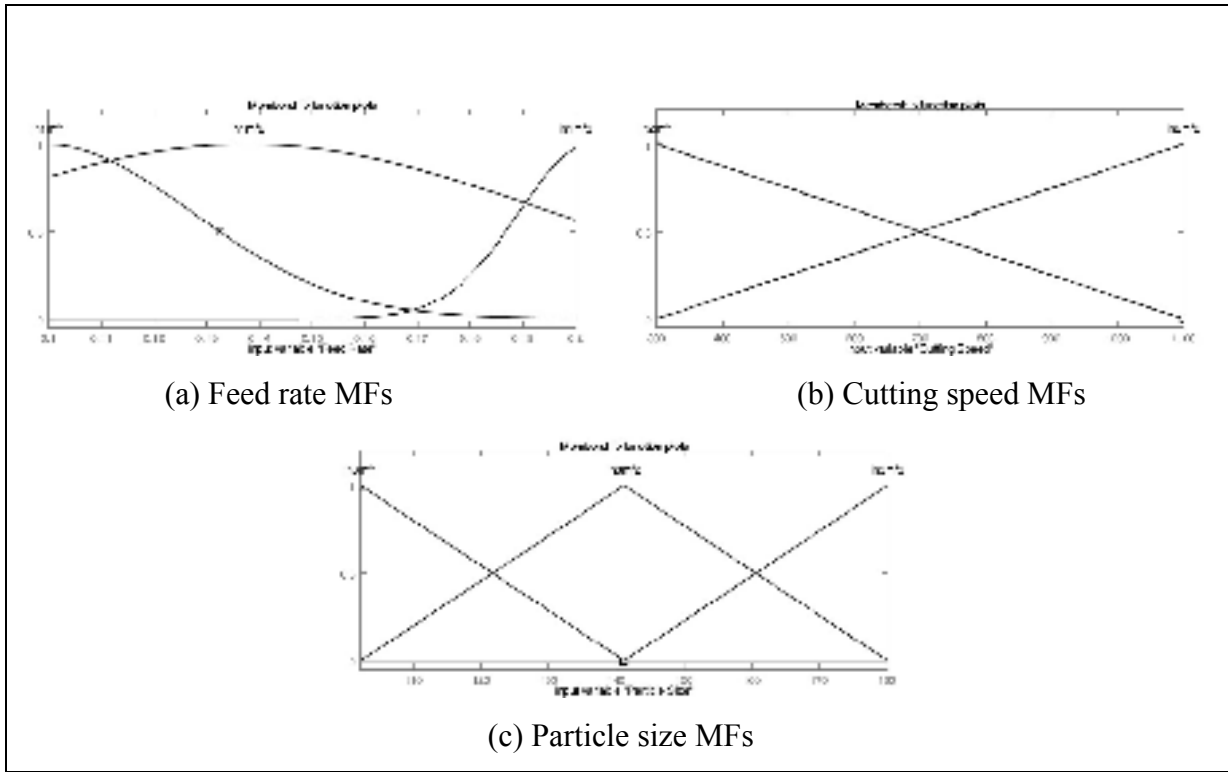
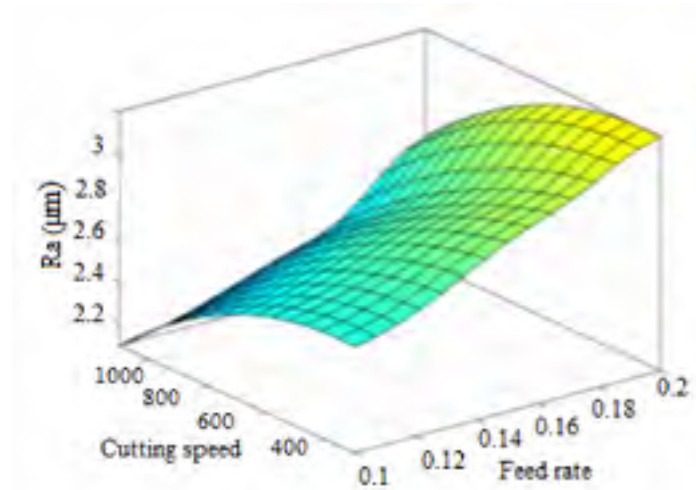
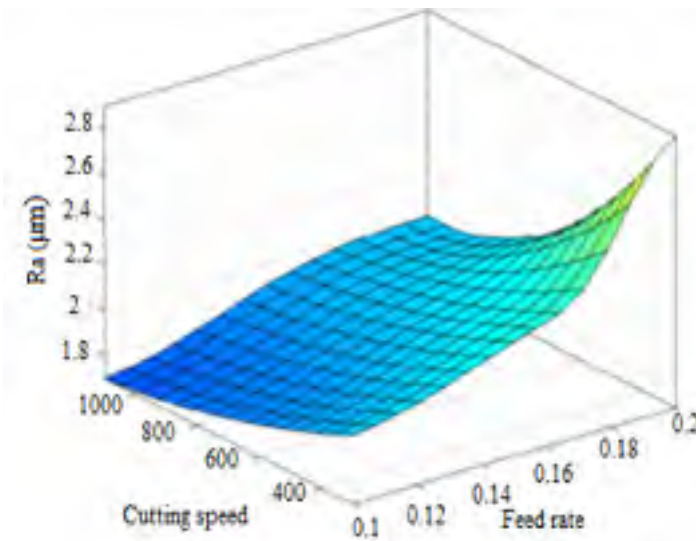


Figure 6.2 Plots of MFs for (a) feed rate, (b) cutting speed and (c) particle size inputs in prediction model of surface roughness

The surface roughness ( $R_a$ ) predicted by ANFIS as function of feed rate, cutting speed and workpiece material is represented in Figure 6.3. The model shows that the surface roughness value improved by increasing the cutting speed from 300 to 1100 m/min and deteriorates by increasing the feed rate from 0.1 to 0.2 mm/tooth for all workpieces. The model also approved that Bi-containing composite (Figure 6.3b) has the best surface roughness value as compared with other workpieces. The unsatisfactory surface roughness at high feed rates is due to increasing amounts of built-up edge (BUE) in the cutting zone (Barzani *et al.*, 2015).



(a) Ba-containing



(b) Bi-containing

Figure 6.3 The surface roughness predicted by ANFIS as function of cutting speed, feed rate and workpiece material: (a) Ba-containing composite (b) Bi-containing composite, (c) Base composite

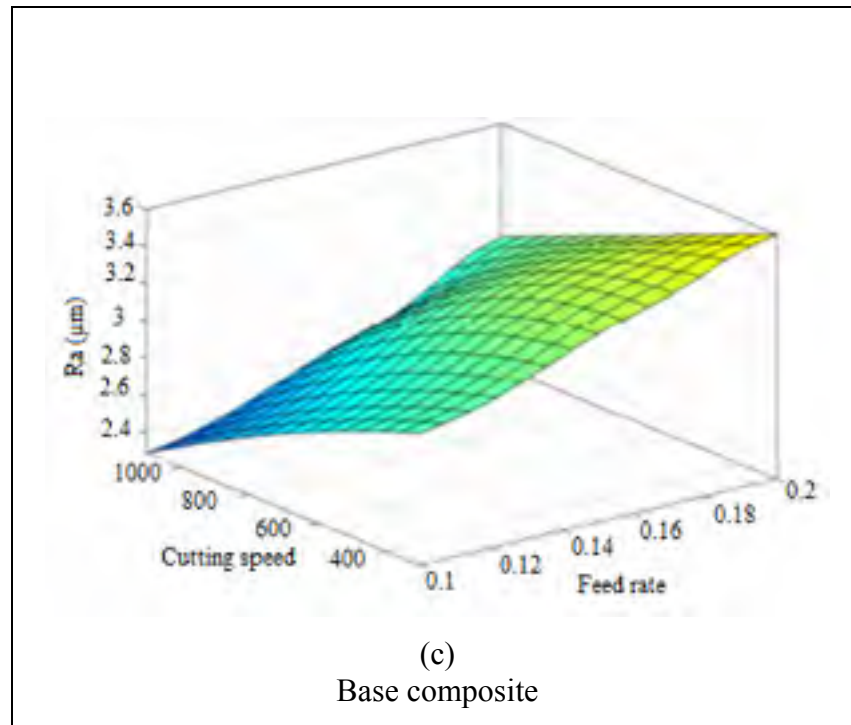


Figure 6.3 Continued

Figure 6.4 (a, b and c) shows the optical microstructure and feed mark images of machined subsurfaces for an unmodified composite, a Ba-containing composite, and a Bi-containing composite, respectively. As can be seen in Figure 6.4a, primary  $Mg_2Si$  particles exist in a coarse shape, as well as being bigger in size compared with the other workpieces. It was found that coarse shape particles have high stress concentrations at their sharp edges and lead to an increase in the fracture surface of the structure, and finally, that they weaken the composite performance (Azmah *et al.*, 2015). The addition of certain amount of modifier elements affects the shape and size of particles by refining them from coarse to a fine polyhedral shape (Marani *et al.*, 2018).

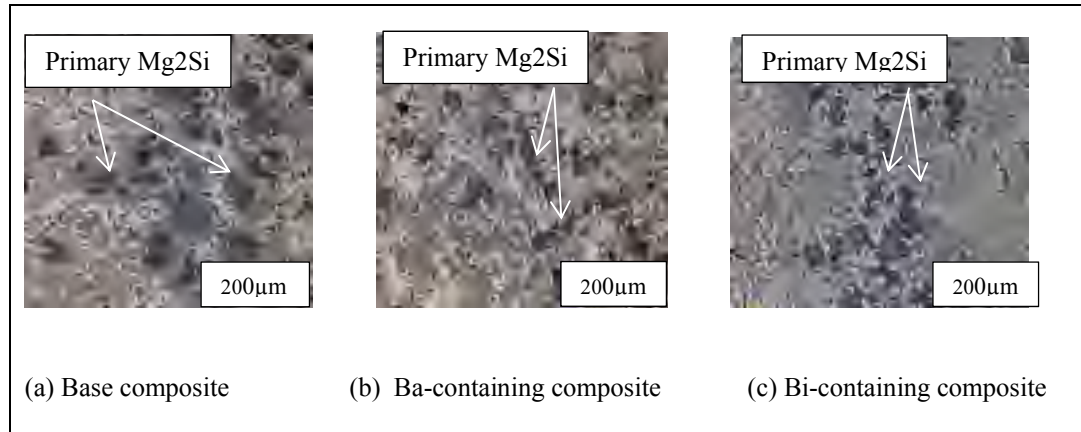


Figure 6.4 Optical microstructure of (a) Base composite, (b) Ba-containing composite, (c) Bi-containing composite.

The selected ANFIS model's structure has three different MFs for each input: 3, 2, and 3 MFs, for feed rate, cutting speed, and particle size, respectively. Therefore, the model has 18 rules. The relationship between feed rate, cutting speed and particle size as inputs and surface roughness as output can be mathematically modeled as follows:

Hence, the equation for second layer will be,

$$w_r = \mu_{1i}(F) \times \mu_{2j}(V) \times \mu_{3k}(P_s) \quad (2)$$

Then, the output of each rule in third layer is as,

$$\bar{w}_r = \frac{\mu_{1i}(F) \times \mu_{2j}(V) \times \mu_{3k}(P_s)}{\sum_{k=1}^3 \sum_{j=1}^2 \sum_{i=1}^3 (\mu_{1i}(F) \times \mu_{2j}(V) \times \mu_{3k}(P_s))} \quad (3)$$

and the relationship between rules number and MF numbers is as,

$$r = 6(i - 1) + 3(j - 1) + k \quad (4)$$

Hence, the prediction of the outputs (surface roughness ( $R_a$ )) can be calculated as:

$$\begin{aligned}
Ra &= \sum_{r=1}^{18} \bar{w}_r f_r = \sum_{r=1}^{18} \bar{w}_r (p_r F + q_r V + r_r P_s + s_r) \\
&= \frac{\sum_{k=1}^3 \sum_{j=1}^2 \sum_{i=1}^3 (\mu_{1i}(F) \times \mu_{2j}(V) \times \mu_{3k}(P_s)) (p_r F + q_r V + r_r P_s + s_r)}{\sum_{k=1}^3 \sum_{j=1}^2 \sum_{i=1}^3 (\mu_{1i}(F) \times \mu_{2j}(V) \times \mu_{3k}(P_s))} \quad (5)
\end{aligned}$$

Tables 6.8 depicts the values of premise parameters,  $a$ ,  $b$ ,  $c$ , and  $\sigma$ , and consequent parameters for surface roughness prediction models. In addition, the comparison of estimated values, using the prediction model, with experimental results (new twelve experiments) is shown in Table 6.11.

Table 6. 8 Values of premise and consequent parameters in proposed ANFIS structure for surface roughness prediction

<i>Premise parameters</i>			<i>Consequent parameters value</i>				
<i>MF</i>	<i>Parameter</i>	<i>Value</i>	<i>Rule No.</i>	<i>p</i>	<i>q</i>	<i>r</i>	<i>s</i>
$\mu_{11}(F)$	$\sigma, c$	[0.02833 0.09913]	1	1.14E-05	3.03E-03	1.31E-02	1.07E-04
			2	4.61E-06	-2.63E-03	8.92E-03	7.86E-05
$\mu_{12}(F)$	$\sigma, c$	[0.05851 0.1376]	3	6.07E-06	1.84E-03	1.16E-02	6.46E-05
			4	-2.68E-06	1.99E-03	-3.15E-03	-2.46E-05
$\mu_{13}(F)$	$\sigma, c$	[0.01378 0.2029]	5	-1.37E-06	7.91E-04	-2.62E-03	-2.31E-05
			6	-1.29E-06	2.18E-03	-2.51E-03	-1.40E-05
$\mu_{21}(V)$	$a, b, c$	[-500 300 1100]	7	2.92E-05	3.04E-03	2.08E-02	2.01E-04
			8	6.25E-06	-7.37E-04	9.89E-04	8.71E-06
$\mu_{22}(V)$	$a, b, c$	[300 1100 1900]	9	1.01E-05	3.84E-03	1.27E-02	7.03E-05
			10	-7.21E-06	2.65E-03	-5.13E-03	-4.96E-05
$\mu_{31}(P_s)$	$a, b, c$	[63.25 102.2 141.1]	11	-1.70E-06	1.07E-03	-2.35E-04	-2.07E-06
			12	-1.83E-06	2.87E-03	-2.35E-03	-1.31E-05
$\mu_{32}(P_s)$	$a, b, c$	[102.2 141.1 180.1]	13	1.97E-05	4.05E-03	2.04E-02	9.86E-05
			14	7.47E-05	-7.40E-03	4.24E-02	3.73E-04
			15	1.75E-05	2.84E-03	1.58E-02	8.77E-05
$\mu_{33}(P_s)$	$a, b, c$	[102.2 141.1 180.1]	16	-4.08E-06	3.09E-03	-5.05E-03	-2.04E-05
			17	-2.15E-05	1.26E-03	-1.22E-02	-1.07E-04
			18	-3.65E-06	3.41E-03	-3.28E-03	-1.82E-05

### 6.5.2. Cutting force prediction

According to Figure 6.5, the best ANFIS models for predicting the cutting force were those with the following characteristics: three MFs and Gaussian-shaped MF for feed rate, two MFs and Triangular-shaped MF for cutting speed, and three MFs and second type

Gaussian-shaped MF for particle sizes. They had the best accuracy among all examined models. The input MFs equations for cutting force modeling are shown in Table 6.9.

Table 6. 9 ANFIS model for cutting force prediction

ANFIS model for cutting force prediction	
Input	MF Equation
$F$	$\mu_{1i} = e^{-\frac{(x-c)^2}{2\sigma^2}}$
$V$	$\mu_{2j} = \max\left(\min\left(\frac{x-a}{b-a}, 1, \frac{c-x}{c-b}\right), 0\right)$
$P_s^*$	$\mu_{3k} = \begin{cases} e^{-\frac{(x-c_1)^2}{2\sigma_1^2}} & x \leq c_1 \\ 1 & c_1 \leq x \leq c_2 \\ e^{-\frac{(x-c_2)^2}{2\sigma_2^2}} & x \geq c_2 \end{cases}$

\* The proposed equation can be used when  $c_1 \leq c_2$ . In this model  $c_1$  is less than  $c_2$

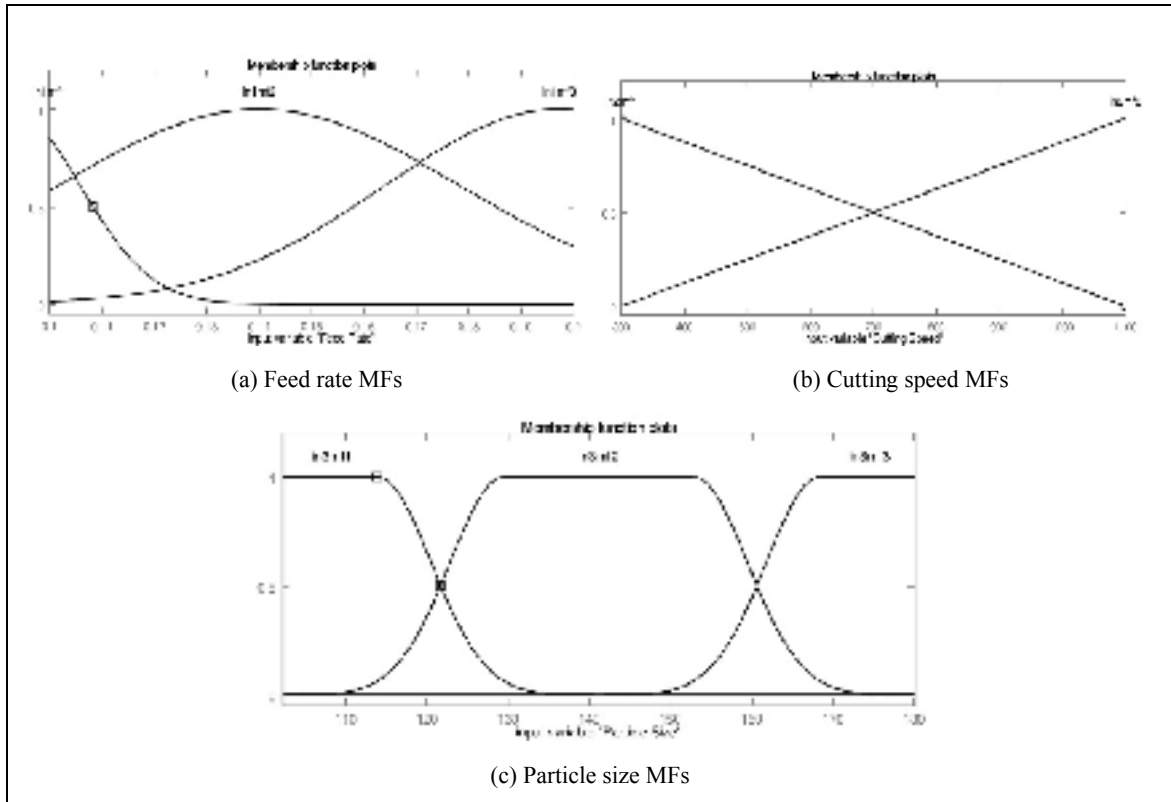


Figure 6.5 Plots of MFs for (a) feed rate, (b) cutting speed and (c) particle size inputs in cutting force prediction model.

Figure 6.6 shows the cutting force ( $F_c$ ) prediction using ANFIS as function of cutting speed, feed rate and workpiece material. The Bi-containing workpiece (Figure 6.6b) shows the lowest cutting force as compared to other workpieces. In addition, the ANFIS model shows that the cutting force decreased as the cutting speed increased and increased when the feed rates increased for all workpieces. This result is also seen in experimental results. The base composite shows a higher value for cutting force than other workpieces due to the coarse shape of  $Mg_2Si$  particles. On the other hand, high energy is required to pull-off brittle  $Mg_2Si$  particles from the machined surface during machining of the base composite, while the

addition of modifier elements decreases the cutting force by decreasing the size of  $Mg_2Si$  particles in the microstructure (Marani et al., 2018).

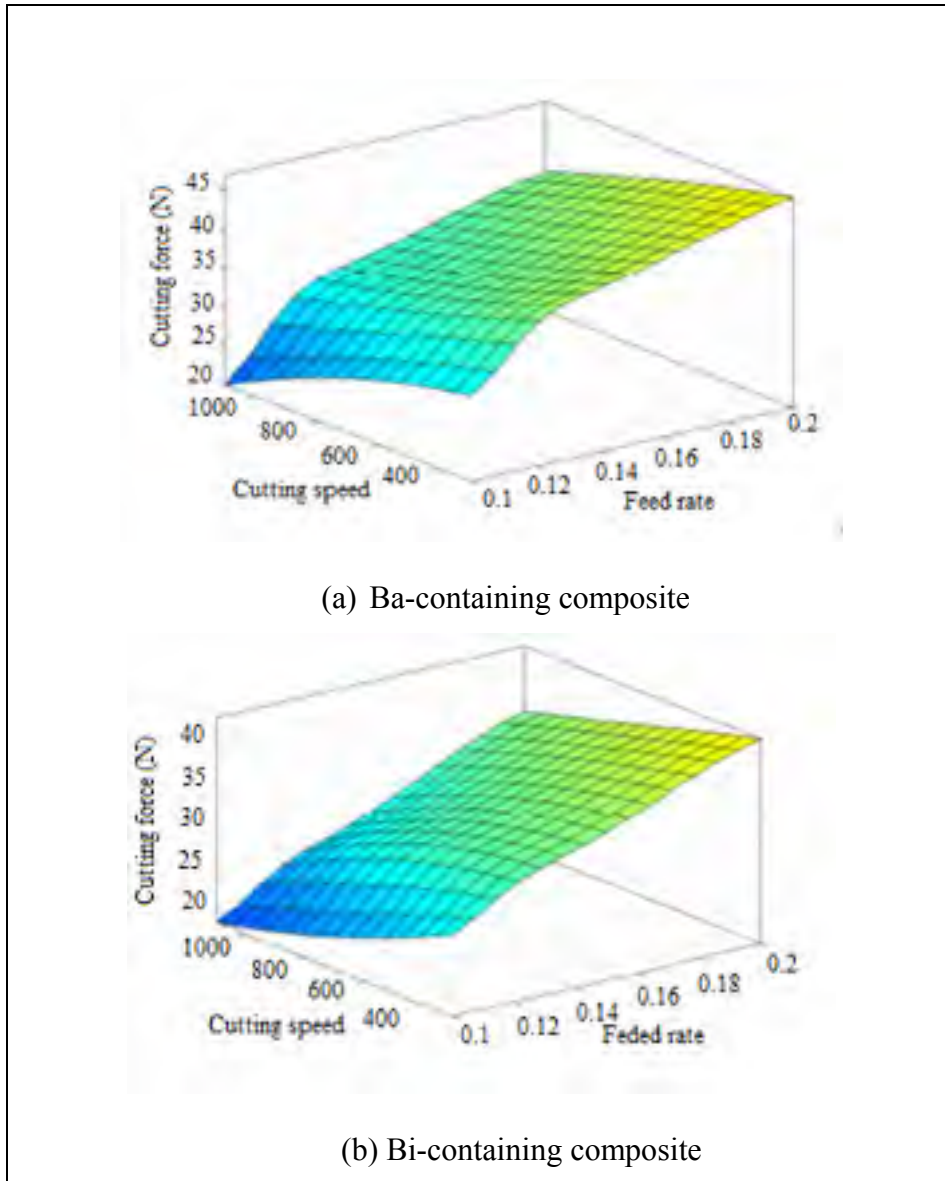


Figure 6.6 Cutting force predicted by ANFIS in relation to cutting speed, feed rate and workpiece material: (a) Ba-containing composite, (b) Bi-containing composite, (c) Base composite.

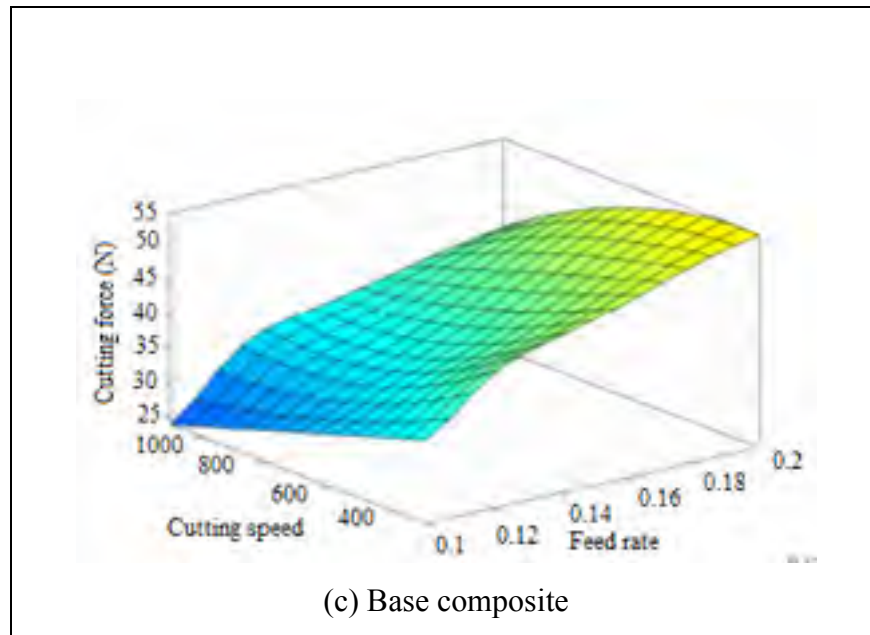


Figure 6.6 Continued

It has been concluded that, the friction between the freshly formed chip surface and the tool has a direct effect on the metal cutting process, and finally in reducing cutting forces (Rath *et al.*, 2018). An optical microscopy of the chips produced during machining of the metal matrix composites illustrates that the chips are highly strained and leads to separation of chip segments at outer surfaces for all workpieces. However, the brittle  $Mg_2Si$  particles caused significant fracturing of chips for the base composite. In the case of a modified composite (Figure 6.7b and c), secondary crack formation is evident at the inner surface of the chips, and leads to improved chip breakability (Kannan & Kishawy, 2008). The addition of Bi to the composite acts as a lubricant in the machining process and improves machinability due to the low melting point of Bi as compared to the base composite (Marani *et al.*, 2017).

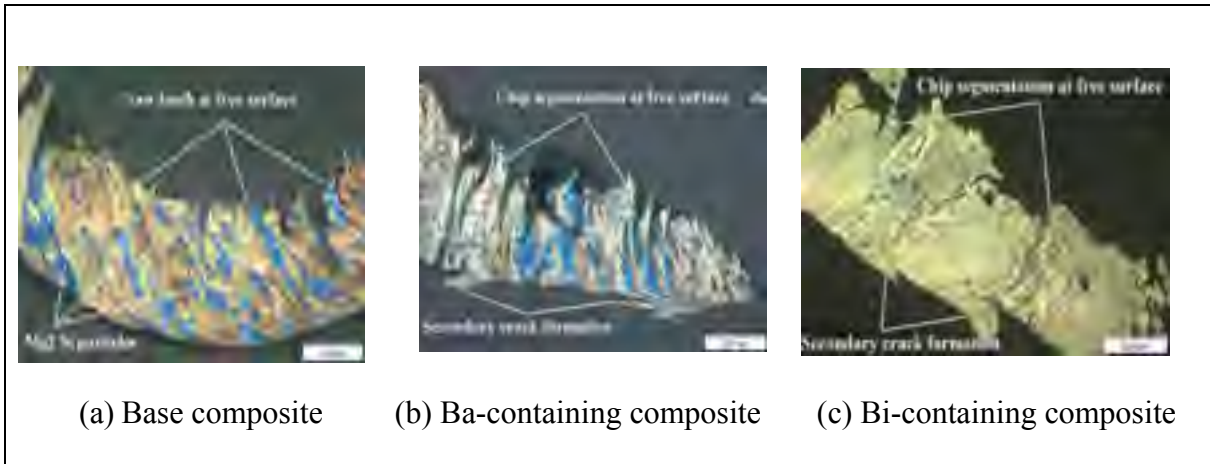


Figure 6.7 Optical images of chips during machining of the (a) base composite, (b) Ba-containing composite, and (c) Bi-containing composite

For modeling the cutting force, 18 rules (Figure 6.1) are considered due to the number of MFs for each input (3, 2, 3 for feed rate, cutting speed, and particle size, respectively). In fact, the formula structures for predicting the surface roughness and the cutting force are similar. However, the MF types, formula and consequent parameters (if-then rules) such as  $P_r$ ,  $q_r$ ,  $r_r$ , and  $s_r$  are different. Table 6.10 illustrates the values of the premise parameters, a, b, c, and  $\sigma$ , and consequent parameters for surface roughness and cutting force prediction models. Hence, the prediction of the outputs cutting force ( $F_c$ ) can be calculated as:

$$\begin{aligned}
 F_c &= \sum_{r=1}^{18} \bar{w}_r f_r = \sum_{r=1}^{18} \bar{w}_r (p_r F + q_r V + r_r P_s + s_r) \\
 &= \frac{\sum_{k=1}^3 \sum_{j=1}^2 \sum_{i=1}^3 (\mu_{1i}(F) \times \mu_{2j}(V) \times \mu_{3k}(P_s)) (p_r F + q_r V + r_r P_s + s_r)}{\sum_{k=1}^3 \sum_{j=1}^2 \sum_{i=1}^3 (\mu_{1i}(F) \times \mu_{2j}(V) \times \mu_{3k}(P_s))} \quad (6)
 \end{aligned}$$

Table 6. 10 Values of premise and consequent parameters in proposed ANFIS structure for cutting force prediction

<i>Premise parameters</i>			<i>Consequent parameters value</i>				
<i>MF</i>	<i>Parameter</i>	<i>Value</i>	<i>Rule No.</i>	<i>p</i>	<i>q</i>	<i>r</i>	<i>s</i>
$\mu_{11}(F)$	$\sigma, c$	[0.01353 0.09238]	1	-2.20E-03	3.80E-02	1.34E-01	-2.20E-02
			2	1.14E-03	-5.13E-01	1.30E+00	1.14E-02
$\mu_{12}(F)$	$\sigma, c$	[0.03844 0.14]	3	5.78E-05	3.78E-02	1.04E-01	5.78E-04
			4	6.05E-04	2.16E-02	-1.08E-01	6.05E-03
$\mu_{13}(F)$	$\sigma, c$	[0.03333 0.1972]	5	-3.49E-04	1.06E-01	-3.96E-01	-3.49E-03
			6	-1.07E-05	1.83E-02	-1.92E-02	-1.07E-04
$\mu_{21}(V)$	$a, b, c$	[-500 300 1100]	7	6.11E-03	2.87E-02	3.00E-01	3.69E-02
			8	-2.78E-03	1.76E-01	-1.89E+00	-1.66E-02
$\mu_{22}(V)$	$a, b, c$	[300 1100 1900]	9	1.82E-04	1.07E-02	2.27E-01	1.26E-03
			10	-1.66E-03	3.41E-02	-7.06E-02	-1.00E-02
$\mu_{31}(P_s)$	$\sigma_1, c_1$	[6.616 90.52]	11	7.72E-04	-1.48E-01	5.18E-01	4.56E-03
	$\sigma_2, c_2$	[6.616 113.9]	12	-4.27E-05	3.99E-02	-5.37E-02	-2.98E-04
$\mu_{32}(P_s)$	$\sigma_1, c_1$	[6.616 129.5]	13	8.72E-04	5.11E-02	3.32E-01	9.41E-03
	$\sigma_2, c_2$	[6.616 152.8]	14	-1.20E-04	-1.37E-01	-3.43E-01	-3.02E-03
				15	2.04E-04	7.71E-02	1.95E-01
$\mu_{33}(P_s)$	$\sigma_1, c_1$	[6.616 168.4]	16	-2.20E-04	4.63E-02	-1.04E-01	-2.48E-03
	$\sigma_2, c_2$	[6.616 191.8]	17	5.55E-06	1.93E-02	8.14E-02	7.16E-04
				18	-3.29E-05	4.57E-02	-3.31E-02

In Table 6.11, the accuracy of the selected ANFIS models is investigated by using twelve additional experimental data sets for testing. As can be seen, ANFIS prediction models are in good agreement with experimental data. The testing data RMSE values of the ANFIS models when it comes to predicting surface roughness and cutting force are 0.2846 and 2.4053, and the average errors are 8% and 6%, respectively.

Table 6. 11 Comparison of estimated outputs and RMSE

Input			Actual Value		Predicted Value			
Feed Rate (mm/tooth)	Cutting Speed (m/min)	Particle Size ( $\mu\text{m}$ )	Ra ( $\mu\text{m}$ )	Cutting Force (N)	Ra ( $\mu\text{m}$ )	Error	Cutting Force (N)	Error
0.13	400	102.2	2.8	35	2.74	2%	38.69	11%
0.13	400	113.5	2.5	30	2.04	18%	33.29	11%
0.13	400	180.1	3	38	3.11	4%	42.35	11%
0.13	600	102.2	3.1	33	2.66	14%	36.05	9%
0.17	600	113.5	2.4	37	2.12	11%	36.65	1%
0.17	600	180.1	3.3	47	3.31	0%	46.75	1%
0.17	800	102.2	3	36	2.71	10%	38.51	7%
0.17	800	113.5	2.5	34	2.04	19%	34.51	2%
0.19	800	180.1	3.2	49	3.21	0%	48.41	1%
0.19	1000	102.2	2.8	37	2.75	2%	38.51	4%
0.19	1000	113.5	2.4	33	2.00	17%	34.89	6%
0.19	1000	180.1	2.9	42	3.03	5%	43.95	5%
Root mean square error (RMSE)					0.2846		2.4053	

## 6.6. Conclusion

Based on the performance and test results for the experiments regarding the influence of modifier elements on the machinability of Al-20 Mg<sub>2</sub>Si metal matrix composite, an Adaptive Network-based Fuzzy Inference System (ANFIS) was used to predict the machinability of the composite. The following observations can be made:

- 1- According to ANFIS structures, it was found that the precision of the prediction model is related to the type and number of membership functions.
- 2- ANFIS models show that Bi-containing composite has the best surface roughness value and lowest cutting force compared to other workpieces.
- 3- In all, 3584 ANFIS structures were examined for each output in which Gaussian-shaped

with three MFs for feed rate, Triangular-shaped with two MFs for cutting speed and three MFs for particle size were selected as the best accurate model for predicting surface roughness. In addition, for predicting cutting force, Gaussian-shaped with three MFs for feed rate, Triangular-shaped with two MFs for cutting speed and second type Gaussian-shaped with three MFs for Particle sizes were selected as the best precise model among all examined models.

4- The validation of model shows that the proposed ANFIS models and resulting mathematical models for predicting the surface roughness and cutting force are in good agreement with experimental data. These models illustrate the capability of neuro-fuzzy models to describe machinability phenomena and minimize experimental repetition.



## CONCLUSION

This research work was carried out to comprehensively understand the machinability of Al-20Mg<sub>2</sub>Si-Cu metal matrix composite. In addition, the effect of modifier elements on microstructure, mechanical properties and machinability indicators such as cutting force, surface roughness and chip morphology have been considered. Furthermore, the effect of modifier elements and cutting conditions on fine and ultrafine particle emission during the machining process was studied.

Moreover, two adaptive network-based fuzzy inference system (ANFIS) structures, being the most precise models, were constructed to evaluate the effects of feed rate, cutting speed and particle size on surface roughness and cutting force.

In the first article, the effect of Bi addition on the machinability, microstructure and mechanical properties of Al-20Mg<sub>2</sub>Si-Cu metal matrix composite was investigated. In light of the above considerations, it was found that the addition of Bi has a significant effect on the microstructure and machinability of the metal matrix composite. In the second article, an experimental investigation of mechanical properties and dust emissions was carried out when milling Al-20Mg<sub>2</sub>Si-Cu metal matrix composite containing Bi and Ba as modifier elements.

In the third article, two adaptive network-based fuzzy inference system (ANFIS) models were selected as the most precise to predict the machinability of the composite and used as artificial intelligence to predict the machinability of Al-20 Mg<sub>2</sub>Si-Cu metal matrix composite with modifier elements. The ANFIS models were introduced to evaluate the effect of feed rate, cutting speed and particle size on the machinability of the composite. The ANFIS

models were used to reduce costs and total experiment time. Since two ANFIS models were selected, two mathematical models were obtained based on these models.

In the light of the results obtained, the major conclusions are summarized as follows:

- It was found the morphology of primary  $Mg_2Si$  particles changed from a coarse shape to fine polygonal structure by the addition of Bi. Moreover, the flake-like eutectic morphology became lamellar-shaped. The addition of Bi decreased the average particle size from 180.1  $\mu m$  to 113.5  $\mu m$ . Elongation (EL %), and hardness of composite improved by 75%, and 12%, respectively with the addition of Bi.
- The addition of Bi improved the machinability of the composite. Bi acted like a lubricant by making a boundary layer between the tool and workpiece and improved chip breakability and surface roughness values. Bi decreased BUE formation and cutting force during the machining process.
- The mean size and mean aspect ratio of the primary  $Mg_2Si$  particles decreased by 37 and 11%, respectively. The addition of 0.2wt%. The addition of Ba decreased the mean size and aspect ratio by 43 and 8%, respectively. In addition, Ba changed the morphology of primary  $Mg_2Si$  particles from a coarse shape to a polyhedral shape.
- It was found that metal matrix composites containing Bi and Ba have a high density of dimples on their fracture faces with a few decohered primary  $Mg_2Si$  particles as a ductile fracture. The addition of Bi and Ba increased hardness value from 62 HV to 80 and 66 HV, respectively. It was found that microstructure and cutting condition have a direct effect on dust emission during the milling process.
- Particle emission increased with increasing cutting speeds from 300 to 700 m/min and then decreased with increasing cutting speed to 1100 m/min. It could be related to the

role of temperature in the primary and secondary shear zones. The addition of Bi and Ba decreased ultrafine particle emission (number, surface, and mass concentration) compared to the base composite by factors of 4 and 8, respectively. It could be related to the ductility of metal matrix composite which strongly controlled the dust emission level during the machining processes.

- According to ANFIS structures, it was found that the precision of the prediction model is related to the type and number of membership functions. ANFIS models show that Bi-containing composite has the best surface roughness value and lowest cutting force compared to other workpieces.
- In all, 3584 ANFIS structures were examined for each output in which Gaussian-shaped with three MFs for feed rate, Triangular-shaped with two MFs for cutting speed and three MFs for particle size were selected as the best accurate model for predicting surface roughness. In addition, for predicting cutting force, Gaussian-shaped with three MFs for feed rate, Triangular-shaped with two MFs for cutting speed and second type Gaussian-shaped with three MFs for Particle sizes were selected as the best precise model among all examined models.
- The proposed ANFIS models and resulting mathematical models for predicting the surface roughness and cutting force are in good agreement with experimental data. These models illustrate the capability of neuro-fuzzy models to describe machinability phenomena and minimize experimental repetition.

## CONTRIBUTIONS

The main contributions made by this research work can be summarized as follows:

- Demonstration of the role of Ba and Bi (modifier elements) on the microstructure and mechanical properties of Al-20Mg<sub>2</sub> metal matrix composite. The application of this composite can be used in automotive and aerospace industries.
- Investigation on the effect of modifier elements (Ba or Bi) on machinability and particle emission when machining Al-20Mg<sub>2</sub>Si-Cu metal matrix composite. It will improve the machinability of this composite and decrease dust emissions during the machining process. It would be helpful for the operator's health.
- Usage of an adaptive network-based fuzzy inference system (ANFIS) as an artificial intelligence method to predict the machinability of Al-20Mg<sub>2</sub> metal matrix composite. The proposed mathematical model's approach showed the capability of neuro-fuzzy models to describe machinability phenomena with fewer experimental repetitions.

## RECOMMENDATIONS

Future research work related to this study will concentrate on the following aspects:

- Performing comprehensive mechanical properties studies such as tensile, impact and wear tests in different temperatures on the unmodified and modified Al-20Mg<sub>2</sub>Si-Cu metal matrix composite in order to clarify the enhancement of the composite performance.
- Using other modifier elements such as tin (Sn), strontium (Sr), and lithium (Li) to investigate the effect of these modifier elements on the microstructure and mechanical properties of the metal matrix composite; Studying the effect of new modifier elements on the machinability of the composite such as surface roughness, cutting force and chip morphology; and investigating the effect of these elements on dust emission during the machining process.
- Investigation on the tool wear characteristics when machining metal matrix composite containing different modifier elements.



## LIST OF BIBLIOGRAPHICAL REFERENCES

- Abdulshahed, A. M., Longstaff, A. P., & Fletcher, S. (2015). The application of ANFIS prediction models for thermal error compensation on CNC machine tools. *Applied Soft Computing Journal*, 27, 158–168.
- Andrewes, C. J., Feng, H.Y., & Lau, W. (2000). Machining of an aluminum/SiC composite using diamond inserts. *Journal of Materials Processing Technology*, 102(1–3), 25–29.
- Arumugam, P. U., Malshe, A. P., & Batzer, S. A. (2006). Dry machining of aluminum–silicon alloy using polished CVD diamond-coated cutting tools inserts. *Surface and Coatings Technology*, 200(11), 3399–3403.
- Arumugam, P. U., Malshe, A. P., & Bhat, D. G. (2003). Study of Airborne Dust Emission and Process Performance During Dry Machining of Aluminum-Silicon Alloy with PCD and CVD Diamond-Coated Tools. *Journal of Manufacturing Processes*, 5, 163–169.
- Azarbarmas, M., Emamy, M., Karamouz, M., & Rassizadehghani, J. (2011). The effects of boron additions on the microstructure, hardness and tensile properties of in situ Al–15%Mg<sub>2</sub>Si composite. *Materials & Design*, 32(10), 5049–5054.
- Azmah, N., Universiti, N., Bzte, S. F., Abubakar, T., Teknologi, U., Hamzah, E., & Teknologi, U. (2015). Alteration by cerium element on primary and eutectic Mg<sub>2</sub>Si phases in Al-20 % Mg<sub>2</sub>Si In-Situ composite, *Advanced Materials Research*, 28(11), 125–143.
- Azwadi, C. S. N., Zeinali, M., Safdari, A., & Kazemi, A. (2013). Adaptive-network-based fuzzy inference system analysis to predict the temperature and flow fields in a lid-driven cavity. *Numerical Heat Transfer; Part A: Applications*, 63(12), 906–920.
- Bahrani, A., Razaghian, A., Emamy, M., & Khorshidi, R. (2012). The effect of Zr on the microstructure and tensile properties of hot-extruded Al–Mg<sub>2</sub>Si composite. *Materials & Design*, 36, 323–330.
- Balout, B., Songmene, V., & Masounave, J. (2007). An experimental study of dust generation during dry drilling of pre-cooled and pre-heated workpiece materials. *Journal of Manufacturing Processes*, 9(1), 23–34.
- Barzani, M. M., Farahany, S., Yusof, N. M., & Ourdjini, A. (2013). The influence of bismuth, antimony, and strontium on microstructure, thermal, and machinability of aluminum-silicon alloy. *Materials and Manufacturing Processes*, 28(11), 1184–1190.
- Barzani, M. M., Sarhan, A. D., Farahani, S., & Singh, R. (2015). Investigation into effect of cutting conditions on surface roughness while dry machining Al-11%Si and Al-11%Si-1% Bi die casting alloy. *Advanced Materials Research*, 1119, 617–621.

- Barzani, M. M., Sarhan, A. A. D., Farahany, S., Ramesh, S., & Maher, I. (2015). Investigating the machinability of Al-Si-Cu cast alloy containing bismuth and antimony using coated carbide insert. *Measurement: Journal of the International Measurement Confederation*, *62*, 170–178.
- Barzani, M. M., Yusof, N. M., Farid, A. A., Farahany, S., & Davoudinejad, A. (2013). Effects of cutting condition on surface roughness when turning untreated and Sb-treated Al-11%Si Alloys Using PVD coated tools. *Applied Mechanics and Materials*, *315*, 413–417.
- Barzani, M. M., Zalnezhad, E., Sarhan, A. A. D., Farahany, S., & Ramesh, S. (2015). Fuzzy logic based model for predicting surface roughness of machined Al-Si-Cu-Fe die casting alloy using different additives-turning. *Measurement*, *61*, 150–161.
- Basavakumar, K. G., Mukunda, P. G., & Chakraborty, M. (2007). Influence of melt treatments and turning inserts on cutting force and surface integrity in turning of Al-12Si and Al-12Si-3Cu cast alloys. *Surface and Coatings Technology*, *201*(8), 4757–4766.
- Bell, D., Chou, J., Nowag, L., & Liang, S. (1999). Modeling of the Environmental Effect of Cutting Fluid. *Tribology Transactions*, *204*, 37–41.
- Bordin, A., Sartori, S., Bruschi, S., & Ghiotti, A. (2017). Experimental investigation on the feasibility of dry and cryogenic machining as sustainable strategies when turning Ti6Al4V produced by Additive Manufacturing. *Journal of Cleaner Production*, *142*, 4142–4151.
- Brevern, P., El-Tayeb, N. S. M., & Vengкатesh, V. C. (2009). GUI Based ANFIS Modeling: Back Propagation Optimization Method for CO<sub>2</sub> Laser Machining. *International Journal of Intelligent Information Technology Application*, *2*(4), 123-135.
- Cai, W., Liu, F., Zhang, H., Liu, P., & Tuo, J. (2017). Development of dynamic energy benchmark for mass production in machining systems for energy management and energy-efficiency improvement. *Applied Energy*, *202*, 715–725.
- Dabade, U. A., & Joshi, S. S. (2009). Analysis of chip formation mechanism in machining of Al/SiCp metal matrix composites. *Journal of Materials Processing Technology*, *209*(10), 4704–4710.
- Davim, J. P. (2010). *Surface Integrity in Machining*. Springer.
- Davim, J. P. (2012). *Machining of Metal Matrix Composites*. London: Springer .
- Debnath, S., Reddy, M. M., & Yi, Q. S. (2014). Environmental friendly cutting fluids and cooling techniques in machining : a review. *Journal of Cleaner Production*, *83*, 33–47.
- Deiab, I., Waqar, S., & Pervaiz, S. (2014). Analysis of Lubrication Strategies for Sustainable

- Machining during Turning of Titanium Ti-6Al-4V alloy. *Procedia CIRP*, 17, 766–771.
- Djebara, A., Zedan, Y., Kouam, J., & Songmene, V. (2013). The Effect of the Heat Treatment on the Dust Emission During Machining of an Al-7Si-Mg Cast Alloys. *Journal of Materials Engineering and Performance*, 22(12), 3840–3853.
- Dong, M., & Wang, N. (2011). Adaptive network-based fuzzy inference system with leave-one-out cross-validation approach for prediction of surface roughness. *Applied Mathematical Modelling*, 35(3), 1024–1035.
- Ebtehaj, I., Bonakdari, H., Khoshbin, F., & Azimi, H. (2015). Pareto genetic design of group method of data handling type neural network for prediction discharge coefficient in rectangular side orifices. *Flow Measurement and Instrumentation*, 41, 67–74.
- Ekici, S. (2009). Expert Systems with Applications An adaptive neuro-fuzzy inference system ( ANFIS ) model for wire-EDM, 36, 6135–6139.
- El-Gallab, M. S., & Sklad, M. P. (2004). Machining of aluminum/silicon carbide particulate metal matrix composites. *Journal of Materials Processing Technology*, 152(1), 23–34.
- Elder, A. C. P., Gelein, R., Azadniv, M., Frampton, M., Finkelstein, J., & Oberdörster, G. (2004). Systemic effects of inhaled ultrafine particles in two compromised, aged rat strains. *Inhalation Toxicology*, 16(6–7), 461–471.
- Elgallad, E. M., Samuel, F. H., Samuel, A. M., & Doty, H. W. (2010). Machinability aspects of new Al–Cu alloys intended for automotive castings. *Journal of Materials Processing Technology*, 210(13), 1754–1766.
- Emamy, M., Emami, A. R., Khorshidi, R., & Ghorbani, M. R. (2013). The effect of Fe-rich intermetallics on the microstructure, hardness and tensile properties of Al–Mg<sub>2</sub>Si die-cast composite. *Materials & Design*, 46, 881–888.
- Emamy, M., Jafari Nodooshan, H. R., & Malekan, A. (2011). The microstructure, hardness and tensile properties of Al–15%Mg<sub>2</sub>Si in situ composite with yttrium addition. *Materials & Design*, 32(8–9), 4559–4566.
- Emamy, M., Nemati, N., & Heidarzadeh, A. (2010). The influence of Cu rich intermetallic phases on the microstructure, hardness and tensile properties of Al–15% Mg 2 Si composite. *Materials Science and Engineering: A*, 527(12), 2998–3004.
- Fadavi Boostani, A., Tahamtan, S., Jiang, Z. Y., Wei, D., Yazdani, S., & Gong, D. (2015). Enhanced tensile properties of aluminium matrix composites reinforced with graphene encapsulated SiC nanoparticles. *Composites Part A: Applied Science and Manufacturing*, 68, 155–163.
- Farahany, S., Azmah, N., Ourdjini, A., Abu, T., Hamzah, E., Hasbullah, M., & Hekmatardakan, A. (2014). Materials Characterization The sequence of intermetallic formation

and solidification pathway of an Al-13Mg-7Si-2Cu in-situ composite. *Materials Characterization*, 98, 119–129.

Farahany, S., Bozorg, M., & Nordin, N. A. Study the Effect of Strontium Addition on Microstructure, Impact Toughness and Corrosion Behaviour of Al-Mg<sub>2</sub>Si In-situ Composite.

Farahany, S., Ghandvar, H., Nordin, N. A., Ourdjini, A., & Idris, M. H. (2016). Effect of primary and eutectic Mg<sub>2</sub>Si crystal modifications on the mechanical properties and sliding wear behaviour of an Al-20Mg<sub>2</sub>Si-2Cu-xBi composite. *Journal of Materials Science & Technology*, 32(11), 1083–1097.

Farahany, S., Nordin, N. A., Ourdjini, A., Bakar, T. A., Hamzah, E., Idris, M. H., & Hekmat-Ardakan, A. (2014). The sequence of intermetallic formation and solidification pathway of an Al-13Mg-7Si-2Cu in-situ composite. *Materials Characterization*, 98, 119–129.

Fox-Rabinovich, G., Dasch, J. M., Wagg, T., Yamamoto, K., Veldhuis, S., Dosbaeva, G. K., & Tauhiduzzaman, M. (2011). Cutting performance of different coatings during minimum quantity lubrication drilling of aluminum silicon B319 cast alloy. *Surface and Coatings Technology*, 205(16), 4107–4116.

Gaitonde, V. N., Karnik, S. R., & Davim, J. P. (2012). Machining of Metal Matrix Composites.

Galoppi, G. de S., Filho, M. S., & Batalha, G. F. (2006). Hard turning of tempered DIN 100Cr6 steel with coated and no coated CBN inserts. *Journal of Materials Processing Technology*, 179(1–3), 146–153.

Geneva, W. (1999). Hazard Prevention and Control In The Work Environment: Airbone Dust, (August), 1–246.

Goindi, G. S., & Sarkar, P. (2017). Dry machining : A step towards sustainable machining e Challenges and future directions. *Journal of Cleaner Production*, 165, 1557–1571.

Gradus, L. Y., & Popov, Y. A. (1984). Methods of decontaminating emissions during machining of materials. *Chemical and Petroleum Engineering*, 20(2), 57–59.

Grum, J., & Kisin, M. (2006). The influence of the microstructure of three Al-Si alloys on the cutting-force amplitude during fine turning. *International Journal of Machine Tools and Manufacture*, 46(7), 769–781.

Guo, E. J., Ma, B. X., & Wang, L. P. (2008). Modification of Mg<sub>2</sub>Si morphology in Mg-Si alloys with Bi. *Journal of Materials Processing Technology*, 206(1), 161–166.

Gupta, A., Singh, H., & Aggarwal, A. (2011). Taguchi-fuzzy multi output optimization (MOO) in high speed CNC turning of AISI P-20 tool steel. *Expert Systems with Applications*, 38(6), 6822–6828.

- Hadian, R., Emamy, M., & Campbell, J. (2009). Modification of cast Al-Mg<sub>2</sub>Si metal matrix composite by Li. *Metallurgical and Materials Transactions B*, 40(6), 822–832.
- Hadian, R., Emamy, M., Varahram, N., & Nemati, N. (2008). The effect of Li on the tensile properties of cast Al–Mg<sub>2</sub>Si metal matrix composite. *Materials Science and Engineering: A*, 490(1–2), 250–257.
- Hengcheng, L., Y., S., & Guoxiong, S. (2003). Restraining effect of strontium on the crystallization of Mg<sub>2</sub>Si phase during solidification in Al–Si–Mg casting alloys and mechanisms. *Materials Science and Engineering: A*, 358(1), 164–170.
- Ho, W., Tsai, J., Lin, B., & Chou, J. (2009). Adaptive network-based fuzzy inference system for prediction of surface roughness in end milling process using hybrid Taguchi-genetic learning algorithm. *Expert Systems With Applications*, 36(2), 3216–3222.
- Hwang, Y.K., Lee, C.M., & Park, S.H. (2009). Evaluation of machinability according to the changes in machine tools and cooling lubrication environments and optimization of cutting conditions using Taguchi method. *International Journal of Precision Engineering and Manufacturing*, 10(3), 65–73.
- Kaynak, Y., Lu, T., & Jawahir, I. S. (2014). Cryogenic Machining-Induced Surface Integrity: A Review and Comparison with Dry, MQL, and Flood-Cooled Machining, 18(2), 149-198.
- Yusof, N. M., Razavykia, A., & Farahany, S. (2016). Effect of modifier elements on machinability of Al-20Mg<sub>2</sub>Si metal matrix composite during dry turning, 20(3), 460-474.
- Kadam, G. S., & Pawade, R. S. (2017). Surface integrity and sustainability assessment in high-speed machining of Inconel 718 e An eco-friendly green approach. *Journal of Cleaner Production*, 147, 273–283.
- Kamguem, R., Djebara, A., & Songmene, V. (2013). Investigation on surface finish and metallic particle emission during machining of aluminum alloys using response surface methodology and desirability functions. *International Journal of Advanced Manufacturing Technology*, 69(5–8), 1283–1298.
- Kannan, S., & Kishawy, H. (2006). Surface characteristics of machined aluminium metal matrix composites. *International Journal of Machine Tools and Manufacture*, 46(15), 2017–2025.
- Kannan, S., & Kishawy, H. (2008). Tribological aspects of machining aluminium metal matrix composites. *Journal of Materials Processing Technology*, 198(1–3), 399–406.
- Kannan, S., Kishawy, H., & Deiab, I. (2009). Cutting forces and TEM analysis of the generated surface during machining metal matrix composites. *Journal of Materials Processing Technology*, 209(5), 2260–2269.

- Khettabi, R., Fatmi, L., Masounave, J., & Songmene, V. (2013). On the micro and nanoparticle emission during machining of titanium and aluminum alloys. *CIRP Journal of Manufacturing Science and Technology*, 6(3), 175–180.
- Khettabi, R., Songmene, V., & Masounave, J. (2007). Effect of tool lead angle and chip formation mode on dust emission in dry cutting. *Journal of Materials Processing Technology*, 193(1–3), 100–109.
- Khettabi, R., Songmene, V., & Masounave, J. (2010). Effects of speeds, materials, and tool rake angles on metallic particle emission during orthogonal cutting. *Journal of Materials Engineering and Performance*, 19(6), 767–775.
- Khettabi, R., Songmene, V., Zaghbani, I., & Masounave, J. (2010). Modeling of particle emission during dry orthogonal cutting. *Journal of Materials Engineering and Performance*, 19(6), 776–789.
- Koch, S., & Antrekowitsch, H. (2008). Free-Cutting Aluminium Alloys with Tin as Substitution for Lead. *BHM Berg-und Hüttenmännische Monatshefte* 153(7), 278-281.
- Koch, S., & Antrekowitsch, H. (2011). Alloying Behaviour of Cu , Mg and Mn in Lead-free Al-Cu Based Alloys Intended for Free Machining. *BHM Berg-und Hüttenmännische Monatshefte* 156(1), 22–27.
- Kouam, J. (2012). Dry high-speed machining : a cost effective and green process Victor Songmene, Riad Khettabi & Jules Kouam, *International Journal of Manufacturing Research* 7(3), 229–256.
- Kouam, J., Songmene, V., & Balhoul, A. (2013). Experimental investigation on PM2.5 particle emission during polishing of granite. *Health* 29. 5(10), 29–35.
- Kouam, J., Songmene, V., Zedan, Y., Djebara, A., & Khettabi, R. (2013). on Chip Formation During Drilling of Cast Aluminum Alloys. *Machining Science and Technology*, 17(2), 228–245.
- Kumar, S., & Satsangi, P. S. (2013). Multiple-response optimization of turning machining by the taguchi method and the utility concept using uni-directional glass fiber-reinforced plastic composite and carbide (k10) cutting tool. *Journal of Mechanical Science and Technology*, 27(9), 2829–2837.
- Lee, D.Y., & Yoon, D. H. (2014). Properties of alumina matrix composites reinforced with SiC whisker and carbon nanotubes. *Ceramics International* 40(9):14375-14383.
- Li, C., Wu, Y., Li, H., & Liu, X. (2009). Microstructural formation in hypereutectic Al–Mg2Si with extra Si. *Journal of Alloys and Compounds*, 477(2), 212–216.
- Li, Q., Xia, T., Lan, Y., Li, P., & Fan, L. (2013). Effects of rare earth Er addition on microstructure and mechanical properties of hypereutectic Al-20% Si alloy. *Materials*

*Science and Engineering A*, 588, 97–102.

- Li, Q., Xia, T., Lan, Y., Zhao, W., Fan, L., & Li, P. (2013). Effect of in situ  $\gamma$ -Al<sub>2</sub>O<sub>3</sub> particles on the microstructure of hypereutectic Al–20% Si alloy. *Journal of Alloys and Compounds*, 577, 232–236.
- Maher, I., Sarhan, A. A. D., Barzani, M. M., & Hamdi, M. (2015). Increasing the productivity of the wire-cut electrical discharge machine associated with sustainable production. *Journal of Cleaner Production*, 108, 247–255.
- Manna, A., & Bhattacharyya, B. (2002). A study on different tooling systems during machining of Al/SiC-MMC. *Journal of Materials Processing Technology*, 123(3), 476–482.
- Marani Barzani, M., Zalnezhad, E., Sarhan, A. a. D., Farahany, S., & Ramesh, S. (2015). Fuzzy logic based model for predicting surface roughness of machined Al–Si–Cu–Fe die casting alloy using different additives-turning. *Measurement*, 61, 150–161.
- Marani, M., Farahany, S., & Songmene, V. (2017). Machinability characteristics , thermal and mechanical properties of Al-Mg 2 Si in-situ composite with bismuth. *Measurement*, 110, 263–274.
- Marani, M., Songmene, V., Kouam, J., & Zedan, Y. (2018). Experimental investigation on microstructure , mechanical properties and dust emission when milling Al-20 Mg2Si-2Cu metal matrix composite with modifier elements, *The International Journal of Advanced Manufacturing Technology* 99.1-4 (2018): 789-802.
- McLellan, R. O., & Miller, F. J. (1997). An overview of EPA’s proposed revision of the particulate matter standard. *CIIT Activities*, 17(4), 1–22.
- Mohammad, H., Bee, K., & Ang, C. (2015). Prediction and characterization of surface roughness using sandblasting and acid etching process on new non-toxic titanium biomaterial : adaptive-network-based fuzzy inference System. *Neural Computing and Applications*, 1751–1761.
- Mohd, A., & Habibollah, Z. (2015). Fuzzy logic for modeling machining process : a review, *Artificial Intelligence Review* 43 (3), 345-379.
- Mulyana, T., Abd, E., & Nazrein, S. (2017). The in fl uence of cryogenic supercritical carbon dioxide cooling on tool wear during machining high thermal conductivity steel. *Journal of Cleaner Production*, 164, 950–962.
- Nami, H., Adgi, H., Sharifitabar, M., & Shamabadi, H. (2011). Microstructure and mechanical properties of friction stir welded Al/Mg2Si metal matrix cast composite. *Materials & Design*, 32(2), 976–983.
- Nasiri, N., Emamy, M., Malekan, A., & Norouzi, M. H. (2012). Microstructure and tensile

properties of cast Al-15%Mg<sub>2</sub>Si composite: Effects of phosphorous addition and heat treatment. *Materials Science and Engineering: A*, 556, 446–453.

Noordin, M. Y., Venkatesh, V. C., Chan, C. L., & Abdullah, A. (2001). Performance evaluation of cemented carbide tools in turning AISI 1010 steel. *Journal of Materials Processing Technology*, 116(1), 16–21.

Nordin, N. A., Farahany, S., Ourdjini, A., Abu Bakar, T. A., & Hamzah, E. (2013). Refinement of Mg<sub>2</sub>Si reinforcement in a commercial Al–20%Mg<sub>2</sub>Si in-situ composite with bismuth, antimony and strontium. *Materials Characterization*, 86, 97–107.

Nordin, N. A., Farahany, S., Ourdjini, A., Abubakar, T. A., & Hamzah, E. (2014). Evaluation of The Effect of Bismuth on Mg 2 Si Particulate Reinforced in Al-20 % Mg 2 Si in-situ Composite, 845, 22–26.

Nordin, N. A., Farahany, S., Ourdjini, A., Bakar, T. A. A., & Hamzah, E. (2013). Refinement of Mg<sub>2</sub>Si reinforcement in a commercial Al–20%Mg<sub>2</sub>Si in-situ composite with bismuth, antimony and strontium. *Materials Characterization*, 86, 97–107.

Oberdrster, G., & Oberdrster, J. (2005). Nanotoxicology: An emerging discipline evolving from studies of ultrafine particles. *Environmental Health Perspectives*, 113(7), 823–839.

Ozben, T., Kilickap, E., & Cakır, O. (2008). Investigation of mechanical and machinability properties of SiC particle reinforced Al-MMC. *Journal of Materials Processing Technology*, 198(1), 220–225.

Ozcatalbas, Y. (2003). Chip and built-up edge formation in the machining of in situ Al<sub>4</sub>C<sub>3</sub>–Al composite. *Materials & Design*, 24(3), 215–221.

Palanikumar, K., & Karthikeyan, R. (2007). Assessment of factors influencing surface roughness on the machining of Al/SiC particulate composites. *Materials & Design*, 28(5), 1584–1591.

Palanikumar, K., & Muniaraj, A. (2014). Experimental investigation and analysis of thrust force in drilling cast hybrid metal matrix (Al–15% SiC–4% graphite) composites. *Measurement*, 53, 240–250.

Peach, W. D. (2009). The effect of near-surface metallurgy on the machinability of cast iron. *Missouri University of Science and Technology*, Thesis T10211.

Pourtousi, M., Zeinali, M., Ganesan, P., & Sahu, J. N. (2015). RSC Advances Prediction of multiphase flow pattern inside a 3D bubble column reactor using a combination of CFD and ANFIS, 85652–85672.

Rai, R. N., Datta, G. L., Chakraborty, M., & Chattopadhyay, A. B. (2006). A study on the machinability behaviour of Al–TiC composite prepared by in situ technique. *Materials Science and Engineering: A*, 428(1), 34–40.

- Ramulu, M., Young, P., & Kao, H. (1999). Drilling of graphite/bismaleimide composite material. *Journal of Materials Engineering and Performance*, 8(3), 330–338.
- Rath, D., Panda, S., & Pal, K. (2018). Prediction of surface quality using chip morphology with nodal temperature signatures in hard turning of AISI D3 steel. *Materials Today: Proceedings*, 5(5), 12368–12375.
- Raynor, P. C., Cooper, S., & Leith, D. (1996). Evaporation of polydisperse multicomponent oil droplets. *American Industrial Hygiene Association Journal*, 57(12), 1128–1136.
- Razaghian, A., Bahrami, A., & Emamy, M. (2012). The influence of Li on the tensile properties of extruded in situ Al–15%Mg2Si composite. *Materials Science and Engineering: A*, 532, 346–353.
- Saidi, M. N., Songmene, V., Kouam, J., & Bahloul, A. (2015). Experimental investigation on fine particle emission during granite polishing process. *The International Journal of Advanced Manufacturing Technology*, 81(9–12), 2109–2121.
- Schultheiss, F., Johansson, D., Bushlya, V., Zhou, J., Nilsson, K., & Ståhl, J. (2017). Comparative study on the machinability of lead-free brass. *Journal of Cleaner Production*, 149, 366–377.
- Schultheiss, F., Zhou, J., Gröntoft, E., & Ståhl, J. (2013). Sustainable machining through increasing the cutting tool utilization. *Journal of Cleaner Production*, 59, 298–307.
- Farahany, S., Idris, M. H., & Ourdjini, A. (2015). Effect of bismuth and strontium interaction on the microstructure development, mechanical properties and fractography of a secondary Al-Si-Cu-Fe-Zn alloy. *Materials Science and Engineering: A* 6(21), 28-38.
- Seeman, M., Ganesan, G., & Karthikeyan, R. (2010). Study on tool wear and surface roughness in machining of particulate aluminum metal matrix composite-response surface methodology approach. *Journal of Advanced Manufacturing Technology*, 48 (5-8), 613–624.
- Shahrom, M. S., & Yusoff, A. R. (2014). Review of aluminum chip machining using direct recycling process. *Advanced Materials Research* 9 (3), 157–162.
- Shaw, M. C. (2005). *Metal cutting principles*, Oxford university press.
- Shokrani, A., Dhokia, V., & Newman, S. T. (2016). Investigation of the effects of cryogenic machining on surface integrity in CNC end milling of Ti–6Al–4V titanium alloy. *Journal of Manufacturing Processes*, 21, 172–179.
- Sidik, C., Azwadi, N., Zeinali, M., & Safdari, A. (2013). Numerical heat transfer, Part A : Applications adaptive-network-based fuzzy inference system analysis to predict the temperature and flow fields in a lid-driven cavity. *Applications*, 63 (12), 906-920.

- Smolej, A., Breskvar, B., Sokovic, M., Dragojevic, V., Slacek, E., & Smolar, T. (2002). Properties of aluminium free-cutting alloys with tin. Part II. *Aluminium*, 78(5), 388–391.
- Songmene, V., & Balazinski, M. (1999). Machinability of graphitic metal matrix composites as a function of reinforcing particles. *CIRP Annals-Manufacturing Technology*, 48(1), 77–80.
- Songmene, V., Balout, B., & Masounave, J. (2004). Clean Machining: Experimental investigation on dust formation-Part II: Influence of machining parameters and chip formation. *Int. J. of Environmentally Conscious Design and Manufacturing*, 14(1), 1–16.
- Songmene, V., Kouam, J., & Balhoul, A. (2018). Effect of minimum quantity lubrication (MQL) on fine and ultra fine particle emission and distribution during polishing of granite. *Measurement*, 114(June 2017), 398–408.
- Sun, J., Ju, C., Yue, Y., Gunter, K. L., Michalek, D. J., & Sutherland, J. W. (2004). Character and Behavior of Mist Generated by Application of Cutting Fluid to a Rotating Cylindrical Workpiece, Part 2: Experimental Validation. *Journal of Manufacturing Science and Engineering*, 126(August), 426.
- Sun, Y., & Ahlatci, H. (2011). Mechanical and wear behaviors of Al–12Si–XMg composites reinforced with in situ Mg<sub>2</sub>Si particles. *Materials & Design*, 32(5), 2983–2987.
- Sutherland, J. W., Kulur, V. N., King, N. C., & von Turkovich, B. F. (2000). An experimental investigation of air quality in wet and dry turning. *CIRP Annals - Manufacturing Technology*, 49(1), 61–64.
- Wright, E. M. T. and P. K. (2000). *mettal cutting*. Butterworth-Heinemann.
- Yang S.L. Lee, C.K. Lee and J.C. Lin, C.Y. (2006). Effects of Sr and Sb modifiers on the sliding wear behavior of A357 alloy under varying pressure and speed conditions. *Wear*, 261: 1348-.
- YANG, M., PAN, F., Jia, S., & Liang, B. A. I. (2009). Comparison of Sb and Sr on modification and refinement of Mg<sub>2</sub>Si phase in AZ61-0.7 Si magnesium alloy. *Transactions of Nonferrous Metals Society of China*, 19(2), 287–292.
- Yue, Y., Gunter, K. L., Michalek, D. J., & Sutherland, J. W. (2000). Cutting fluid mist formation in turning via atomization part 1: Model development. *IMECE Proc. of ASME: Manufacturing Engineering Division*, 843–850.
- Yusof, N. M., Razavykia, A., Farahany, S., & Esmailzadeh, A. (2016). Effect of modifier elements on machinability of Al-20%Mg<sub>2</sub>Si metal matrix composite during dry turning. *Machining Science and Technology*, 20(3), 460–474.
- Zaghbani, I., Songmene, V., & Khettabi, R. (2009). Fine and ultrafine particle characterization and modeling in high-speed milling of 6061-T6 aluminum alloy.

*Journal of Materials Engineering and Performance*, 18(1), 38–48.

Zedan, Y. (2010). *Machinability aspects of heat-treated Al-(6-11)% Si cast alloys: role of intermetallics and free-cutting elements*. Université du Québec à Chicoutimi.

Zeinali, M., & Mazlan, S. A. (2013). A phenomenological dynamic model of a magnetorheological damper using a neuro-fuzzy system. *Smart Materials and Structures*, 22(12), 125013.

Zhang, Q., Kusaka, Y., & Donaldson, K. (2000). Comparative pulmonary responses caused by exposure to standard cobalt and ultrafine cobalt. *Journal of Occupational Health*, 42(4), 179–184.